Solar Desalination Systems

Research and Modeling Process

by

Rodrigo Barraza

A thesis submitted in partial fulfillment of

the requirements for the degree of

Master of Science

(Mechanical Engineering)

at the

UNIVERSITY OF WISCONSIN – MADISON

2011

Abstract

Desalination is a process of removing dissolved minerals (principally, salt) from seawater or brackish water to produce fresh water. Desalination systems are a reliable option to supply a supply of sustainable fresh water in coastal areas where fresh water may be in shortage. In costal locations where fresh water is scarce and high levels of solar radiation are available, the use of desalination technologies driven by solar energy systems may be a suitable option.

This thesis describes and compares different conventional seawater desalination technologies analyzing their features, energy performance, and fresh water yields. Two technologies that use solar-derived thermal energy directly to desalinate are evaluated. The two most promising desalination technologies that can be combined with solar thermal energy include multi-effect desalination (MED) and multi-effect desalination combined with a thermo-compressor (MED-TC). Models for both of these technologies are developed and validated against operational data from the ALBA MED-TC plant installed in Bahrain. The desalination models are then coupled with a parabolic trough system with thermal storage to supply the necessary thermal energy to drive the plant.

The performance of the solar plant and the desalination plant both working together is tested in a case study. The case study locates both plant solar steam generator and desalination plants in the city of Antofagasta, Chile. This city faces a shortage of fresh water and it is located in a coastal region that receives high levels of solar radiation. The desalination plant is sized to produce 10,800 metric tons of fresh water per day continuously. The solar steam generation plant supplies saturated steam at three

alternative plant design steam pressures. The solar energy is capable of covering up to 70% of the total thermal energy required using storage capacity by the desalination plant with annual solar field efficiency of about 55%. The solar field oriented along a north-south axis presents the best performance, and the solar fraction does not change significantly as the pressure of the saturated steam generated varies.

Acknowledgements

This thesis is dedicated to my Mom, Ines, my Dad, Eugenio, and my wife, Ana Maria.

First, I would like to thank my primary advisor, Sanford Klein. I feel quite honored when you selected me to work with you. I have enjoyed this time in Wisconsin and worked in the SEL group. I have learned a lot taking your classes and working with you. I look forward to working with you more in the future. Thank you for your patience, kindness and time to explain all the details.

I would like to thank my second advisor, Douglas Reindl. I am honored to work for you. I appreciate your constructive criticisms. I am glad that I have vastly improved as a writer during my Masters career. I look forward to working with you more in the future. Thank you for your dedication and patience explaining different problems

Dad and Mom, I do not know what to say, really! I am indebted to your encouragements, your patience answering all my questions when I was growing up. I feel honored being born in this family. I really don't know how to thank both of you; I hope I have answered part of your wishes with my work.

Ana Maria, my lovely wife, without you I would not have been able to come back to school. Thank you for your love, support, and encouragement. Also, you provide me a stress free atmosphere every day.

Thank you to John Tonner from Water Consultants International for all your help, encourage and willingness to provide many technical material, it was really useful.

Greatly acknowledged financial support was provided by Fulbright fellowship and by Conicyt of the government of Chile through my Master's career.

Table of Contents

Table of Figures

List of Tables

Nomenclature

a	frictional pressure gradient for all the flow liquid
A	surface area (m^2)
AA	parameter of equation 4.19
b	frictional pressure gradient for all the flow vapor
BPE	boiling point elevation (°C)
c	specific heat capacity (kJ/kg-°C)
C	sound velocity (m/s^2)
C	Concentration ratio
$\dot{C}$	capacitance (kW/°C)
C_1	parameter of equation 4.28
C_2	parameter of equation 4.28
C_P	specific heat capacity at constant pressure (kJ/kg-°C)
C_v	specific heat capacity at constant volume (kJ/kg-°C)
CR	compression ratio
$\frac{dp}{dz}$	pressure gradient

$\frac{dT_i}{dt}$	the change in average temperature of the node "i" as a function of time
ER	expansion ratio
f	friction factor
Fr	frounde number
$F_R(\tau\alpha)_n$	intercept efficiency
$F_R U_L$	efficiency slope
g	gravitational acceleration (m/s^2)
G	mass flux (kg/m^2)
Ga	galileo number
GOR	gain output ratio
h	specific enthalpy (kJ/kg)
$\overline{H}_{1-tube}$	(W/m^2-°C)
H	local heat transfer coefficient associated with convection (W/m2-K)
$\overline{H}$	average heat transfer coefficient associated with convection (W/m2-K)
HTF	heat transfer fluid
I_b	incident beam radiation

IAM	incidence angle modifier
ID	internal diameter
k	thermal conductivity (W/m-K)
L	length of tube (m)
m	mass (kg)
$\dot{m}$	mass flow rate (kg/s)
N	number of tube
N	number of nodes
N_p	number of collector in parallel
N_s	number of collector in series
NTU	number of transfer units
Nu_{fc}	nusselt number related to forced convection in the bottom pool
Nu_D	nusselt number
OD	external diameter
P	pressure (kPa)
Pr	Prandt number
PR	Performance ratio (kg/kJ)
PP	pinch point (°C)
ppm	part per million

q''	heat flux (kW/m^2)
$\dot{Q}$	rate of heat (kW)
Q_u	solar energy absorbed by the fluid (kW)
R	Thermal resistance (K/kW)
R_1	correction factors due to flow rate
R_2	correction factors due to number of collector in series
R_f''	fouling factor
Re_D	Reynold number
$Re_{D,l}$	superficial liquid Reynold number
S	concentration (mg/kg)
SEC	specific energy consumption (kJ/kg)
St	solar time (h)
T	temperature (°C)
TBT	brine temperature (°C)
U	overall heat transfer coefficient (W/m2-K)
UA	loss coefficient from the tank (W/°C)
V	velocity (m/s^2)
vf	void fraction

$\dot{W}$	rate of work (kW)
x	quality
X_{tt}	Lockhart Martinelly parameter
Z	factor equation 4.11

Greek Symbols

α	collector control function
ζ	collector control function
θ	angle of incidence
θ_z	zenith angle
δ	declination angle
ω	entrainment ratio
ω	hour angle
β	surface slope
γ_s	solar azimuth angle
γ	surface azimuth angle
ϕ	latitude
ε	effectiveness

η	efficiency
μ	viscosity (Pa-s)
ν	kinematic viscosity (m^2/s)
ρ	density (kg/m^3)
$\Delta\dot{G}$	Gibbs energy rate difference (kW)
Δh	enthalpy difference (kJ/kg)
$\Delta\dot{H}$	enthalpy rate difference (kW)
ΔP	pressure difference (kPa)
$\Delta\dot{S}$	entropy rate difference (kW/K)
ΔT	temperature difference (°C)

Subscripts

a	ambient
a	aperture
avg	average
b	brine
brine	brine
FB	flashing box
c	condensing

C	condenser
co	condensation
cond	condensate water
cool	cooling water
d	discharge
e	evaporatorating
E	evaporator
effect	effect
ext	external
Ej	ejector
Feed	feed water
flashing	vapor water by flashing
fd	fully developed
frict	frictional
fw	fresh water
H	solar field
HTF	heat transfer fluid
i	number of node
i	effect i

int	internediate
is	isentropic
n	effect n, last effect
in	inlet
l	liquid
L	load
m	mixed-flow rate
min	minimum
max	maximum
out	outlet
p	primary
Ph	pre-heater
R	ratio
s	secondary
s	surface
salt	salt
sat	saturated
sc	subcooling
sh	superheat

sw	seawater
t	tube
TC	turbo compressor
tot	total
v	vapor
vap	vaporization
vapor	vapor water
vapor − heat	vapor water condensing inside of tubes
vert	vertical
wv	vapor water
0	before effect 1
1	effect 1
2	effect 2
3	effect 3

Chapter 1 : Introduction

1.1. Water availability and use

The existence of human and animal life, environment, and any human activity requires an adequate supply of freshwater. Water is an abundant resource on the earth, and it covers 75% of the planet's surface. Figure 1-1 shows how water is distributed on the earth's surface.

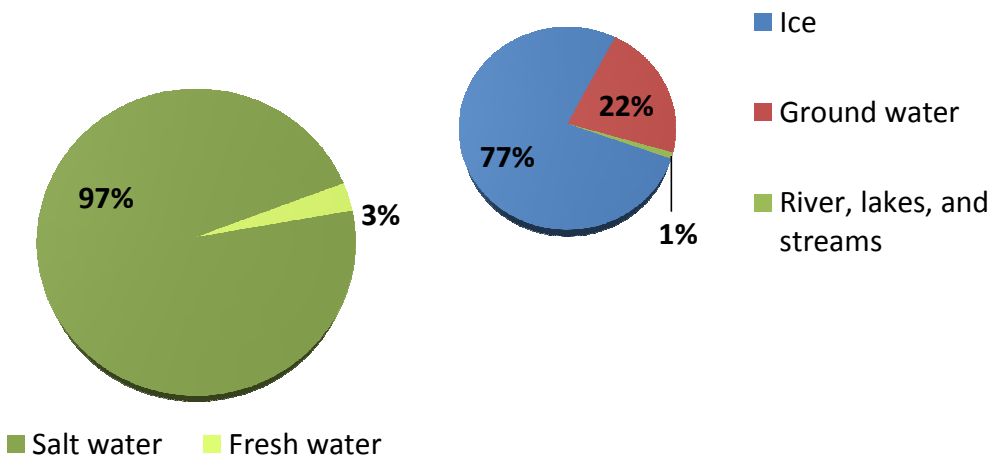

Figure 1 - 1 : Distribution of water on the earth's surface (U.S. EPA, 2011)

Seawater (salt water) of the oceans represents 97% of the total water in the earth but only about 36 million km^3 of the earth's water is fresh (3%). Fresh water is found mostly in the form of ice (77%), mainly in the poles, in the ground water (22%), and only 1% is in

lakes and rivers (U.S. EPA, 2011). Humans and animals obtain most of the fresh water to meet their needs from lakes and rivers.

A portion of the total fresh surface water available is used finally for human activities. The other portion flows free to the oceans. Agriculture uses 70% of the total of fresh water used for human activities, 20% is used by the industry and only 10% is used for household needs (United Nations, 2008). In a developed country as United States, one American resident uses an average of 380 liters of fresh water per day (100 gal/day) (U.S. EPA, 2011).

1.2. Water scarcity

1.2.1. Problem description

For many years, civilizations have settled and founded cities near large source of fresh water such as rivers, lakes, and oases because water is essential for life. However, demand for freshwater have risen due to the combination of several factors: growth of population, developing of economic, accelerated urbanization, and improvements in the living standard. In the past century, the use of fresh water has grown at more than twice the rate of the population (United Nations, 2008). Although there is not yet a global water shortage, nowadays, some cities, which decades ago had plenty of water for human consumption and its activities, suffer water shortages.

Figure 1.2. shows the river's basins that are currently stresses and how severe it is. Scarcity or high stress is defined when the zone has a lower annual fresh water

availability than 1,000 cubic meter per person (Revenga, Brunner, Henninger, Kassem, & Payne, 2000), indicated with a red label. Stress is indicated with an orange label, and it is produced when the annual availability of water is between 1,000 and 1,700 cubic meter per person (Revenga et al., 2000). Labels yellow, green and blue light indicate sufficient quantity of water.

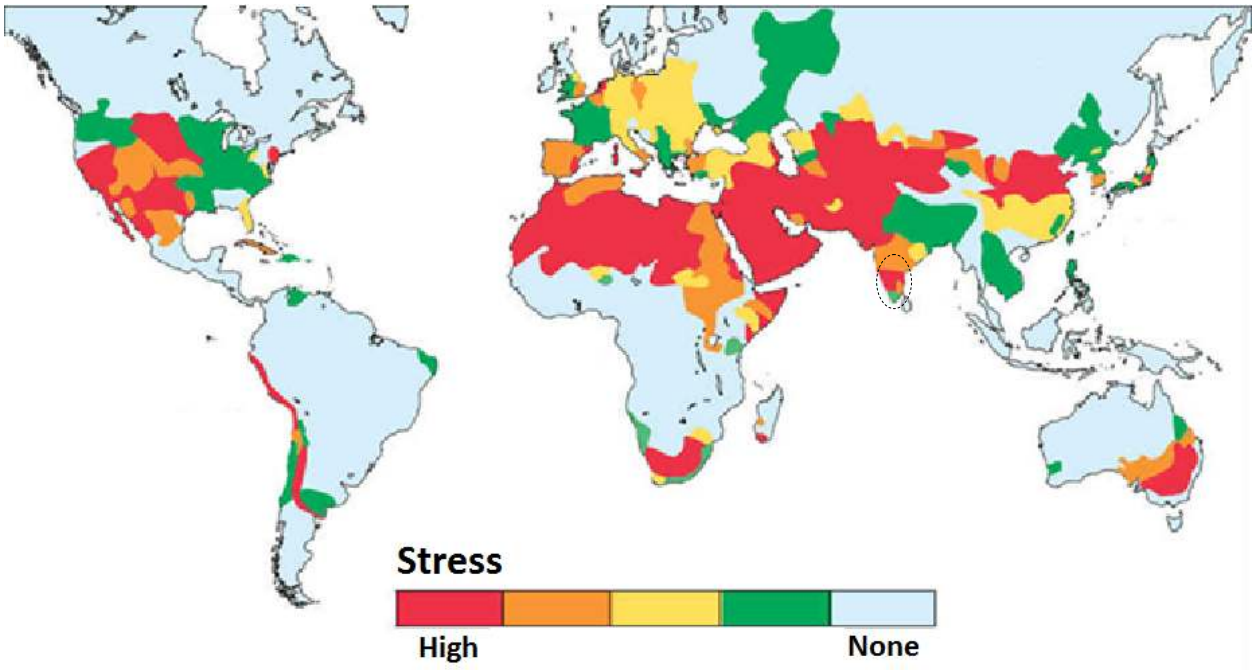

Figure 1 - 2 : Stress on World's River Basins (Revenga et al., 2000)

More than 40% of the world's population (about 2.8 billion people) lives in river basins with some form of water scarcity (United Nations, 2008). Northern Africa and Western Asia are seriously compromised, as are some regions within countries such as China, India, United States, Mexico, Australia, South Africa, Peru, Chile, and Argentina.

The fresh water provision through the time has become an important issue in many areas of the world, and it is expected to increase its importance in the future as the world's population and the global economy continues growing. The water shortage could be the cause of future conflict due to the fact that this affects the food security and human life.

1.2.2. Problem causes

Water scarcity may be explained by a diversity factors such as population growth population, developing of economic and social systems, accelerated urbanization, improvements in the standard of living, water pollution and climate change. Maybe, the most important factor is the increment of water consumption caused by the increment of population. Figure 6-3 shows the variation world's population between 1950 and 2011, and its projection up to 2050.

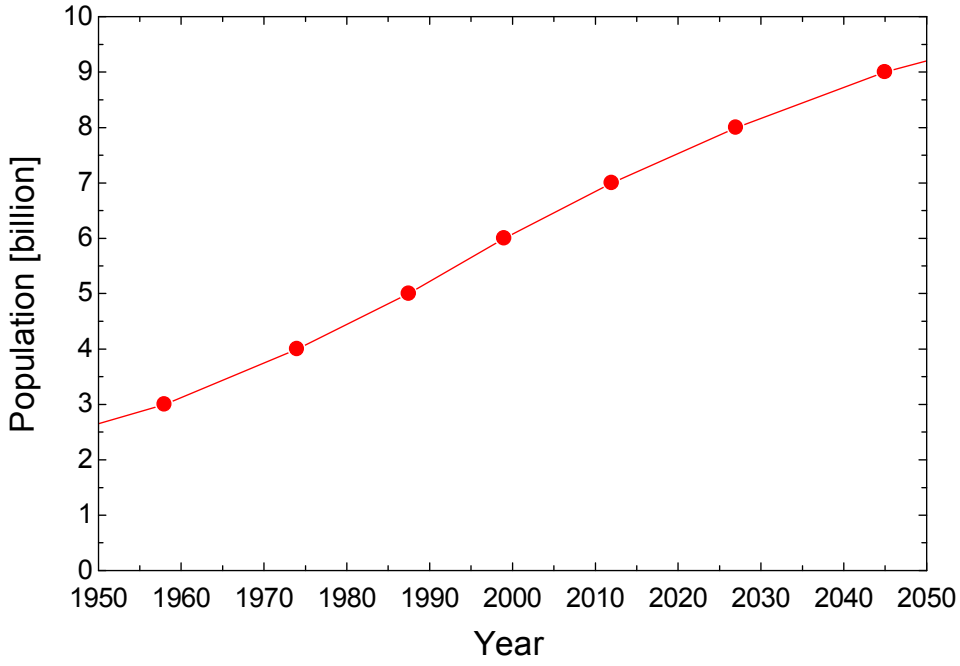

Figure 1 - 3 : World population variation between 1950 and 2050 (U.S Census Bureau, 2011)

The world's population has doubled over the past of 40 years achieving 7 billion in 2011, and it is projected to be 9 billion in 2050 (U.S Census Bureau, 2011). The growth of population can be expected to increase water shortages because the consumption is increased, but also more people will require more food increasing the agriculture activities that demand more water for irrigation. Additionally with the growing population, more services and products will be demanded increasing the global economy that required more industries and it means more water consumption for industrial processes. The other factor is the increment of urbanization and the improving of living standards that significantly increase water requirements for human consumption and its activities. Nowadays, the average per capita water consumption in urban China is about

200 liters per day and in rural areas is near to 70 liters per day (Cheng, Hu, & Zhao, 2009). If these water consumptions are compared with the fresh water consumption of a developed country as United State (380 liters), the potential of increment is high. In addition, in some places, there are problems of pollution of water sources (rivers and lakes) by industrial wastes and the large amounts of sewage discharged. Global climate change might be other big cause of water scarcity. The greenhouse effect is likely to increase the number of intense precipitation days and flood frequencies in northern latitudes and snowmelt-driven basins. Also, the frequency and severity of droughts could worsen as a result of a regional decrease in total rainfall.

1.2.3. Problem solutions

Water scarcity can be remedied applying several solutions: water conservation measures and water reuse, water reservoirs and water transfer, and desalination. Maybe, any of these measures is the solution for itself, but if they are applied together, the water shortage can be overcome.

1.2.3.1. Water Conservation and water reuse

Water use efficiency may be one of the most important strategies to preserve fresh water supply as the world's demand grows. Agricultural, household and industrial water uses have many opportunities to reduce their fresh water consumption. One example is in irrigation. Agriculture uses more than 70% of world's fresh water. Water shortages in important grain producing regions may seriously compromise agricultural production

potential. If some water saving irrigation technologies are implemented, reduction of fresh water in irrigation can be reduced to use between 30 and 70% less water than traditional methods and increases crop yield (Soteris A., 2005). In addition, it is possible to treat and purify water from industrial or municipal wastewater restoring water quality.

1.2.3.2. Water reservoirs and water transfer

Many countries suffer from a common problem: too much water in the wrong place and time. Unfortunately, in many places the distributions of population and economy do not coincide with that of the water resources. In these cases, inter-basin transfer (water transfer) plays a key role in supplying freshwater in huge quantities and balancing the unevenly distributed water resources. Water reservoirs are useful when regions suffer extreme climate alternating drought and flood periods, so water reservoirs and dams are effective to manage the water resources. China is a pioneer in both water transfer and water reservoir because they have the greatest number of large dams in the world and they plan to complete in 2050 a project that connect the four major rivers allowing adjustment and allocation of nearly 10% of the nation's surface water resources (Cheng et al., 2009). These kinds of projects involve many complex environmental impacts, which limit its application.

1.2.3.3. Desalination

Seawater desalination is a technology that offers the potential to alleviate the problem of fresh water shortage. The desalination technology is to clean or purify

seawater by removing the salt contained in it. Seawater has salinity in the range of 35,000 and 45,000 parts per million (ppm), and it is converted into fresh water that should contain as a maximum concentration of 500 ppm according to World Health Organization. Many cities in the world that face water scarcity are located in coastal areas (see figure 1-2). Desalination is an effective and important strategic approach to alleviate the shortage of water resources in coastal regions. For example, China plans to meet between 26 and 37% of the total water demand in the coastal cities by 2020 (Cheng et al., 2009). Currently, the installed capacity of desalination water systems in the world is over 60 million m^3/day, which is expected to increase drastically in the next decades. Figure 1-4 shows the evolution of the installed capacity of desalination water systems in the world since 1980 to 2010.

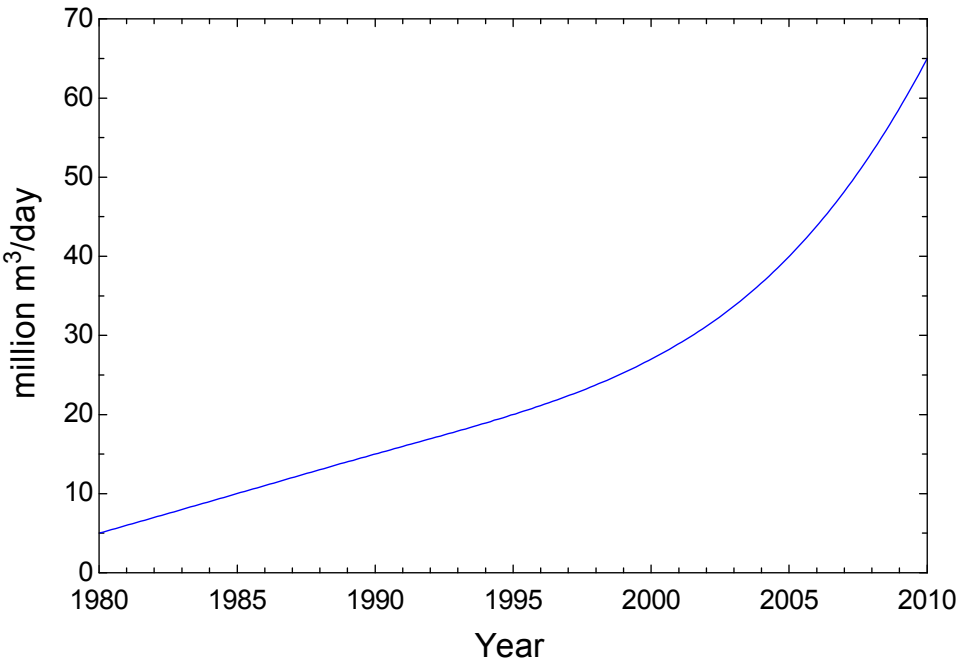

Figure 1 - 4 : Installed desalination capacity (Pankratz, 2010)

The dramatic increase of desalinated water supply will create a series of problems. The most significant of which are those related to energy consumption and environmental pollution caused by the use of fossil fuels. Given current understanding of the greenhouse effect and the importance of CO_2 levels, the use of oil as a primary energy source for desalination is debatable. Thus, apart from satisfying the additional energy demand, environmental pollution would be a major concern. If desalination is accomplished by conventional technology, then it will require burning of substantial quantities of fossil fuels. Given that conventional sources of energy are polluting, sources of energy that are not polluting will have to be developed.

1.3. Desalination driven by solar

The main drawback of desalination technologies are the high requirement of fossil fuels required (some technologies requires electricity, but it is produced from fossil fuels) and the pollution effect that they produce. Both problems can be overcome if desalination plants are driven by an energy source freely available in nature and friendly to the environment, which means renewable energies. Many places in the world are short of water, but some of them are located in coastal zones and have good level of solar radiation that could be used to drive desalination processes. Figure 1-5 shows the combination of the stress on world's river basin map with zones that present of high solar radiation.

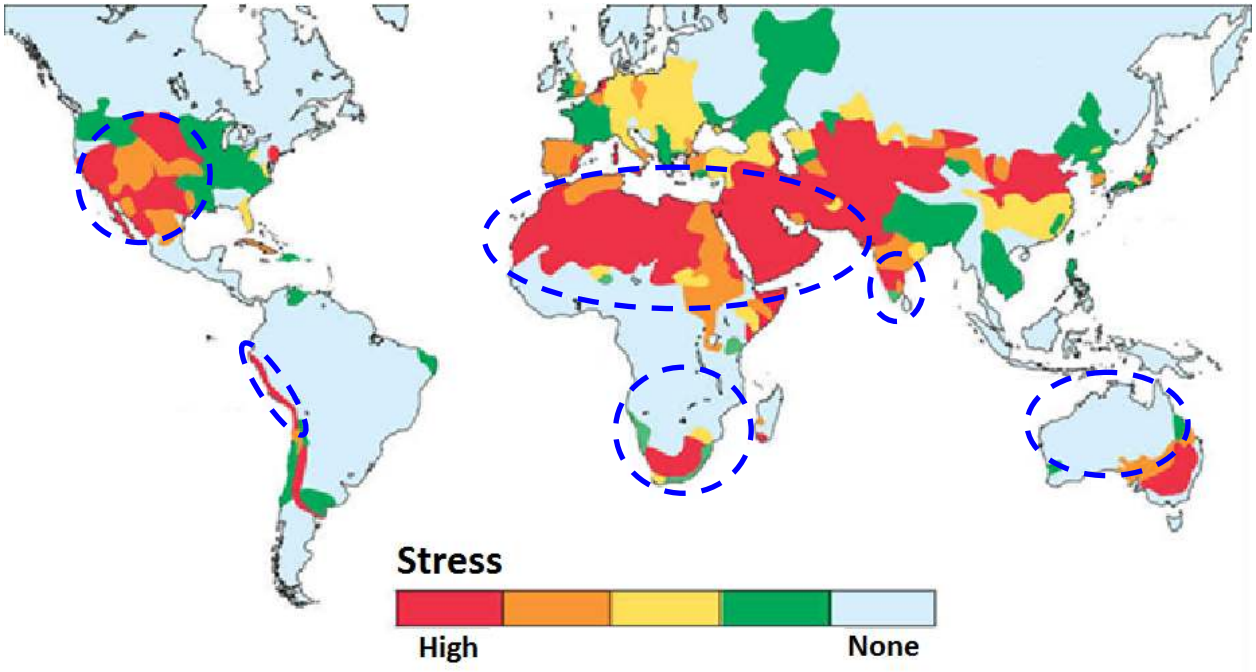

Figure 1 - 5 : Stress on World's River Basins Map combines with zones of high solar radiation (Revenga et al., 2000) **and** (Meteonorm, 2011)

Many regions simultaneously suffer shortage of water and receive high solar radiation such as the west cost of United States and Mexico, north of Chile and Peru, north and south of Africa, Arab countries, and some areas of India and Australia. If it is taken advantages of this simultaneity, solar energy has strong potential to drive seawater desalination processes.

1.4. Conclusions

Water scarcity can be remedied by the means of water conservation measures and water reuse, water reservoirs and water transfer, and desalination. The only option really

that increases the amount of fresh water is desalination, which permit a sustainable fresh water supply. However, conventional desalination technologies face a big drawback because they are intensive fossil fuel systems that cause environmental hazards. In many places where there are abundant seawater resources and a good level of solar radiation, production of fresh water using desalination technologies driven by solar energy systems is thought to be a viable solution to the water scarcity. Although everybody recognizes the strong potential of solar thermal energy to seawater desalination, the process is not yet developed at commercial level.

1.5. Objectives

The objectives of this work may be stated into the following points:

- Study different seawater desalination technologies.
- Compare different conventional seawater desalinization technologies operated with electrical energy with desalination technologies operated using directly fossil fuels (thermal energy). The analysis will include comparative energy performance and fresh water yield.
- Study and model the most promising technology for use with thermal solar energy.
- Model a solar steam generation plant using parabolic trough solar collectors.
- Study the interaction of both desalination and solar steam generation models working together. The analysis will include the portion of the total energy that is provided from solar energy as a function the size of the solar field.

Chapter 2 : Review desalination technologies

2.1. Introduction

Desalination is a process of removing dissolved minerals (principally, salt) from seawater or brackish water. Seawater or brackish water desalination is generally performed either by evaporation or by filtration. Evaporation is a thermal process, which uses a heat source such as conventional fossil fuel, nuclear energy, solar energy, or geothermal energy to distillate seawater. In the evaporation process, pure water is vaporized leaving behind the dissolved solids in solution. Subsequent condensing of the pure vapor yields salt-free or fresh water. In effect, this is a distillation process. The filtration method approach uses a reverse-osmosis process whereby the salt solution is pressurized and applied to one side of a membrane. The membrane allows pure water to pass while holding back the concentrated salt water (Borsani & Rebagliati, 2005).

The most important desalination processes driven by thermal energy are multi-stage flash (MSF), and multi-effect distillation (MED). The electrical driven desalination process are reverse osmosis (RO) and electrodialysis (ED). Figure 2-1 shows the distribution of the total worldwide installed capacity by technology. MSF process represents about 80% of the thermal desalination processes (26.8% of world capacity) while RO processes about 95% of membrane processes for fresh water production (60% of world capacity).

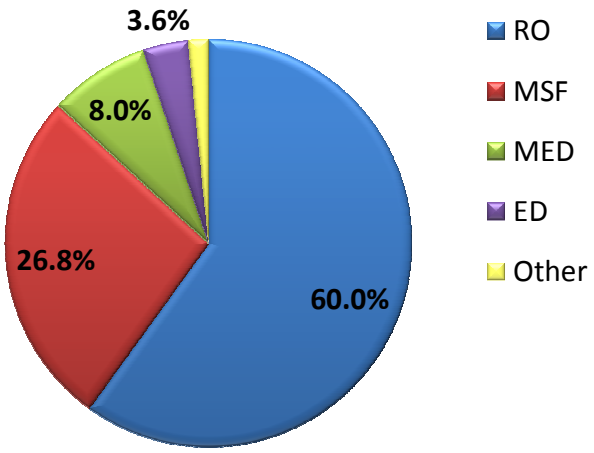

Figure 2 - 1 : Desalination Technologies (Pankratz, 2010)

2.2. Energy requirement

The minimum energy requirement to desalinate can be calculated assuming an isothermal and reversible process to separate salt from seawater and produce fresh water. The first and second law balances applied to a system that receives seawater and releases fresh water and brine are presented on equations 2.1 and 2.2.

$$\Delta \dot{H} + \dot{W} - \dot{Q} = 0 \tag{2.1}$$

$$\Delta \dot{S} - \frac{\dot{Q}}{T} = \dot{S}_{gen} \tag{2.2}$$

If the process is assumed reversible, $\dot{S}_{gen} = 0$.

Substituting equation 2.2 into 2.1 leads to:

$$-\dot{W} = \Delta\dot{H} - T\,\Delta\dot{S} = \Delta\dot{G} \tag{2.3}$$

Consequently, the minimum energy requirement to desalinate is defined as:

$$-\dot{W} = \dot{G}_{fw} + \dot{G}_{b} - \dot{G}_{sw} \tag{2.4}$$

where subscripts fw, b, and sw refer to fresh water, brine, and seawater, respectively. Assuming a seawater salinity of 35 g/kg, the same inlet and outlet temperature (25 °C), and recovery ratio (ratio of fresh water mass flow rate and seawater mass flow rate) of 50% the minimum specific energy consumption (SEC) to produce one cubic meter of fresh water is 1.09 kWh/m^3. Figure 2.2 show the minimum SEC to desalinate seawater with a salinity of 35 g/kg as a function of recovery ratio, where recovery ratio is the ratio of fresh water produced to brine refused.

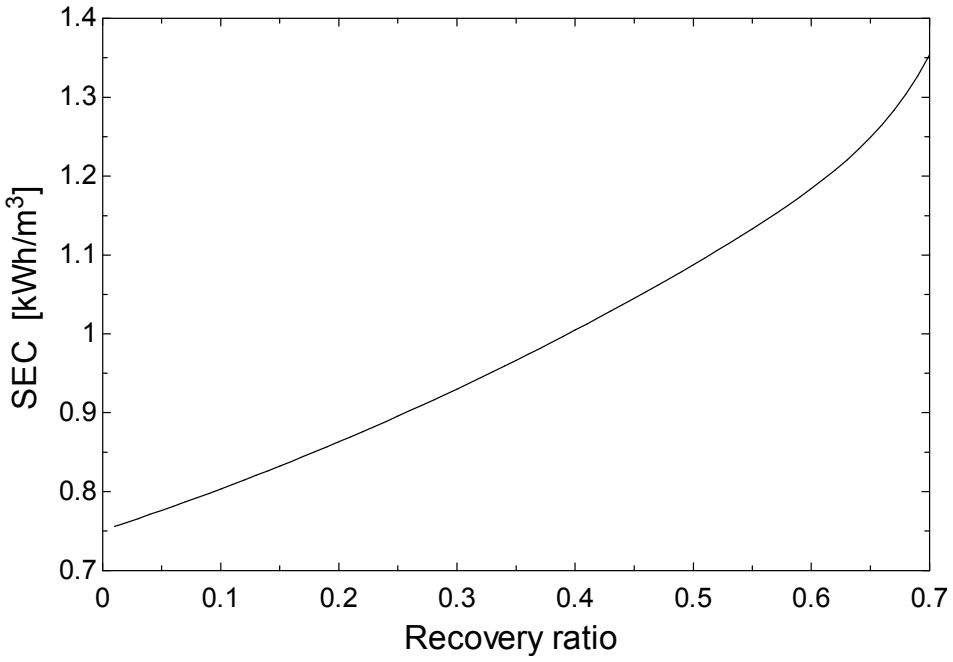

Figure 2 - 2 : Minimum energy requirement to desalinate

The energy required in distillation-based separation processes is virtually independent of concentration of dissolved solids in feed water. However, the energy required in membrane processes depends on salt concentration of seawater (Miller, 2003). The simplest distillation technique, single-stage evaporation of seawater, consumes a large amount of thermal energy, around 650 kWh/m^3 of fresh water. However, by recycling the latent heat of vaporization repeatedly, the energy intensity of thermal distillation becomes competitive. Field applications of both MSF and MED utilize multiple stages to increase desalination performance. The efficacy of heat recycling in distillation is expressed in terms of the performance ratio (PR) or gained output ratio (GOR). GOR and PR are related with the number of units of distillate, stages

in a MSF and effects in a MED. When the number of units of distillate increases, GOR and PR also increase because the distillation process is more efficient.

Generally, the efficiency of a desalination plant based on distillation is defined in terms of consumed of thermal energy. There are two main definitions to present this efficiency: gain output ratio (GOR) and performance ratio (PR).Gain output ratio (GOR) is defined as the ratio between the distillate output and the steam supplied, both in mass units.

$$GOR = \frac{kg\ of\ fresh\ water}{kg\ of\ steam} \tag{2.5}$$

GOR does not take into account the effects of steam enthalpy difference, the quality of steam supplied (temperature and pressure), and pumping work (Narayan et al., 2010). Performance ratio (PR) represents the amount of fresh water produced by condensing one kilogram of steam at an average temperature corresponding to 2330 kJ/kg latent heat.

$$PR\ [{}^{kg}/_{kJ}] = \frac{kg\ of\ fresh\ water}{kg\ of\ steam \cdot 2330\ [kJ/kg]} \tag{2.6}$$

PR takes into account the enthalpy drop of the supplied steam, but it does not account the pumping work (Narayan et al., 2010).

2.3. Desalination processes

2.3.1. Multi stage flash (MSF)

MSF is a desalination technology that evaporates seawater due to successive reductions in pressure of heated seawater resulting flashing at each stage of pressure reduction. The process begins by heating seawater and then injecting the hot seawater in a vessel under low-pressure conditions. As the seawater flows from higher to lower pressure, a portion of the seawater flashes to a vapor leaving behind the dissolved solids. This isenthalpic process results in a temperature reduction for both the vapor and remaining liquid to the saturation temperature corresponding to the vessel's lower pressure. A schematic multi-stage flash distillation plant is shown in Figure 2-3.

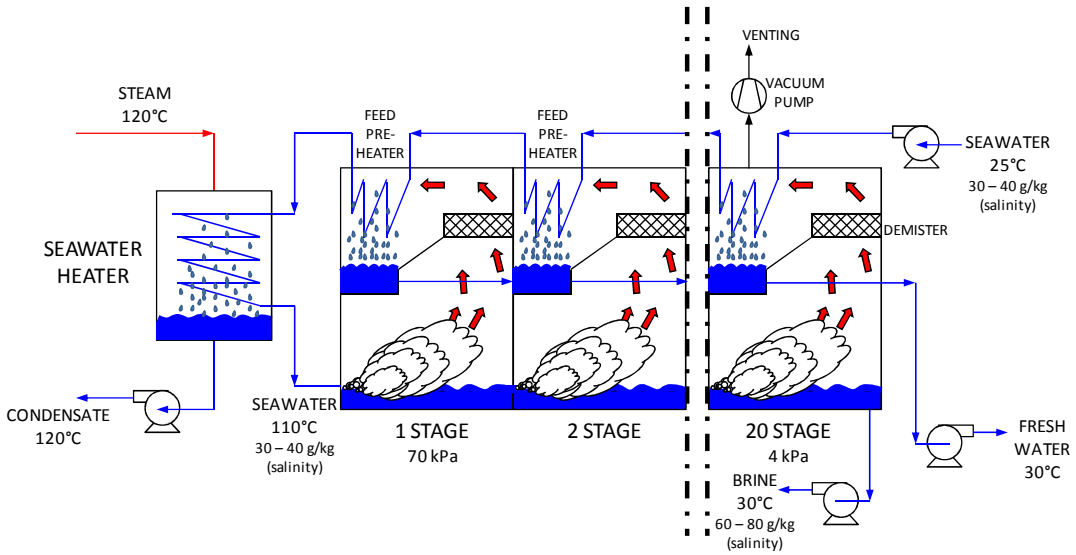

Figure 2 - 3 : Schematic diagram of a multi-stage flash distillation plant (Pankratz & Tonner, 2003)

Before seawater enters to MSF, it is pre-treated by adding some chemicals to avoid scale and corrosion. The incoming cold seawater is pre-heated in cascade in each stage by the outgoing stream when vapor distillate is condensing and cooling to fresh water. In the seawater heater, pre-heated seawater is heated to 90 – 120°C. Even though high seawater temperatures increases the MSF performance, it also accelerates corrosion and scaling. The highest seawater temperature limitation is about 120°C due to risks of scale and corrosion (Pankratz & Tonner, 2003). The heat is supplied by low-pressure saturated steam (200 – 300 kPa) from a boiler, a cogeneration plant, or solar thermal. Heat supplied by cogeneration is either by using a heat recovery steam generator or by steam turbine extraction or by backpressure turbine. In the first stage, the heated seawater is flashed in a vessel under low-pressure conditions (pressure below to the corresponding saturation temperature generally 70 – 90 kPa), where partial evaporation occurs. The evaporated fraction of seawater condenses when it comes in contact with the cooler feed seawater pipe while the incoming seawater is preheated. The mass outlet streams of the first stage are fresh water and brine. The brine goes to the next stage where it is flashed. The pressure in this stage is lower than the preceding stage. The results in this stage are similar to the previous stages. The vacuum in each stage is established and maintained by a venting system driving by a vacuum pump or by a steam jet ejector (Khawaji, Kutubkhanah, & Wie, 2008). The fresh water produced in a MSF plant contains about 2 to 10 ppm of dissolved solids (Khawaji et al., 2008). The fresh water is not completely pure because a lower portion of seawater is carried by the steam and passes through the demisters.

The thermal performance of these systems is proportional to the number of stages, with capital cost limiting the number of stages to be used (Borsani & Rebagliati, 2005). The number of stage of these plants varies between 20 and 30 stages. MSF manufacturers provide a GOR design in the range of 8 – 12, depending on the steam feed temperature (R. Semiat, 2008). Thermal energy based on fuel consumption is in the range of 55 – 80 kWh/m^3 of product (R. Semiat, 2008). Pumping energy is around 1.2 – 4.5 kWh/m^3 (R. Semiat, 2008). Energy consumption of MSF may be reduced considerably when MSF is coupled with a power plant (cogeneration) using steam from a turbine extraction or from a backpressure turbine to provide the primary thermal energy required for MSF. The thermal energy consumption on this condition is around 4 – 7 kWh/m^3 and the pumping energy is similar to one purpose plants (R. Semiat, 2008).

Existing MSF plants typically have capacities ranging from 100,000 to 880,000 m^3/day (Shoaiba 3). The production cost of fresh water in a dual-purpose plant (cogeneration) varies between 0.52 and 1.75 $\$/m^3$ of fresh water yield (Karagiannis & Soldatos, 2008). It includes energy costs, operation and maintenance costs, and plant investment. Figure 2-4 shows the cost breakdown for MSF desalination of water.

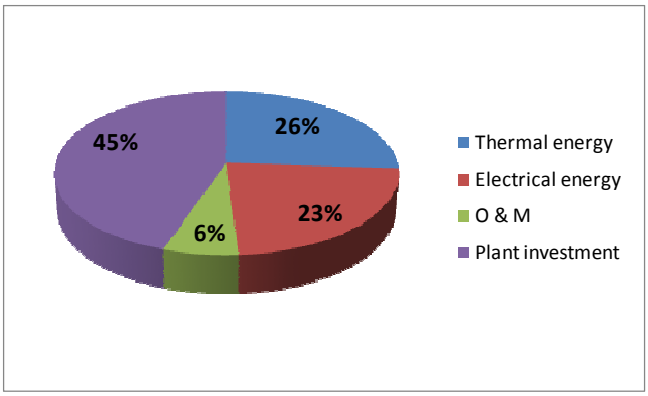

Figure 2 - 4 : Cost breakdown for MSF desalination of water in a dual-purpose plant (Borsani & Rebagliati, 2005)

The main advantage of MSF is the reduction of the effects of scaling on heat transfer surfaces by eliminating boiling (Khawaji et al., 2008), The lower scale formation is controlled by including high temperature additives and continuously rejecting a blowdown stream to avoid overconcentration (Khawaji et al., 2008). One of the drawbacks of this technology is the presence of brine in the vapor stream of certain stages that affects purity of the fresh water. The presence of brine may be diminished installing demisters, or by using effective antifoam agents to reduce foam levels and allow sufficient disengagement height, before the demisters (Khawaji et al., 2008). Another drawback is the accumulation of non-condensable gases at the condenser zone. For this reason, non-condensable gases are evacuated continuously by the venting system.

2.3.2. Multi effect distillation (MED)

MED is a desalination technology that evaporates seawater by two phenomena. First, a portion of the incoming brine (or seawater) is initially flashed to a vapor upon throttling into downstream stages due to the pressure difference between the brine (or seawater) and the main chamber of the downstream desalination stage. An additional contribution to the production of fresh water vapor is generated by boiling of brine due to heat addition from higher temperature fresh water vapor condensing from the upstream stage. This process takes place in several evaporators (effects), and each effect has a lower pressure than the preceding effect. All the system operates with a pressure lower than the atmospheric pressure (Khawaji et al., 2008). A schematic MED is shown in Figure 2-5.

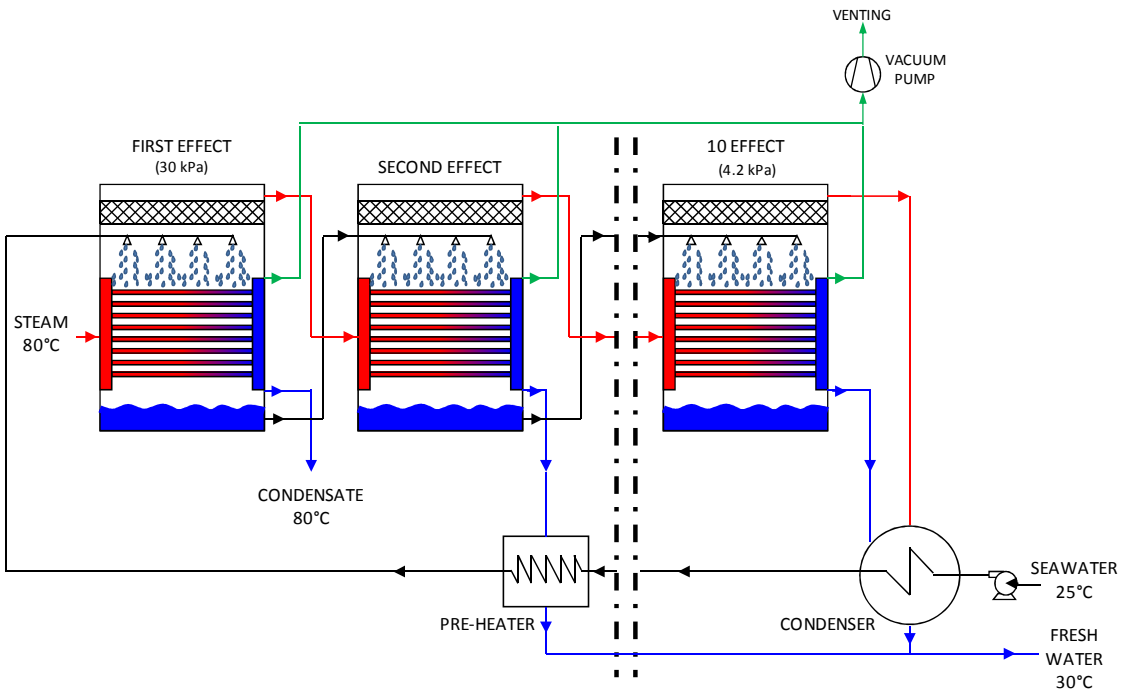

Figure 2 - 5 : Schematic MED (Pankratz & Tonner, 2003)

The incoming seawater is pre-heated in the condenser and by the pre-heaters from intermediate stages before entering to the first effect. In the first effect, external thermal energy (steam or hot water) is added to distill fresh water from incoming seawater. The first effect operates with a temperature (or top brine temperature) of about 70°C (Khawaji et al., 2008). Consequently, a portion of the incoming seawater is vaporized, and water vapor is generated. This water vapor is the incoming stream thermal energy source in the downstream effect. The concentrated brine portion of the first effect is directed to the chamber of the second effect where it is throttling. A portion of the incoming brine stream is flashed to vapor upon entering the evaporator chamber due to the fact that this effect operates at a lower pressure than the previous effect. The remaining portion of the brine falls to the bottom of the chamber while it absorbs additional heat from the higher temperature freshwater that is condensing within tubes. As the brine absorbs heat from the condensing water vapor, more water (fresh water) vapor is produced. The repetition of the processes several times, multiplying the effectiveness of the primary external thermal energy supplied. The secondary steam generated in the last effect passed to a steam condenser. A vacuum pump or a steam ejector is used to maintain gradual pressure difference in effects and to remove non-condensable gases. The condensate is collected as the product water. The fresh water produced in a MED has a similar quality than produce in MSF (Khawaji et al., 2008).

The thermal performance of this plant increases with the number of the effects. The typical number of effects varies between 4 and 16 effects and the total range of

temperature limits this number (Khawaji et al., 2008). MED manufacturers claim a GOR of 10 – 16 in working units and up to 30 in designed prototypes (R. Semiat, 2008). Thermal energy based on fuel consumption in typical single-purpose plants is in the range of 40 – 65 kWh/m^3 of fresh water (R. Semiat, 2008). Pumping energy is about 0.5 kWh/m^3. Similar to MSF, energy consumption of thermal desalination processes may be reduced considerably in dual-purpose plants (cogeneration). Thermal energy is reduced up to around 4 – 7 kWh/m^3, similar to MSF (R. Semiat, 2008). Pumping energy is maintained at approximately 0.5 kWh/m3.

MED production cost in a dual-purpose plant varies between 0.95 and 1.95 $/m3 of fresh water for medium plants and between 0.52 and 1.01 $/$m^3$ for large plants (Karagiannis & Soldatos, 2008). It includes energy costs, operation and maintenance costs, and plant investment. Figure 2-6 shows the cost breakdown for MED desalination of water.

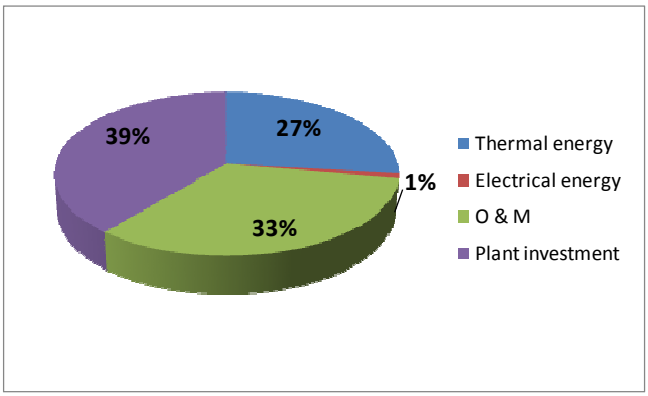

Figure 2 - 6 : Cost breakdown for MED desalination of water in a dual-purpose plant (Miller, 2003)

A drawback of this system is the accumulation of non condensable gases in the condensing zone. This phenomenon reduces the heat transfer. The elimination of these non condensable gases can be accomplished using a venting system. If this venting is excessive part of the vapor is lost, and the efficiency of this system is reduced (Leblanc, Andrews, & Akbarzadeh, 2010). In addition, this technology operates at low temperature because of the necessity of boiling, which increases the risk of scale formation and corrosion, but it means that is necessary to increase the heat transfer area of equipment (Khawaji et al., 2008).

2.3.3. Reverse Osmosis (RO)

Reverse osmosis is the process where pressurized seawater is separated by membranes to produce fresh water and concentrated saline solution. The membranes are polymers that block salt transport but permit water transport because of a pressure difference across the membrane. In order to achieve this separation, a high pressure between 55 and 65 bar is required (Fritzmann, Löwenberg, Wintgens, & Melin, 2007).

The osmosis phenomenon occurs when a semi permeable membrane separates two liquids with different concentration. At the same temperature and pressure, water flows from low concentration to high concentration across a permeable membrane to achieve same conditions in both sides (Figure 2-7 a). If pressure is applied to high concentration liquid, the flow can be stopped (Figure 2-7 b). The pressure required to stop the flow is directly proportional to the solution concentration and is called osmotic pressure. When the applied pressure is greater than the osmotic pressure, the flow occurs

in the other direction, resulting in water flowing from the concentrate to dilute side; this phenomenon is called reverse osmosis (Figure 2-7 c) (Fritzmann et al., 2007). Part of feed water is released without passing through the membrane, but with increased concentration of salt. The discharge of water is about 35-100% of outgoing fresh water.

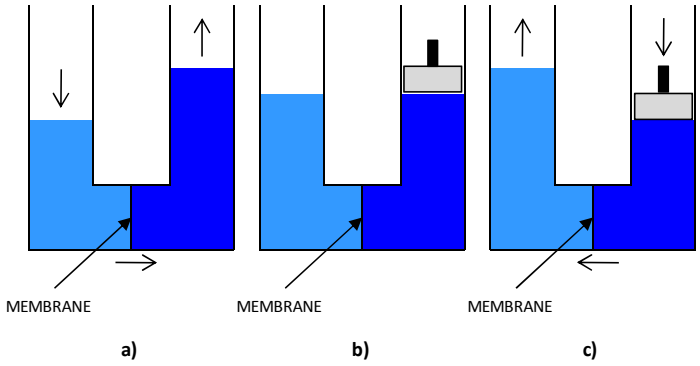

Figure 2 - 7 : Reverse osmosis phenomenon (Pankratz & Tonner, 2003)

Figure 2.8 shows a schematic diagram of a reverse osmosis plant.

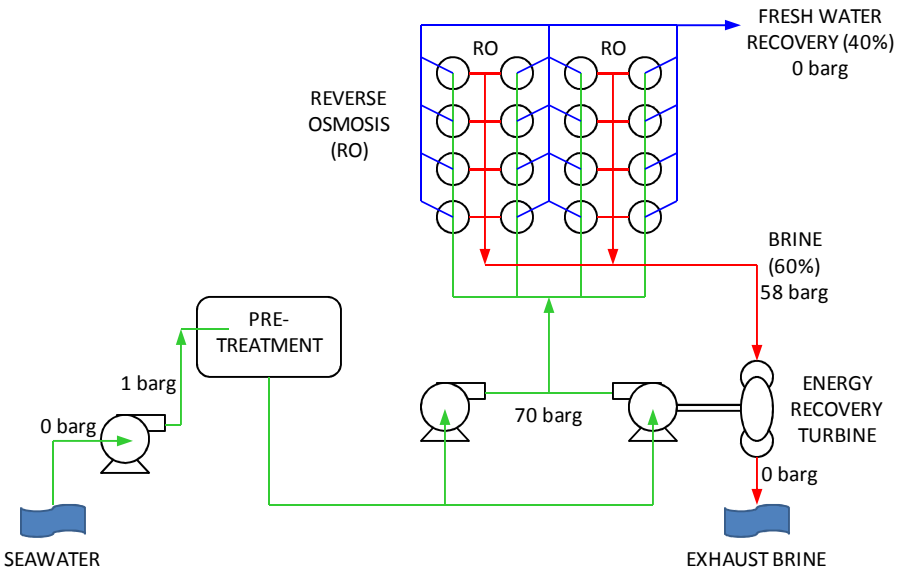

Figure 2 - 8 : Schematic diagram of a reverse osmosis plant (Pankratz & Tonner, 2003)

Pre-treatment consists in adjusting the inlet water composition, removing particular matter and adding chemicals to avoid scaling and fouling, and to adjust the pH-value (Fritzmann et al., 2007). RO membranes are sensitive to feed seawater conditions. For example, pH, oxidizers, a wide range of organics such as algae, bacteria, particulates and other foulants (Fritzmann et al., 2007).

The energy requirements of a reverse osmosis system are due to intake system, pumping system, pre-treatment operation, and (most important) to high-pressure pumps (84% of total energy consumption). The major energy input for RO desalination is for pressurizing the incoming seawater. Two improvements have aided in reducing the energy consumption of this technology. First is the development of membranes that can

operate efficiently with lower pressure and the second is the use of energy recovery devices (Al-Karaghouli, Renne, & Kazmerski, 2009). An energy recovery system permits the use high pressure from brine to supply high pressure on the feed. There are two types of these units. One is a Pelton turbine, which drives a feed pump using the high pressure of brine with efficiencies of up to 90% (Fritzmann et al., 2007). The other system is a pressure exchange, which directly transfers pressure from brine to the feed. A duct is filled with feed water, and a valve is closed while the other side of the duct is filled with brine water pressuring feed water. Pressured feed water is then introduced to the system. The efficiency of this last technology is about 96-98% (Fritzmann et al., 2007). Energy recovery in reverse osmosis, which drives seawater, is reaching 60%.

The energy consumption in seawater reverse osmosis plants is approximately 3–6 kWh/m^3 without energy recovery (Khawaji et al., 2008) and about 1.9 – 2.5 kWh/m^3 with energy recovery (Fritzmann et al., 2007). It is important to note that energy consumption for small RO plants may increase due to lower efficiency of smaller pumps. The desalination water produced in a RO plant contains about 300 ppm dissolved solids (Vyas, 2003).

Water production cost for reverse osmosis plant are about 0.48 to 1.62 $/m3 for medium plants and between 0.45 and 0.66 $/m3 for large plants (Karagiannis & Soldatos, 2008). It includes energy costs, operation and maintenance costs, and plant investment. Figure 2-9 shows the cost breakdown for RO desalination of water.

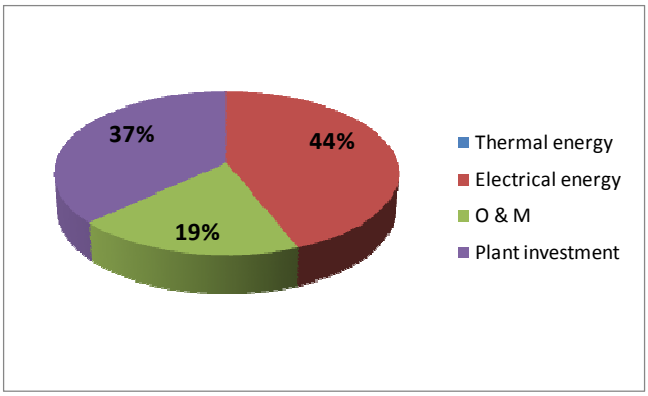

Figure 2 - 9 : Cost breakdown for RO desalination of water (Miller, 2003)

2.3.4. Electrodialysis (ED)

Electrodialysis is a desalination technology, which is used for desalination of brackish water. An electric field removes salt ions from the brackish water. Brackish water passes between pairs of cation-exchange (CEM) and anion-exchange membranes (CEM). Cations (K+, Na+) moves from the brackish water towards the negative electrode passing through the cation exchange membranes those allow only cations to pass. Moreover, anions such as Cl- and NO3- are attracted to the anode, and they pass through the anion exchange membranes (Al-Karaghouli et al., 2009).

In an ED plant, the cation exchange and anion-exchange membranes are alternate to provide anion and cation exchanges in alternating sequences. There are a large number of membranes stacked together. Brackish water passes by flow spacers, which separate the membranes. The streams in flow spacers alternate in a sequence of diluted and concentrated water flowing in parallel to each other. To prevent scaling, the process

utilizes inverters, which reverse the polarity of the electric field about every 20 minutes. Figure 2-10 shows a schematic diagram of an electrodialysis cell.

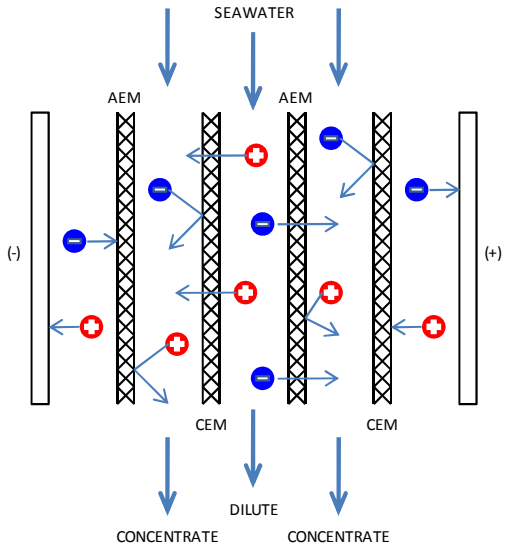

Figure 2 - 10 : Schematic diagram of an electrodialysis cell

Electrodialysis presents advantages when it is managed to have a low ion concentration. Consequently, this technology is used to desalinate brackish water with total dissolved solid (TDS) levels of up to 4,000 to 5,000 g/kg (Al-Karaghouli et al., 2009), and it is not useful to desalinate seawater.

2.3.5. Vapor-compression distillation

They are two versions of this technology. One is called mechanical vapor-compression (MVC) and another is named thermal vapor-compression or thermo compressor (TVC) (Al-Karaghouli et al., 2009). Vapor compression is used in small and

medium applications. MVC is used in the range of 20 – 4,000 m^3/day, and TVC may range in size up to 20,000 m^3/day. This technology evaporates seawater using the heat from the compression of vapor. The main idea is to take advantage of reducing the boiling point by reducing the pressure in the vessel where the seawater is contained (Al-Karaghouli et al., 2009). The feed water is heated to a temperature above the saturation temperature maintained in the evaporator by the outgoing brine and fresh water produced in a heat exchanger. The evaporator has an operating temperature of about 64 - 70°C. The heated feed water then is flashed into the evaporator. The vapor generated by flashing and by heat addition in the evaporator is compressed, either mechanically (compressor) or thermally (steam ejector). This compressed superheated vapor is then used as a heat source for evaporation of brine in the evaporator obtaining and additional portion of vapor. The vapor produced in the evaporator is always superheated due to the boiling point elevation. Figure 2-11 shows a schematic diagram of a mechanical vapor-compression system.

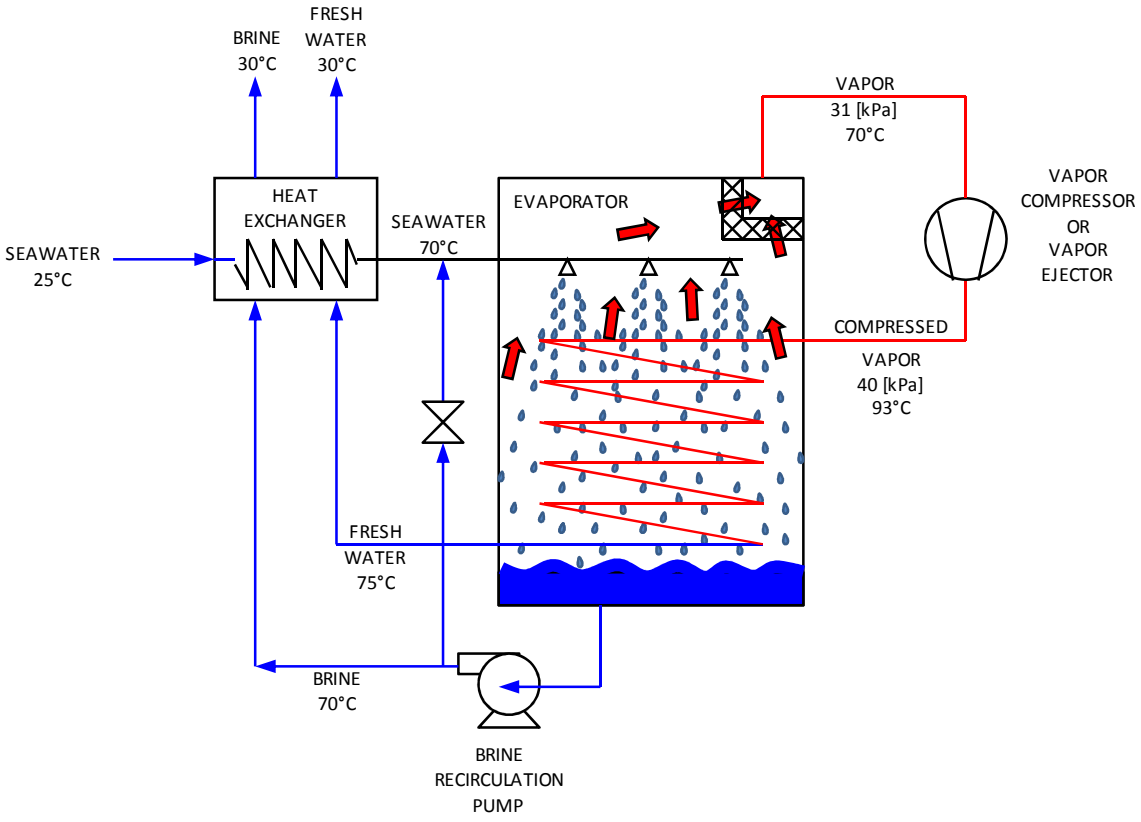

Figure 2 - 11 : Schematic diagram of a mechanical vapor-compression system

The specific power consumption of electrical energy in MVC plants varies in the range of 6 - 8 kWh/m^3 and the water production costs are about 2.0 – 2.6 US$ /m^3 for fresh water production of about 1,000 and 1,200 m^3/day (Karagiannis & Soldatos, 2008). Generally, TVC are combined with a conventional MED. It increases the MED performance. The thermo-compressor recycles low-pressure water vapor generally from the MED last effect by the means to inject high-pressure steam into an ejector avoiding releasing the heat in the condenser and reusing as heat source in the first effect. The recycled heat is used as energy source in the first effect (Pankratz & Tonner, 2003).

2.4. Desalination processes using solar energy

Solar energy can be used for seawater desalination in the following ways: 1) Solar collectors can provide by the thermal energy required by conventional distillation processes; 2) using photovoltaic cells or other methods, solar energy can provide the electricity required to drive membrane processes; or 3) solar energy can directly power some desalination technologies such as solar stills and humidification-dehumidification desalination.

2.4.1. Solar stills.

Solar stills use the greenhouse effect to evaporate seawater. The still consists of a basin (Figure 2-12), in which a constant amount of seawater is enclosed in a veeshaped glass envelope. The sun's rays pass through the glass roof and are absorbed by the blackened bottom of the basin. As the water is heated, its vapor pressure is increased. The resultant water vapor is condensed on the underside of the roof and runs down into troughs, which conduct the distilled water to the reservoir. The still acts as a heat trap because the roof is transparent to the incoming sunlight, but it is opaque to the infrared radiation emitted by the hot water (greenhouse effect). The roof encloses all of the vapor, prevents losses and, at the same time, keeps the wind from reaching the salty water and cooling it.

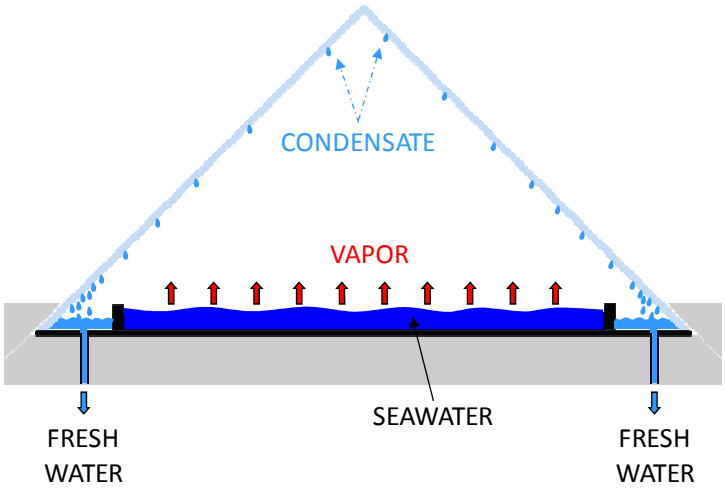

Figure 2 - 12 : Schematic diagram of solar still

This technology has low performance in comparison with other desalination technologies, only 45% of energy received is used to desalinate seawater. The energy consumption rate is about 1,300 kWh/m3 of fresh water. The water production of these of solar stills is about 4 - 6 kg/m^2-day (Al-Karaghouli et al., 2009). However, the initial cost of the still may be lower than alternative technologies. The solar still performance can be improved if the water temperature in the basin is increased, due to higher evaporation and condensation rates. In addition, the production can be raised if an additional source (solar collector) of thermal energy is added (Sampathkumar, Arjunan, Pitchandi, & Senthilkumar, 2010). This solar desalination system is considered as promising device for remote regions that do not have connection to the electrical grid (Al-Karaghouli et al., 2009).

2.4.2. Humidification dehumidification desalination (HDH)

HDH is a desalination process that tries to imitate the natural water cycle (Narayan et al., 2010). In the natural process, seawater is heated by solar irradiation, and it humidifies the air. The air acts as a carrier gas rising and forming clouds. Finally, clouds dehumidify as rain. This kind of plant is formed by three systems as shown in Figure 2-13 (Narayan et al., 2010): water heater (or air heater), evaporator or humidifier, and condenser or dehumidifier. The heat source could be fossil fuel, solar, geothermal or combinations of these i.e., hybrid systems.

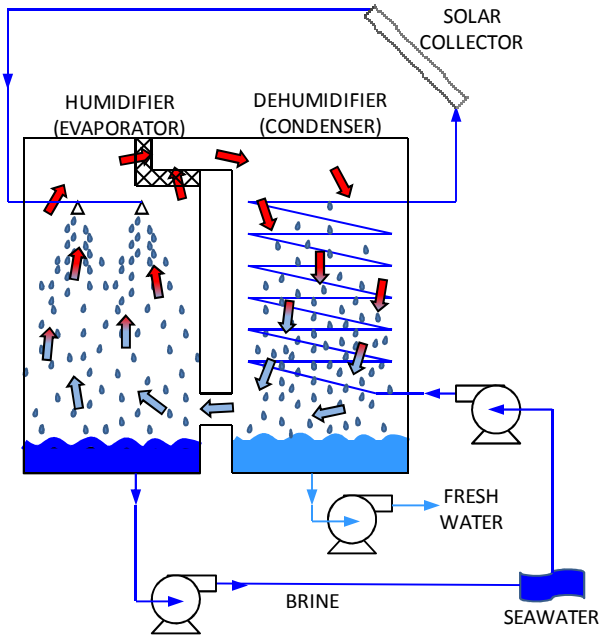

Figure 2 - 13 : Schematic diagram of a humidification dehumidification desalination plant (Narayan et al., 2010)

In the humidifier, air is wetted by hot water being humidified and heated using the energy from the hot water. The humidified air is directed to the dehumidifier where it is cooled by seawater (cold stream) in a heat exchanger. Seawater is preheated in the dehumidifier and is further heated in a solar collector before it is sprayed into the humidifier, The air is then circulated back from the dehumidifier to the humidifier.

This cycle operates under atmospheric conditions, and this system can operate in an open and a close cycle. This technology presents an advantage because it permits to use of low grade energy, specially from renewable sources. The specific fresh water production per collector area was found to be between 4 and 12 kilogram per square meter of solar collector per day. The energy consumption rate is about 140 to 550 kWh/m^3 of fresh water (Narayan et al., 2010).

2.5. Comparison between conventional desalination technologies

Both RO and ED are useful for brackish water desalination; however, RO is also competitive to performance seawater desalination [9]. The energy requirement for RO are highly dependent of salt concentration of seawater. ED can be only economically used to brackish water [11]. For this reason, ED is not taking into account in this comparative analysis.

Both distillation processes are more competitive to desalinate seawater than brackish due to the fact that they always produce distillate of high purity regardless the

quality of feed water. Also, their energy requirements are virtually independent of salt concentration.

The summary of conventional desalination technology is compiled from a number of sources and is presented in Table 2-1.

Table 2 - 1 : Summary of conventional desalination technology

	MSF	MED	RO
Seawater quality	not critical	not critical	critical, require specific pre-treatment
Distillate quality (ppm TDS)	1 -10 ppm	1 -10 ppm	300 ppm
Thermal energy (kWh/m^3)	55 - 80 .@ 120 °C	40 - 65 @ 70 °C	
Electrical energy (kWh/m^3)	1.2 - 4.5	0.5	3.0 - 6.0
Primary energy (kWh/m^3) (*) (**)	68 - 107	48 - 78	8.5 - 17
Maintenance cost	low	low	medium

Notes:
(*) It was assumed
(**) It was assumed

When the energy consumption of each technology is compared referring to primary energy, it is clear that MSF uses the most energy. It is followed by MED and by RO. It is clear that MED is the best distillation process because it requires about 40% less energy than MSF. Even though RO uses lower energy than MED, MED plants are competitive when they use low grade energy such as waste heat or solar or geothermal.

RO uses electrical energy, and its conversion from thermal technology depends in the technology that is used to convert it. It is assumed an efficiency of conversion of 35%. Table 2-2 shows the typical desalination costs for conventional technologies. It includes energy costs (thermal and electrical), operation and maintenance costs, and plant investment.

Table 2 - 2 : Desalination costs conventional technologies (Karagiannis & Soldatos, 2008)**.**

Size of plant (m^3/day)	**MSF**	**MED**	**RO**
Medium Plants (15,000 - 60,000)	0.52 - 1.75	0.95 - 1.95	0.48 - 1.62
Large Plants (> 100,000)	0.52 - 1.75	0.52 - 1.01	0.45 - 0.66

The desalination cost varies widely and depends of a number of factors such as energy prices, feed seawater conditions, environmental requirements, availability of waste heat, and location. For example, RO desalination cost depends highly of seawater feed conditions. When the feed stream contains potential foulants such as particulate, biological components, and scale formers, the pretreatment costs increases dramatically. This is the case of Mid-Eastern countries where thermal distillation is preferred over RO because of feed seawater conditions (high salinity and high temperature). Finally, the water quality provided by thermal desalination plant has high quality (less than 10 ppm) than RO (about 300 ppm).

2.6. Conclusions

Seawater desalination can be performance using solar energy by means providing thermal energy to conventional distillation processes (MSF or MED), or producing electricity required to drive RO, or driving solar stills or humidification-dehumidification desalination systems. The most suitable technologies to desalinate on a large scale are RO and MED. MED is the most efficient distillation process, and RO has the lower energy consumption. Also, MED requires a energy source of low grade (70 - 80°C), which means that it could work with waste heat, solar or geothermal energy. For small scale 1 – 100 m^3/day applications (Narayan et al., 2010), RO, MED and solar desalination technologies are suitable. HDH is the most efficient solar desalination technology, and it could be the best option when the applications is located in an isolated place where there is not a continuous supply of electrical energy (Narayan et al., 2010). However, HDH has worse performance than RO and MED. Finally, in both cases, small and large scale, the most suitable technology using thermal solar energy is MED and RO to use PV.

Chapter 3 : Multi-effect desalination (MED) and Multi-effect desalination with thermal vapor compression (MED-TC)

3.1. Introduction

As explained in Chapter 2, a multi-effect desalination plant (MED) is formed by a sequence of evaporators (effects) as shown in Figure 3-1. Incoming seawater is pre-heated in the condenser and by a series of pre-heaters from each of the intermediate stages before entering the first effect of the plant. In the first effect, external thermal energy (steam or hot water) is added to thermally separate (distill) fresh water from incoming seawater; consequently, a portion of the incoming seawater is vaporized and a stream of pure water vapor is produced. The heat provided when water vapor produced in one effect is recovered by condensing in a heat exchanger known as a pre-heater which warms incoming sea water. The water vapor generated in the *evaporator* is slightly superheated due to the boiling point elevation of the brine relative to pure water. The concentrated brine portion of the first effect is directed to the chamber of the second effect where it is throttled to the lower pressure of the second effect. A portion of the incoming brine stream flashes to a vapor upon entering the evaporator chamber because of its lower pressure operation. In addition, feed seawater at saturated conditions enters in each effect. The incoming seawater is sprayed over the condenser tubes and falls to the bottom of the chamber as it absorbs heat from the higher temperature freshwater that is condensing within tubes. As the seawater absorbs heat from the condensing water

vapor, more water vapor is produced which is condensed to form fresh water. The secondary steam generated in the last effect passed to a steam condenser.

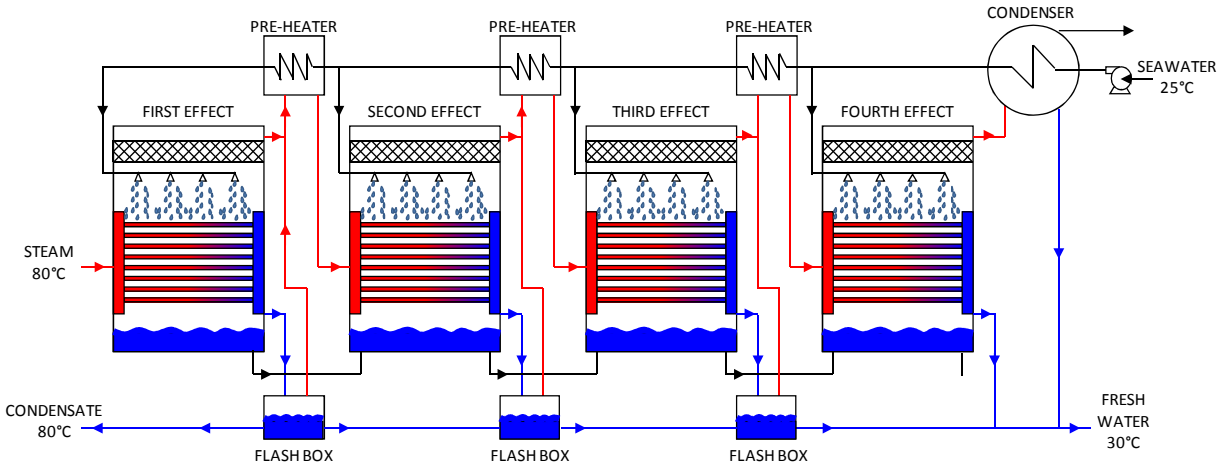

Figure 3 - 1 : Schematic MED (Pankratz & Tonner, 2003)

A MED-TC plant is a variation of a MED plant, which combines a conventional MED plant with a thermal vapor compression plant (TC). In this kind of plant, the external thermal energy, (typically, high pressure steam) is provided to a steam jet ejector or thermo-compressor as motive steam as shown in Figure 3-2. The ejector utilizes the pressure of the motive steam to increase the pressure - generally steam with a pressure greater than 1 atm. (Pankratz & Tonner, 2003). The ejector draws in a portion of the vapor generated which allows the system to "reuse" the energy content associated with a portion of the vapor generated in the last effect to avoid losing this energy in the condenser. The recycled steam from the steam ejector can be used as an energy source for the first effect. This variation of the MED system can work with a steam pressure that is barely above 1 atm and it provides a significant increase in performance. The

efficiency of a conventional MED can be nearly doubled by combining it with a TC. Another advantage of MED-TC is that the plant requires less cooling water. One disadvantage of MED-TC is the unavoidable mixing of condensate from high pressure steam with fresh water produced in the first effect, which may contaminate the fresh water because high pressure steam might contain boiler treatment chemicals (Pankratz & Tonner, 2003).

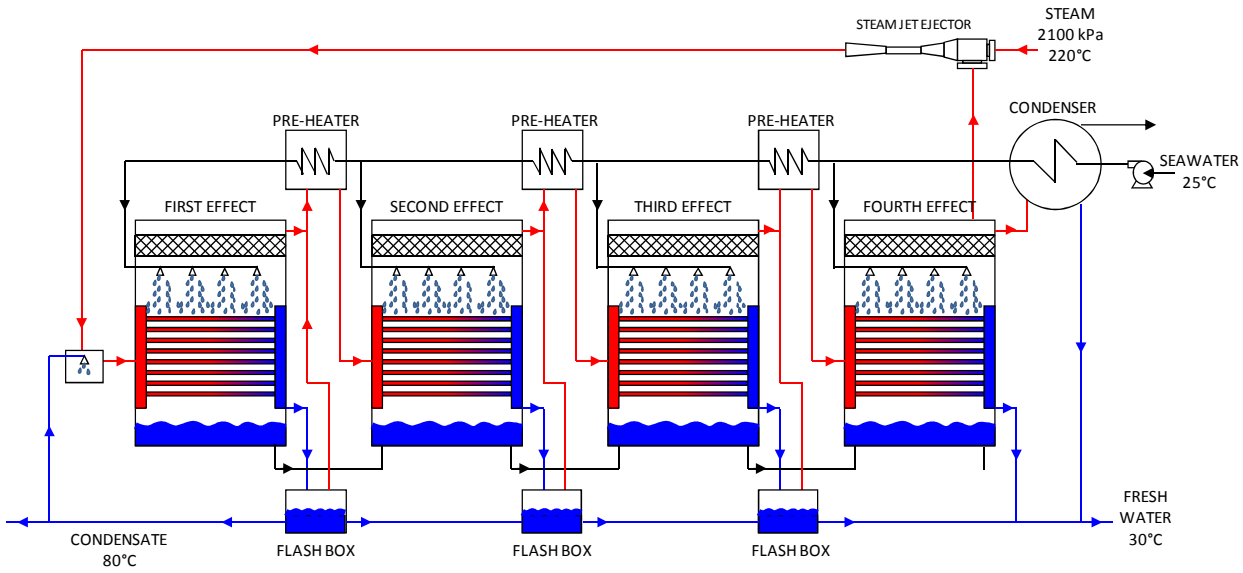

Figure 3 - 2 : Schematic MED-TC (Pankratz & Tonner, 2003)

3.2. Types of feed water configurations

MED plants can be configured in forward (co-current), backward (counter-current), parallel feed, and in combinations of these flow configurations.

3.2.1. Backward feed (counter-current)

In a backward feed configuration, feed seawater and vapor move in opposite directions as shown in Figure 3-3. Seawater enters the last effect operating with low pressure and temperature. Brine pumps are used to move the brine to the next effect where its salinity and temperature increase in each successive effects. Although this configuration provides high thermal efficiency because the brine is pre-heated, it also requires higher electrical energy consumption due to the operation of several brine pumps which lowers the overall efficiency of the plant. Another drawback of this configuration is the high risk of scaling because brine with the highest concentration is exposed to the effect with highest temperature. Backward feed configuration is not a preferred configuration for desalination (Vyas, 2003).

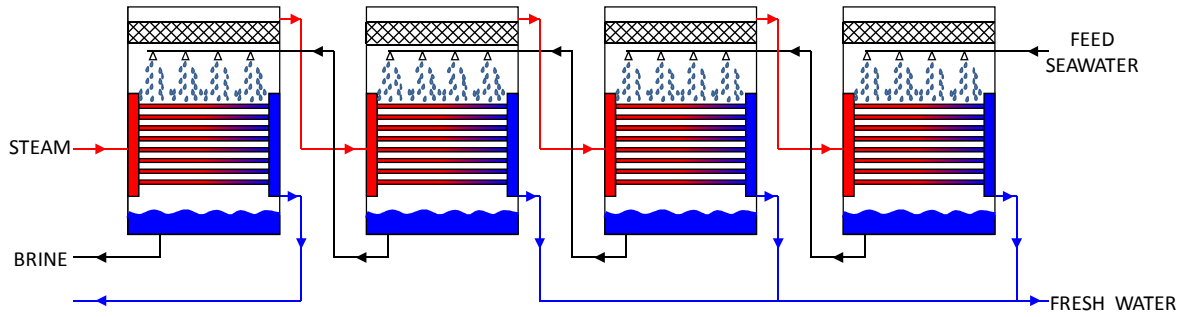

Figure 3 - 3 : Backward feed or counter current configuration (El-Dessouky & Ettouney, 2002)

3.2.2. Parallel feed (co-current)

A parallel feed configuration is the simplest configuration and it is used frequently on desalination industry (El-Dessouky & Ettouney, 2002). Feed seawater is divided into several equal flow rate streams which are delivered to individual effects using a single pump as shown in Figure 3-4. Each effect is fed with seawater at the same temperature and salinity and this water is concentrated to its maximum (Vyas, 2003). The first effect is the most susceptible to the risk of scale because it operates at high temperature and high salinity.

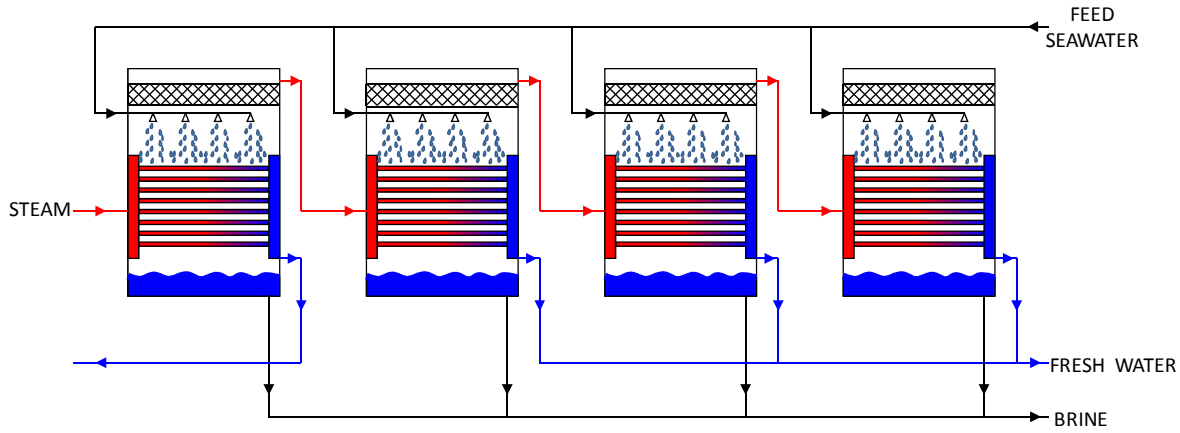

Figure 3 - 4 : Paralel feed or co-current configuration (El-Dessouky & Ettouney, 2002)

3.2.3. Forward feed

Figure 3-5 shows the "forward feed" configuration where the feed seawater and distilled fresh water vapor flow in the same direction - moving from higher to lower temperature effects. Seawater enters in the first effect, and the brine produced in the first

effect is injected to the next effect (second effect) and so on. This type of configuration combines low salinity brine and high temperature which reduces the risk of scaling. Forward feed configuration is not frequently used in the desalination industry because it has a more complex layout than the parallel feed configuration (El-Dessouky & Ettouney, 2002).

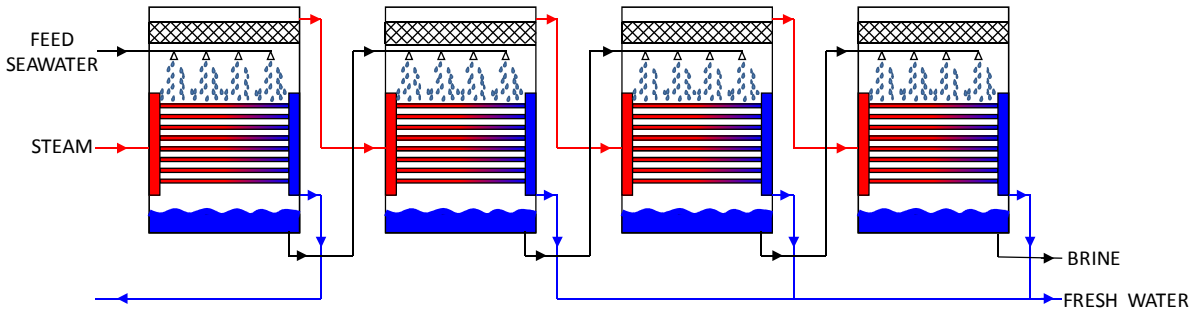

Figure 3 - 5 : Forward feed configuration (El-Dessouky & Ettouney, 2002)

3.3. Types of evaporators

MED configurations generally employ two types of evaporators. horizontal (HTE) and vertical tubes (VTE). In some plant configurations, successive effects are placed sideways and in other configurations the effects are stacked vertically on top of one another with the first effect at the top (Vyas, 2003). Each of these evaporator designs are discussed in more detail below. Heat is transferred across a thin film of liquid falling down by the inside surface of the tube or by the outside of the tubes because the heat transfer is more effective than if the tube is submerged or filled with water (Slesarenko, 1977).

3.3.1. Horizontal tube evaporator (HTE)

HTE configuration is the most common evaporator design in desalination plant applications. In this case, tubes are arranged horizontally in several rows with a square pitch inside a given evaporator stage. Steam flows inside the tubes where it condenses, providing heat to evaporate a falling film of feed brine over the outside the tubes. Because the feed brine is sprayed over the tubes, it forms a thin film that falls due to gravitational forces. The constant motion of brine across the heat exchanger surface allows vapor bubbles to be effectively carried away from the evaporator tube surface which lowers resistance to heat transfer compared to a flooded evaporator design. Horizontal tubes performance well when they are completely wetted. The tube-wetting rate between 0.14 and 0.25 [kg/s-m] (350 and 620 [lb/hr-ft]) seems to be adequate for complete tube wetting (Office of Saline Water (O.S.W), 1973). This condition depends of tube pitch, tube diameter, spray pattern, and liquid flow rate (El-Dessouky & Ettouney, 2002). Although staggering the arrangement of tubes comprising the evaporator can result in enhanced heat transfer, the evaporator tubes are typically arranged in a square pitch to simplify cleaning process (El-Dessouky & Ettouney, 2002).

Thin falling films over horizontal tubes provide an effective heat transfer mechanism because they exhibit high heat transfer coefficients at low film flow rates, low evaporation temperatures and small temperature differences (Yang & Shen, 2008). In addition, falling films provide an efficient disengagement of vapors and non-condensable gases because steam enters the tube at one end and distillate flows out of the other end

allowing positive venting (El-Dessouky & Ettouney, 2002). Moreover, the visual monitoring of scale formation and corrosion outside tube is possible through inspection windows (El-Dessouky & Ettouney, 2002). The main drawbacks the falling film horizontal tube design are scale and fouling formation on the outer surface of the tubes when they do not have an efficient water distribution and dry patches in the tubes are produced (Office of Saline Water (O.S.W), 1973).

3.3.2. Vertical tube evaporator (VTE)

Tubes in a VTE are arranged vertically. Feed brine enters at the top of the tube and flows downward by gravity the inside of the surface of the tubes forming a falling film. Steam flows over the outside surfaces of the tubes (shell-side) giving up its heat while condensing; as a result, thin film is formed both inside and outside surface of the tubes and high heat transfer rates are obtained. The most important aspects in design are to obtain uniform distribution of liquid in the tubes and match tube dimensions with heat transfer rates. The feed can be distributed to tube sheet either by a top nozzle or through side nozzle. The film begins to collapse at certain liquid flow rate and above certain heat flux, thus resulting in poor average heat transfer rates (Palen, 1988).

Similar to HTE, thin falling film in vertical tubes presents high heat transfer rates. The use of fluted tubes in the VTE allows enhanced heat transfer coefficients (Vyas, 2003). The most serious disadvantage of vertical tubes is the possible collapse of the falling film. When falling film collapses, it can produce dry patches or small amount of liquid in some areas. In some cases, complete evaporation of the liquid leaves salt scaling

on the tube surface. In addition, temperature increases in dry zones rising thermal stresses (El-Dessouky & Ettouney, 2002).

3.4. Steam jet ejector or thermo-compressor

The main components of an ejector include a nozzle zone that contains the primary nozzle and the suction chamber, the mixing, and the diffuser zone (Figure 3-6). The primary steam (high pressure) enters to the primary nozzle, a convergent–divergent nozzle, expanding and accelerating to supersonic speed through the nozzle; consequently, it creates a low-pressure region at the nozzle exit in the mixing zone due to its supersonic speed. The pressure difference between the mixing zone and the secondary steam inlet drives the secondary steam flow inside of the ejector (entrainment effect). This phenomenon is considered adiabatic because the velocity is very high and there is not sufficient time for heat transfer to occur (He, Li, & Wang, 2009). At the beginning of the mixing zone, the primary steam and the secondary steam merge without mixing. The primary steam expands diminishing the cross-section area where the secondary steam flows increasing its speed to sonic value and chokes. After the secondary steam chokes, the two incoming primary and secondary streams mix while the primary steam slows and the secondary steam accelerates. The pressure of the two streams is uniform at the mixing zone and remains constant until they reach the constant-area tube section. As the two stream flow into the diffuser zone, the mixture velocity is decreased causing pressure to rise.

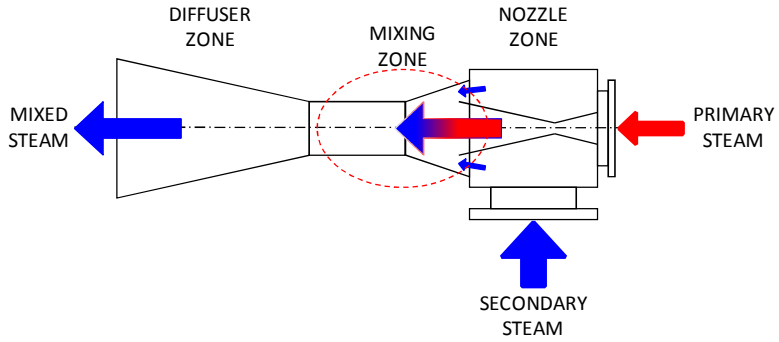

Figure 3 - 6 : Schematic steam jet ejector or thermo-compressor.

The mixing mechanism is modeled using two methods, the constant-area and the constant-pressure model (Keenan, Neumann, & Lustwerk, 1950). The constant-pressure model offers more accurate predictions; therefore, most of the mathematical models assuming constant-pressure. The most essential part in modeling the ME-TVC desalination system is to determine the entrainment ratio (ω) of motive steam (primary steam) to suction vapor (secondary steam) in the ejector.

$$\omega = \frac{\dot{m}_p}{\dot{m}_s} \tag{3.1}$$

An optimal ratio will improve the unit efficiency by reducing the amount of motive steam (Utomo et al., 2008). This ratio is a direct function of discharge pressure (P_d), primary steam pressure (P_p), and secondary pressure (P_s) (Bin Amer, 2009). These pressures are related by the compression ratio (CR) and expansion ratio (ER), and they are generally defined as:

$$CR = \frac{P_d}{P_s} \tag{3.2}$$

$$ER = \frac{P_p}{P_s} \tag{3.3}$$

Several methods are available in the literature to evaluate entrainment ratio (ω). An empirical correlation was proposed by Power (1994), which is a graphical data method shown in Figure 3-7 (Power, 1994). Thermodynamic model have been proposed by Eames (1995), and by Aly (1999). Eames developed the model applying steady-state equations of energy, momentum and continuity at the nozzle, diffuser and mixing zone to determine the pressure and velocity at each zone. In addition, this model accounts for friction losses (Eames, Aphornratana, & Haider, 1995). Aly used the same fundamental relations as Eames, but the flow inside the ejector was considered as an ideal gas with

constant specific heat ratio both for superheated and the wet region. These two models were compared with Power's empirical correlation (Power, 1994), and good agreement was found (He et al., 2009). Finally, El-Dessouky developed a semi–empirical model (El-Dessouky & Ettouney, 2002). It was based on a methodology similar to Aly's model and data extracted from ejector manufacturer and experimental data provided in the literature. El-Dessouky's model avoids iterative procedures and proposes a simple correlation, which facilitates in such optimization and simulation models (He et al., 2009).

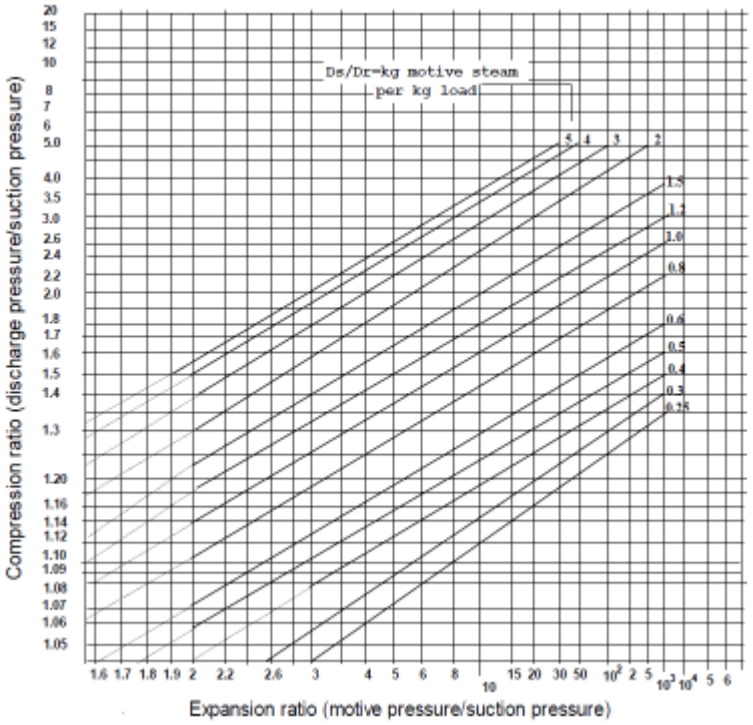

Figure 3 - 7 : Entrainment ratio for different compression and expansion ratios (Power, 1994)

3.5. Overall heat transfer coefficient (U)

The overall heat transfer coefficient, U, in the evaporator can be defined as the sum of thermal resistances in series:

$$\frac{1}{U\,A} = R_{in} + R_{cond} + R_{out} + R_{f,out} \tag{3.4}$$

where R_{in} is the convection resistance between the water-vapor condensing and the inner surface of the tube, R_{cond} is the resistance through the tube wall, R_{out} is the resistance between the brine evaporating and the outer tube surface, $R_{f,out}$ is the fouling resistance that occurs on the external surface of the tube as a result of deposits that accumulate from the flowing brine.

The resistance between the fresh water-vapor condensing and the inner surface of the tube can be represented as:

$$R_{in} = \frac{1}{\bar{H}_{c,t}\,\pi\,ID\,L_{tube}} \tag{3.5}$$

where $\bar{H}_{c,t}$ is the average heat transfer coefficient between the water-vapor condensing and the tube wall, *ID* is the inner diameter of the tube, and L_{tube} is the total length of the tube. Several correlations are available to calculate the average convective heat transfer coefficient on the condensing side in a horizontal tube such as Dobson and Chato (1998), Shah (1979), Traviss (1972), and Cavalini (1974) (Uche, Artal, & Serra, 2003). In this

case, $\bar{h}_{in}$ can be determined using a flow condensation correlation suggested by Dobson and Chato (1998).

The thermal conduction resistance of the tube wall for a cylindrical tube is defined as:

$$R_{cond} = \frac{ln\left(\frac{OD}{ID}\right)}{2\,\pi\,k_m\,L_{tube}} \tag{3.6}$$

where k_m is the conductivity of the tube. This resistance for the selected material and tube thickness is fixed and small in comparison with the other resistances.

The resistance between the evaporating brine and the outer surface of the tube is expressed as:

$$R_{out} = \frac{1}{\bar{H}_{b,t}\,\pi\,OD\,L_{tube}} \tag{3.7}$$

where $\bar{H}_{b,t}$ is the average heat transfer coefficient between the brine evaporating and the outer tube wall, and OD is the outer diameter of the tube. The average convective heat transfer coefficient on the evaporating side can be determined using several experimental correlations such as Barba (1984), Kutateladze (1963) (modified Nusselt), and Parken (1990) (Uche et al., 2003). The Parken (1990) correlation is a falling thin film correlation that predicts the boiling heat transfer coefficient for a thin water film falling over the outside of horizontal smooth tubes.

$$\bar{H}_{b,t}\left(\frac{\nu^2}{g\,k^3}\right)^{1/3} = 0.00082\,Re^{0.10}\,Pr^{0.65}\,q^{"\,0.40}$$

(3.8)

In this correlation (3.8), Re and Pr are Reynolds and Prandt numbers, respectively, $q^{"}$ is the heat flux, ν is the kinematic viscosity, and k is the thermal conductivity of the seawater. The correlation is valid for 2.54 cm diameter tubes over the following ranges $770 \leq Re \leq 7000$, $1.3 \leq Pr \leq 3.6$, 30 kW/m^2 $\leq q^{"} \leq$ 80 kW/m^2, and 49°C $\leq$ T $\leq$ 127°C. The average outside heat transfer coefficient, $\bar{h}_{out}$, is influenced by the flow rate of seawater over the tube. When the flow rate increases, the heat transfer coefficient improves because the velocity of the seawater also increases which enhances the convective heat transfer (Yang & Shen, 2008).

The fouling resistance on the outer surface of the tube can be expressed in terms of fouling factor, R_f''.

$$R_f = \frac{R_f''}{\pi\,OD\,L_{tube}}$$

(3.9)

R_f'', can vary in the range 0.00009 - 0.0002 m^2-C/W depending upon seawater temperature and scale conditions with the lower value being for relatively clean tubes (Holman, 1997).

The overall heat transfer coefficient, U is mainly influenced by the average heat transfer coefficient between the brine evaporating and the outer tube wall, $\bar{h}_{out}$, because

it is about 50% of the average heat transfer coefficient between the water-vapor condensing and the tube wall, $\bar{h}_{in}$ (Yang & Shen, 2008). Experimental values of U range between 3.2 – 6.2 kW/m^2-°C (570 – 1100 BTU/h-ft^2-F) for a feed temperature range of 48 – 86°C (118 – 186 F), a ΔT range of 4 – 8 °C (9.8 – 16.7 F), an average feed wetting rate at the top tube row between 0.15 and 0.23 kg/s-m (370 - 570 lb/h-ft), with a feed salinity of 48 – 52 g/kg, and the feed seawater at saturated conditions (Office of Saline Water (O.S.W), 1973). In order to achieve high U values during evaporator operation, it is necessary for the liquid to be evaporated to enter the evaporator at its saturation temperature; otherwise the system operates as a normal heat exchanger and $\bar{h}_{out}$ is governed by equations for single-phase flow with correspondingly lower U values (Vyas, 2003). Experimental data indicated that U declines in about 10% for a seawater feed that is sub-cooled by 9°C (18 F).

Non-condensable gases and scaling are two additional factors that have a significant effect on the overall heat transfer coefficient. Previous investigators have found that U declines by up to 65% of its original value after injection of 0.11 mole % of nitrogen, and if the scale grows up to 5 mm (3/16 inches) thick, the heat transfer rates decreased to 25% of the original in horizontal tubes evaporator (Office of Saline Water (O.S.W), 1973). The causes, effects, and means to control the detrimental effects of non-condensable gases and scaling are discussed in more detail in the sections that follow. Furthermore, chemical additives change the boiling and the condensing characteristics of the seawater. Surfactant chemicals increase the boiling heat transfer coefficients while the antifoams reduce the overall heat transfer coefficients. The U decreases by the addition of antifoam in the brine feed. A decline in the overall heat transfer coefficient by up to 18%

was noted with the addition of up to 10 ppm of antifoam (Office of Saline Water (O.S.W), 1973).

3.6. Non condensable gases (NCG)

Non condensable gases (NCG) consist mainly of air (N_2 and O_2) and CO_2. Three sources explain the presence of NCG in thermal desalination systems(Bodendieck & Genthner, 1999): Air penetration through leakage (small holes and pores in the containers' flanges, and connections pipes). Liberation of dissolved atmospheric gases entering with the feed seawater. Release of carbon dioxide (CO_2) due to carbonic acid decomposition.

The relevance of CO_2 generated due to carbonic acid decomposition can be illustrated when it is compared with the dissolved atmospheric gases in seawater. The solubility of the atmospheric gases in seawater can be estimated using Henry's law because their concentrations dissolved in seawater are sufficiently small (Glade & Al-Rawajfeh, 2008). The potential liberation of CO_2 by carbonic acid decomposition may be determined from the composition of standard seawater shown in Table 3-1.

Table 3 - 1 : The composition of standard seawater with a salinity of 35 g/kg and pH = 8.1 at 25°C (Millero, 1996)

Species	Concentration [g/kg seawater]	Concentration [mol/kg seawater]	Specific concentration [g/kg] / S
Na^+	10.7838	0.46907	0.30811
Mg^{2+}	1.2837	0.05282	0.03668
Ca^{2+}	0.4121	0.01028	0.01177
K^+	0.3991	0.01021	0.01140
Sr^{2+}	0.0079	0.00009	0.00023
Cl^-	19.3529	0.54588	0.55294
SO_4^{2-}	2.7124	0.02824	0.07750
HCO_3^-	0.1070	0.00175	0.00306
Br^-	0.0672	0.00084	0.00192
CO_3^{2-}	0.0161	0.00027	0.00046
$B(OH^-)_4$	0.0079	0.00010	0.00023
F^-	0.0013	0.00007	0.00004
$B(OH)_3$	0.0193	0.00031	0.00055
Sum	**35.1707**	**1.11993**	**1.00488**

CO_2 is formed by a chemical reaction and will continuously be released during the distillation process. When the system is in equilibrium, any change in the partial pressure of CO_2 in the gas phase induces a state of non-equilibrium between the gas and aqueous phases. When feed seawater enters to the evaporator, the solubility of CO_2 decreases due to pressure drop; consequently, CO_2 is released into the water vapor space. The release of CO_2 disturbs the chemical equilibrium in the carbonate system, and new CO_2 is formed by chemical reaction from HCO_3^-, and CO_3^{2-} (Glade & Al-Rawajfeh, 2008). Table 3-2 presents the potential presence of NCG in a desalination system. The amount

of CO_2 released due to carbonic acid decomposition in each effect of a MED plant can be calculated using the methodology presented by Glade (2008).

Table 3 - 2 : Amounts of atmospheric gases molecularly dissolved chemically react and not chemically react in seawater

Species	Composition in atmosphere	Equilibrium concentration on seawater	
	vol/vol	mol/kg SW	mg/kg SW
(*) N_2	0.7800	0.00048	13.36
(*) O_2	0.2100	0.00027	8.75
(*) Ar	0.1000	0.00001	0.56
(*) CO_2 (no react)	0.0004	0.00001	0.57
(**) CO_2 (react)	0.0004	0.00202	88.88
(***) CO_2 (total)	0.0004	0.00203	89.45

Notes:
(*) Calculate using Henry's law
(**) Calculate from seawater composition including HCO_3^- and CO_3^{2-}
(***) CO_2 (no react) + CO_2 (react)

The heat transfer rate in the condensing side of evaporators is diminished by the presence of NCG that reduce the temperature at which steam condenses. By their very nature, NCG remain in the gaseous state and mix with water vapor. When water vapor condenses, the concentration of NCG increases and tends to accumulate in the interface between the water vapor and the condensed water forming a NCG film. This film of poorly conducting gas insulates the water vapor from reaching the cool tube wall surface where it can effectively condense. This process results in a reduced heat transfer rate (R. Semiat & Galperin, 2001). For example, the overall heat transfer coefficient, U, declines

to 65% of its original value in horizontal tubes evaporator after injection of 0.11 mole % of nitrogen (OSW, 1973). The designer may be sized for 8 – 10% more heat transfer area to offset the drop in U (Bodendieck & Genthner, 1999). Furthermore, the NCG accumulation reduces the local partial pressure of the water vapor next to the wall (interface) diminishing the condensation temperature (R. Semiat & Galperin, 2001). At lower vapor velocities or Reynolds number the heat transfer coefficient declines and the non-condensable present are not properly swept out and subsequently blanket the condensing film (Office of Saline Water (O.S.W), 1973).

The effects of NCG can be minimized by means of installing a deaerator to eliminate dissolved atmospheric gases and a suitable venting system to release CO_2 generated in each effect of desalination plant due to chemical reaction (Glade & Al-Rawajfeh, 2008). When the feed seawater is degassed, the residual concentrations of N_2, O_2, CO_2, and Ar in seawater are negligible. This assumption is supported by Figure 3-8 that shows equilibrium concentration of CO_2 dissolved in seawater as a function of temperature. A typical temperature of operation of this kind of plant is 70°C. If the degassing is made at this temperature, the concentration of CO_2 is reduced by more than 80%. The same behavior is applicable for N_2, O_2 and Ar.

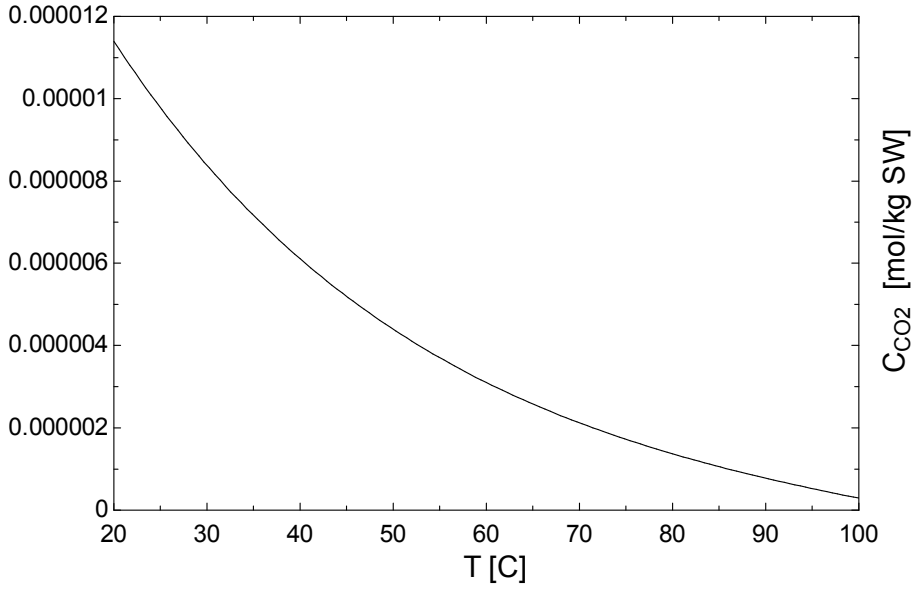

Figure 3 - 8 : CO_2 dissolved, not chemically react, in seawater as a function of temperature

In order to release carbon dioxide (CO_2) due to carbonic acid decomposition and inhibit the adverse effects due to NCG accumulation, evaporators and the condenser must be provided with good gas vents (Bodendieck & Genthner, 1999). Venting usually cascades from the steam chest of one pre-heater to the steam chest of the adjacent one. The vent for the condenser must be connected to vacuum system to compress and release NCG to the atmosphere (El-Dessouky & Ettouney, 2002). Furthermore, feed seawater can be pre-treated and de-carbonated adding chemicals in the deareator.

3.7. Scaling and corrosion

Scale formation is the most commonly operational problem in a desalination plant (Pankratz & Tonner, 2003). Seawater has the tendency for scale formation and fouling problems because it contains ions (see Table 3-1) such as dissolved salts and suspended solids. Certain combinations of these ions form components, which have a low solubility in seawater. Low solubility means that these compounds typically precipitate out as a solids when the solubility limit is exceeded. These precipitated solids will either remain in suspension in the seawater or form scale on the heat transfer surface (Al-Ahmad & Aleem, 1993).

Scale formation is caused by super saturation of scale-forming agents, and it may be alkaline and sulfate scales. In the case of sulfate scale, the saturation is promoted by a reduction in the solubility of the calcium sulfate as the temperature increases (inverse-solubility); consequently, three types of calcium sulfate might be formed: anhydrite ($CaSO_4$), hemihydrate ($CaSO_4$ $1/2H_2O$), and di-hydrate ($CaSO_4$ $2H_2O$). The seawater solubility of these compounds as a function of temperature is given in Figure 3-9 (Ludwig & Hetschel, 1990).

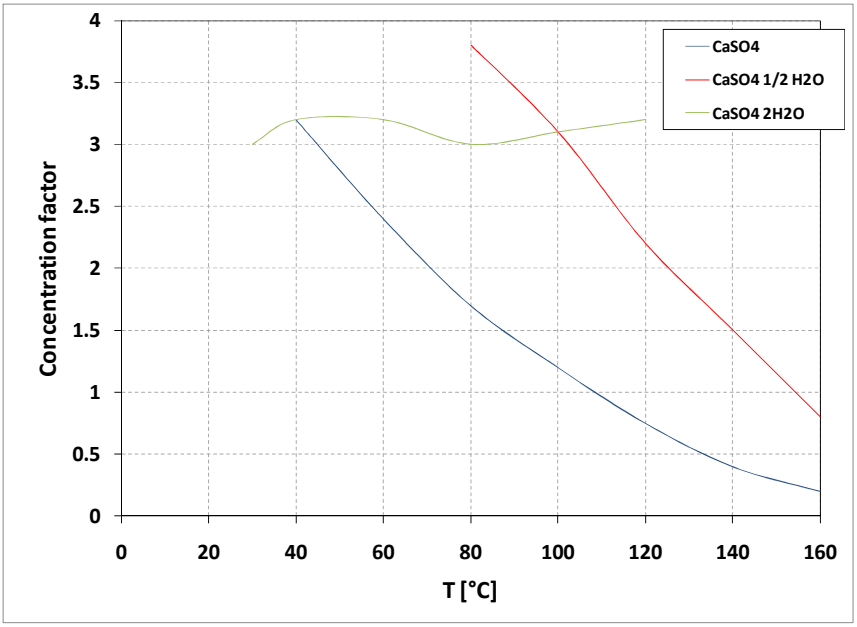

Figure 3 - 9 : The seawater solubility of calcium sulfates as a function of temperature (Ludwig & Hetschel, 1990)

In the case of alkaline scale, $CaCO_3$ and $Mg(OH)_2$, super saturation depends on temperature, pH, the release rate of CO_2 as well as the concentrations of HCO_3^-, CO_3^{2-}, Ca^{2+}, and Mg^{2+} ions. The release of CO_2 from the evaporating brine shifts the pH to higher values and considerably influences the concentrations of HCO_3^- and CO_3^{2-} ions in the brine (Al-Ahmad & Aleem, 1993).

Scale formation on heat transfer surfaces reduces plant performance and efficiency because it increases thermal resistance of the tube walls, which reduces the heat transfer rates and leads corrosion limiting the lifetime of the plant. Also, when deposits build up inside tubes, pressure drop will increase; therefore, the pumping energy increases (Vyas, 2003). In MED with horizontal tubes evaporators, scale is formed on

the outside of the tubes, which is difficult to prevent and remove (Pankratz & Tonner, 2003). Experimental tests have shown when the scale have grown up to 5 mm (3/16 inches) thick, the heat transfer rates decreased to 25% of the original (Office of Saline Water (O.S.W), 1973).

The detrimental effects for potential scale formation cannot be avoided, but they can be reduced increasing the design heat transfer area, operating plants at conditions in which dissolved solids do not precipitate, , and cleaning on-load and off-load. In some cases, the heat transfer area is made 40% larger to reduce fouling and scale problems. This increase in surface are represents about 10% the whole capital cost of the system (Knudsen, 1990). The operational factors that affect scale formation are feed seawater composition, top brine temperature (TBT), and brine concentration. Corrosion problems are also associated with high operating temperatures, presence of dissolved oxygen in water and the heat transfer material used (R. Semiat & Galperin, 2001). Scale can be controlled by treating feed water with chemicals. One alternative is an acid treatment, which maintains low fouling rates by neutralizing the alkalinity of feed water so that the pH is in a range between 7.7 and 8.0 (Knudsen, 1990). Another chemical method is the addition of scale inhibitors (anti-scaling), which can prevent alkaline scale with the addition of certain polyphosphates to supersaturated solutions of various salts, particularly calcium carbonate, preventing precipitation for substantial period of time (Al-Ahmad & Aleem, 1993). Additionally, an external treatment is necessary, which includes water softening, de-areation, and de-carbonation. The scale can be cleaned either by chemical treatment or by mechanical cleaning. The scale should be removed as early as possible brushing the pipes and applying high-pressure water sprays in the

outside surface of the evaporator heat exchanger, the plant should be off-line to the clean process (Pankratz & Tonner, 2003).

3.8. Water quality

The literature reports the product purity of fresh water in MED plants is about 3.5 – 6.5 ppm of total dissolved solids (TDS). In some cases, it is below 1.5 ppm TDS (Office of Saline Water (O.S.W), 1973). The fresh water produced in a desalination plant is generally not used without post-treatment because it tends to corrode pipes during supply (Vyas, 2003). Some plants add at least 50 ppm of TDS to fresh water before transporting it through pipes. These chemicals added convert the fresh water distilled in non-corrosive fresh water, but still is potable (Khan, 1986).

Chapter 4 : Model multi-effect desalination (MED) and multi-effect desalination with thermal vapor compression (MED-TC) plants

4.1. MED model

4.1.1. Model Overview

A steady state model of a desalination plant is developed using the Engineering Equation Solver EES software (Klein, 2010). This model consists of a thermally-driven multi-effect desalination plant (MED) with n-effects, where n is three (3) or greater. Individual effects are denoted with "*i*" where "*i*" varies from 1 to n. The MED model is developed to analyze the specific energy consumption needed to distill seawater while varying the number of effects, the plant configuration, the thermal energy source kind (steam or hot water), conditions (temperature and pressure) of the thermal energy source, and characteristics of the incoming seawater (salinity and temperature). The model is based on mass, salt and energy balances, heat transfer equations, and pressure drops effects.

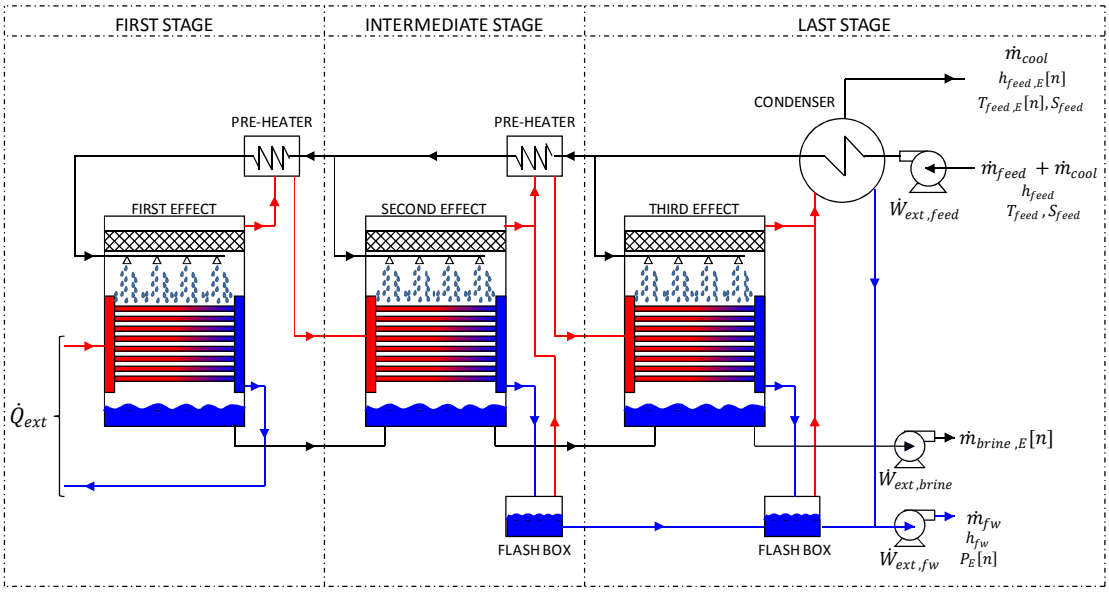

Figure 4 - 1 : Schematic multi-effect desalination plant

The simplest MED plant considered is comprised of three effects as shown in Figure 4-1. The first effect has unique characteristics compared to the other n-1 effects in that it receives pre-heated incoming seawater and thermal energy directly from an external source in order to drive the water purification process. Within the MED cycle, pure water vapor and concentrated seawater leave the first effect to a second effect. One or more "standard effects" follow the first stage. Each "intermediate stage" receives intermediate temperature seawater which is distilled by heat given up by incoming pure water vapor created by the stage immediately upstream… Somewhat like the first effect, the MED plant model includes a separate model for the last effect. The last effect receives fresh water vapor from the effect immediately upstream. The fresh water vapor condenses in a heat exchanger where it gives up its heat of condensation to evaporate

incoming seawater. The condensed fresh water collects with condensate from the upstream stages where it is pumped from the desalination plant for finishing prior to being made available for consumption.

The information required by the model includes:

- thermal source mass flow rate, temperature, pressure, and state
- incoming seawater conditions (temperature and salinity)
- incoming seawater mass flow rate (for each effect)
- number of effects
- dimensions and features of evaporators, pre-heaters and condenser
- temperature of fresh water leaving the plant

The most important results that the model determines are the fresh water production rate ($\dot{m}_{fw}$ in kg/s) and the specific energy consumption (SEC in kWh/m^3). Equation 4-1 presents an overall water mass balance for the plant (Figure 4-1).

$$\dot{m}_{feed} + \dot{m}_{cool} = \dot{m}_{fw} + \dot{m}_{brine,E}[n] + \dot{m}_{cool} \tag{4.1}$$

The specific energy consumption (SEC) of the plant in kWh/m^3 is defined as the ratio of the external thermal and electric energy (kW) provided to the plant in order to produce one (1) cubic meter of fresh water, and it is expressed as:

$$SEC\ [kWh/m^3] = \frac{\dot{Q}_{ext} + \dot{W}_{ext,feed} + \dot{W}_{ext,brine} + \dot{W}_{ext,fw}}{\dot{m}_{fw}/\rho} \tag{4.2}$$

The total energy supplied to the plant takes into account the external thermal provided to the first effect as well as the electrical energy input to the pumps. In addition to the these gross measures of overall plant performance, the model provides the temperature and pressure in each evaporator, and the overall heat transfer coefficient for each evaporator as well as the individual stage pre-heaters and the plant's condenser.

The MED plant model makes the followings assumptions:

- The plant analysis assumes steady-state operation with negligible kinetic energy terms.
- Pressure drops are ignored in the following processes: evaporating water vapor in evaporators, water vapor in pre-heaters (hot stream), condensing water vapor in the condenser, and in pipelines between stages.
- The heat transfer equation in the evaporator ignores the effect that the feed seawater has a temperature slightly lower than saturated temperature. It is assumed that phase change is simultaneously occurring on both sides of the evaporator heat exchangers in each stage.
- External heat losses through the jacket of the equipment are assumed to be negligible.

Enthalpies, specific heat, and boiling point elevation (BPE) of seawater are functions of temperature and salt concentration. Seawater and brine properties are obtained from Thermophysical properties of seawater (Sharqawy, Lienhard, & Zubair, 2010).

4.1.2. Stages of MED model

4.1.2.1.First effect

The incoming seawater, $\dot{m}_{feed,Ph}[1]$, is preheated by the condenser from the last MED stage and by the n-2 pre-heaters in series from intermediate stages. At the first effect, $\dot{m}_{feed,Ph}[1]$ is preheated to a temperature slightly lower than the saturation temperature in the evaporator before being sprayed onto the outside surface of first stage evaporator. In the evaporator, thermal energy is added to the stream of seawater entering the first effect. The thermal energy input to the first effect is steam or high temperature sensible energy change secondary fluid (e.g. hot water) obtained from an external source such as a boiler, power plant, or solar thermal system. As a consequence of this heat addition, a portion of the incoming seawater is vaporized, pure water vapor, is generated at the rate $\dot{m}_{vapor-heat,E}[2]$,. After leaving the first stage, $\dot{m}_{vapor-heat,E}[2]$ flows through the "pre-heater" heat exchanger where it gives up a portion of its thermal energy to pre-heat the incoming seawater. Thereafter, the remaining mass flow of fresh water flows into the subsequent effect where it fully gives up its heat of condensation in order to evaporate seawater flowing into the second stage. The concentrated brine portion that collects in the bottom of the first effect ($\dot{m}_{brine,E}[1]$) is directed to the chamber of the second effect. Figure 4-2 shows the schematic first effect of MED.

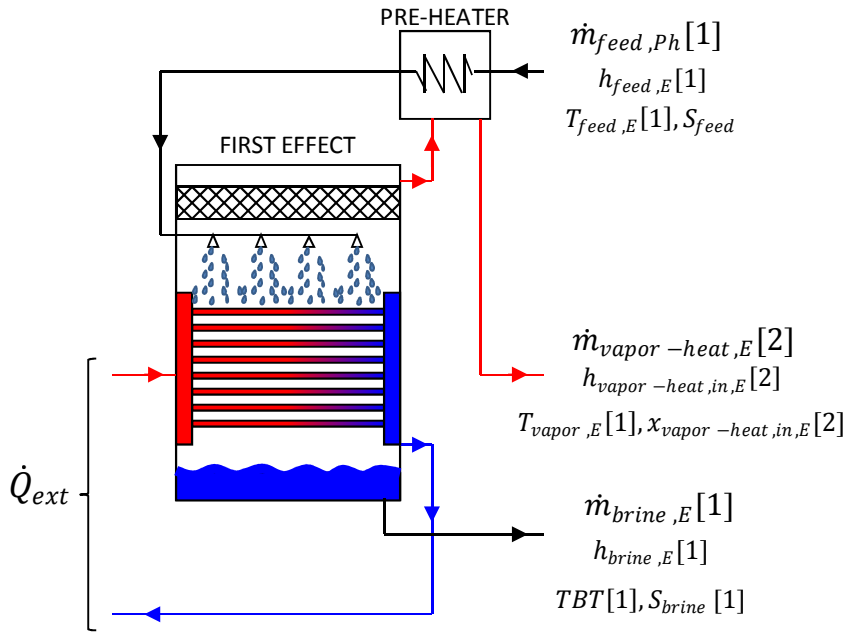

Figure 4 - 2 : Schematic First effect of MED

4.1.2.2.Intermediate stage

Figure 4-3 shows the schematic of an intermediate stage, which consists of an indirect heat exchanger (evaporator), a pre-heater, and a flash box. The model is capable of accommodating any number of intermediate stages varying from a minimum of one (1) to n-2 effects. The pre-heater heats the incoming seawater, $\dot{m}_{feed,Ph}[i]$, up to a temperature slightly lower than the saturation temperature in the evaporator. After passing through the pre-heater, $\dot{m}_{feed,Ph}[i]$ is divided into two streams, one that feeds the evaporator ($\dot{m}_{feed,E}[i]$), and other that feeds the downstream pre-heater ($\dot{m}_{feed,Ph}[i-1]$). Brine at rate $\dot{m}_{feed,E}[i]$ falls by gravity over the outside surface of the evaporator heat exchanger. The high temperature fresh water vapor (steam), $\dot{m}_{vapor-heat,E}[i]$, generated

by the previous effect provides the necessary thermal energy to evaporate the seawater that falls over the outside surface of the heat exchanger (evaporator).

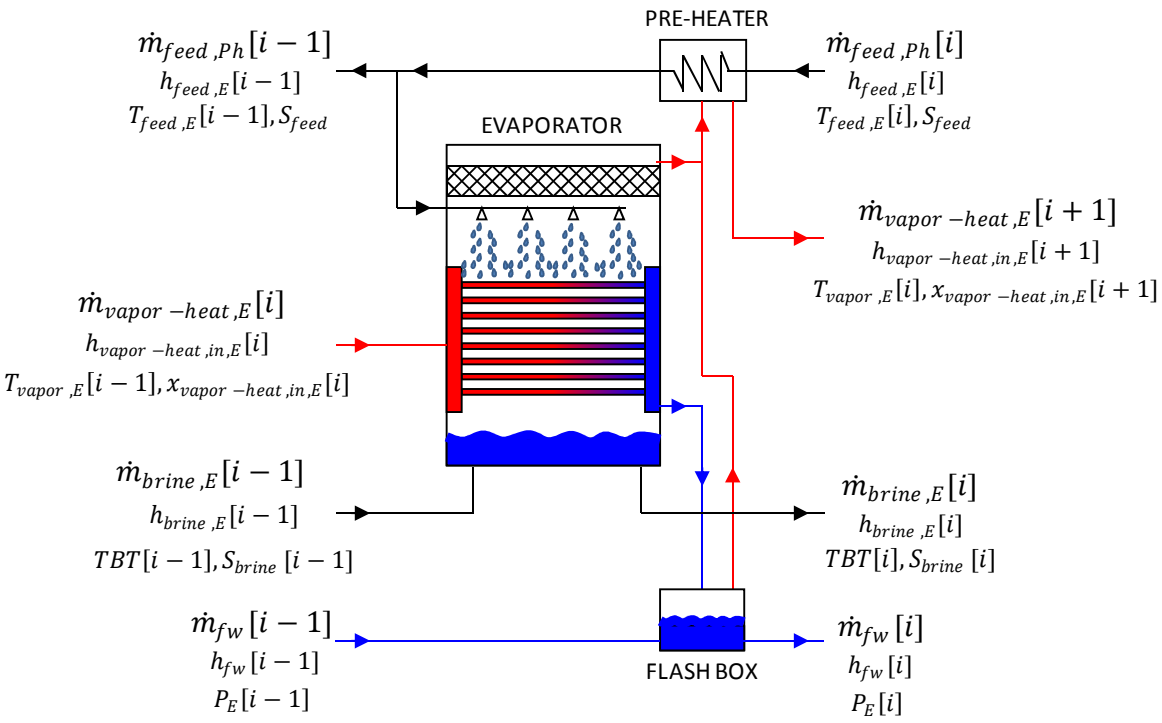

Figure 4 - 3 : Schematic intermediate stage

The fresh water condensing in the evaporator at rate $\dot{m}_{vapor-heat,E}[i]$ leaves the effect and flows to the "flash box," which operates at the same pressure as the evaporating side of the evaporator. A portion of the fresh water is flashed to vapor upon entering the flash box due to the pressure difference between the condensing side of the evaporator and the flash box. The flash vapor is vented to the pre-heater where it merges with fresh water vapor generated directly in the upstream stage. The residual brine ($\dot{m}_{brine,E}[i-1]$) flows downstream to the next effect. A portion of the incoming brine stream will flash to

vapor upon entering the evaporator chamber because of the decreasing pressure in each successive effect. After leaving the evaporator, vapor at rate $\dot{m}_{vapor-heat,E}[2]$ is mixed with the vapor formed in the flash box. The vapor mixture, $\dot{m}_{vapor-heat,E}[i]$, flows through the heat exchanger pre-heater as hot stream heating the incoming seawater, and subsequently it is conducted to the following effect as heat source. The concentrated brine portion of this effect ($\dot{m}_{brine,E}[i]$) is directed to the next evaporator. The "intermediate stage" in the desalination plant is configured identically for multiple subsequent effects that can be added to the overall plant.

4.1.2.3.Last effect

An evaporator, a flash box, and the condenser form the last effect. The condenser initiates pre-heating the incoming seawater, $\dot{m}_{feed}$, to a temperature slightly lower than the saturation temperature in the evaporator. Additional seawater enters to the condenser, $\dot{m}_{cool}$, to completely condense and cool the water vapor leaving the evaporator and the flash box of the last effect. The excess incoming seawater at rate $\dot{m}_{cool}$ is purged after leaving the condenser. Upon leaving the condenser, $\dot{m}_{\text{feed}}$ is divided into two streams: one that feeds the evaporator ($\dot{m}_{feed,E}[n]$), and other that feeds the downstream pre-heater ($\dot{m}_{feed,Ph}[n-1]$). $\dot{m}_{vapor-heat,E}[n]$ provides the necessary thermal energy to distill a portion of the seawater falling on the outside of the surface ($\dot{m}_{feed,E}[n]$) while it is condensing on inside of the heat exchanger. After condensing in the evaporator, vapor at rate $\dot{m}_{vapor-heat,E}[n]$ flows to the flash box, which operates at the lower primary side

of evaporator pressure. A portion of the fresh water is flashed to vapor upon entering the flash box due to the pressure difference. The residual brine ($\dot{m}_{brine,E}[n-1]$) from the previous effect also becomes an incoming stream in the evaporator. A portion of the incoming brine stream will flash to vapor upon entering the lower pressure in the evaporator chamber. After leaving the evaporator, $\dot{m}_{vapor-heat,E}[2]$ is mixed with the vapor formed in the flash box. The vapor mixture, $\dot{m}_{vapor-heat,E}[i]$, flows through the condenser condensing to produce fresh water. The concentrated brine portion of this effect ($\dot{m}_{brine,E}[n]$) is considered as blowdown and it is purged. Figure 4-4 shows the schematic last effect.

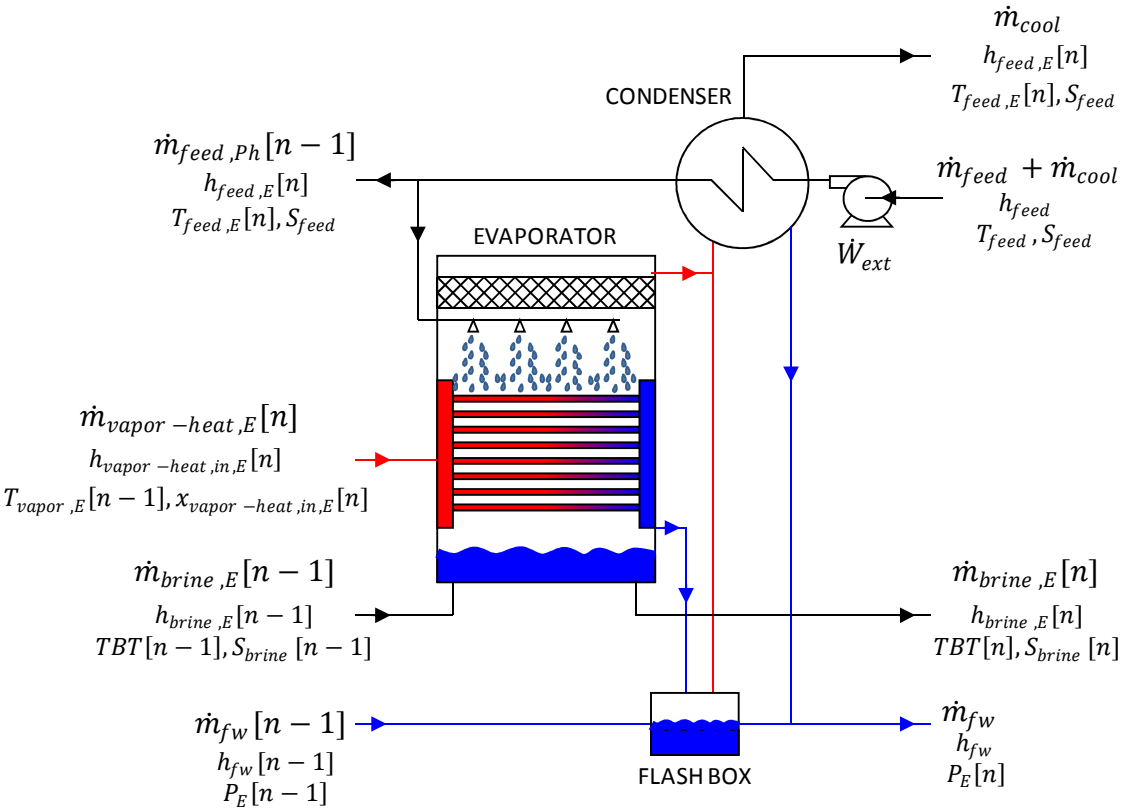

Figure 4 - 4 : Last effect

4.1.3. Components of the MED model

4.1.3.1.Evaporator

The evaporator heat exchanger is modeled as a horizontal tube evaporator. The distillation process occurs on the outside of the evaporator, by two phenomena. First, fresh water vapor is generated by a portion of feed brine ($\dot{m}_{feed,E}[i]$) evaporating as it absorbs heat from the higher temperature stream ($\dot{m}_{vapor-heat,E}[i]$) flowing through inside of the evaporator tubes. The increasingly concentrated brine falls to the bottom of the effect's camber around the outside surface of the evaporator tubes. The heat source for the evaporator in the first effect may be steam or hot water. The heat source from the second to n effect is condensing fresh water vapor generated by the upstream effect. This phenomenon occurs in all of the effects. An additional contribution to the production of fresh water vapor is produced when a portion of the incoming brine ($\dot{m}_{brine,E}[i-1]$) flashes to a vapor upon throttling from a higher pressure upstream to a lower pressure in the downstream effect. This situation takes place from the second effect onward. In a MED plant, the generated water vapor is directed to the pre-heater and subsequently to the downstream evaporator as a heat source; therefore, only $\dot{m}_{vapor,E}[i]$ is generated and $\dot{m}_{vapor,TC}[i] = 0$. In a MED-TC plant, a portion of the water vapor generated may be directed to the ejector as secondary steam, generally in the last effect, and it is denoted $\dot{m}_{vapor,TC}[i]$.

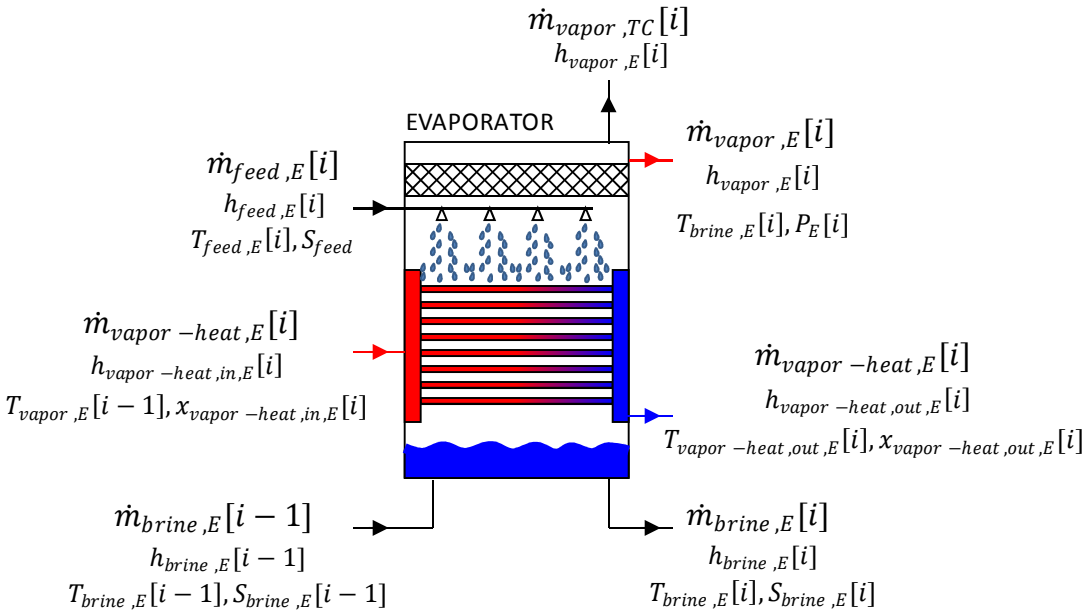

Figure 4 - 5 : Schematic evaporator

The mass, salt, and energy balances in the outside surface of the evaporator heat exchanger (evaporating system) are presented in equations 4-3, 4-4, and 4.5 respectively.

$$\dot{m}_{feed,E}[i] + \dot{m}_{brine,E}[i-1] - \dot{m}_{vapor,E}[i] - \dot{m}_{vapor,TC}[i] - \dot{m}_{brine,E}[i] = 0 \tag{4.3}$$

$$\dot{m}_{feed,E}[i] \cdot S_{feed} + \dot{m}_{brine,E}[i-1] \cdot S_{brine,E}[i-1] - \dot{m}_{brine,E}[i] \cdot S_{brine,E}[i] = 0 \tag{4.4}$$

$$\dot{Q}_E[i] + \dot{m}_{feed,E}[i] \cdot h_{feed,E}[i] + \dot{m}_{brine,E}[i-1] \cdot h_{brine,E}[i-1] - \dot{m}_{vapor,E}[i] \cdot h_{vapor,E}[i] - \dot{m}_{vapor,TC}[i] \cdot h_{vapor,E}[i] - \dot{m}_{brine}[i] \cdot h_{brine,E}[i] = 0 \quad (4.5)$$

The energy balance inside of the pipes of the evaporator heat exchanger (condensing system) is shown in Equation 4.6., where $\dot{Q}_E[i]$ is the heat transfer rate from the condensing system to the evaporating system on the evaporator heat exchanger:

$$\dot{Q}_E[i] = \dot{m}_{vapor-heat,E}[i] \cdot \left(h_{vapor-heat,in,E}[i] - h_{vapor-heat,out,E}[i]\right) \quad (4.6)$$

In the first effect ($i = 1$), $\dot{Q}_E[1]$ is provided by an external source of steam or hot water. From the second effect onward ($i = 2, n$), $\dot{Q}_E[i]$ is provided by condensing fresh water vapor generated from the upstream effect ($i - 1$). Energy balances are based on enthalpies using the temperature, pressure, and quality.

The saturation temperature the seawater or brine depends on its pressure and salt content. At a given pressure, the saturation temperature of the seawater or brine will be elevated slightly with respect to the saturation temperature of pure water; this increment in the saturation temperature is called "boiling point elevation (BPE)" and it is considered in the salt water property functions. Therefore, the saturation temperature of the brine ($T_{brine,E}[i]$) is greater than the saturation temperature of pure water ($T_{vapor,E}[i]$) by the boiling point elevation, which is defined as

$$T_{brine,E}[i] = T_{vapor,E}[i] + BPE_E[i] \tag{4.7}$$

Figure 4-6 shows the variation of BPE as a function of the temperature in the evaporator. The brine is considered to have a salt concentration ($S_{brine,E}$) of 50 [g/kg]. The BPE increases when the temperature in the evaporator increases.

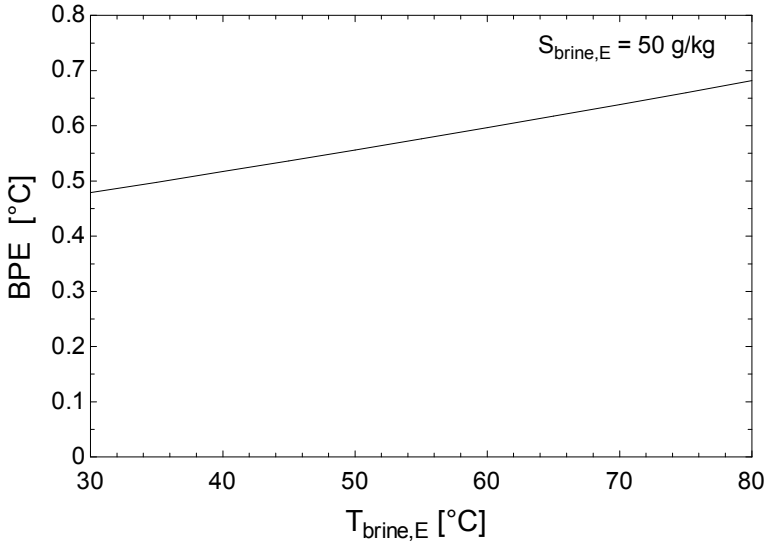

Figure 4 - 6 : BPE as a function of the temperature in the evaporator

The heat transfer rate in the evaporator is modeled assuming phase change on both sides of the heat exchanger, and it is expressed as indicated in equation 4.8:

$$\dot{Q}_E[i] = U_E[i] \cdot A_{tot,E}[i] \cdot \left(T_{avg}[i] - T_{brine,E}[i]\right) \tag{4.8}$$

where $A_{tot,E,i}$ is the total outside surface of the heat exchanger, $T_{brine,E}[i]$ is the temperature in the evaporating side and $T_{avg}[i]$ is the average temperature in the condensing side. $T_{avg}[i]$ is defined as:

$$T_{avg}[i] = T_{vapor-heat,out,E}[i] \; + \; T_{vapor,E}[i-1]$$

(4.9)

$T_{avg}[i]$ is the average between the inlet temperature ($T_{vapor,E}[i-1]$) and the outlet temperature ($T_{vapor-heat,out,E}[i]$) in the tubes of the heat exchanger. The temperature difference between the inlet and the outlet is produced due to the pressure drop in the evaporator tubes while water vapor condenses. The pressure gradient can be determined using the Muller-Steinhagen and Heck correlation (Ould Didi, Kattan, & Thome, 2002) that describes the two-phase frictional pressure gradient as is shown

$$\left(\frac{dp}{dz}\right)_{frict} = Z \cdot (1-x)^{1/3} + b \cdot x^3$$

(4.11)

The pressure drop from inlet to outlet in the tube is determined integrating the pressure gradient.

$$\Delta P = \int_{x_{in}}^{x_{out}} \left(\frac{dp}{dz}\right)_{frict} dx$$

(4.10)

the factor Z is defined as

$$Z = a + 2 \cdot (b - a) \cdot x \tag{4.12}$$

where a is the frictional pressure gradients for all the flow liquid $\left(\frac{dp}{dz}\right)_{Lo}$

$$a = \left(\frac{dp}{dz}\right)_{l} = f_l \cdot \frac{2 \cdot \dot{m}_{total}{}^2}{ID \cdot \rho_L} \tag{4.13}$$

and b is the frictional pressure gradients for all the flow vapor $\left(\frac{dp}{dz}\right)_{Go}$

$$b = \left(\frac{dp}{dz}\right)_{v} = f_v \cdot \frac{2 \cdot \dot{m}_{total}{}^2}{ID \cdot \rho_v} \tag{4.14}$$

The friction factors are obtained using equation 4.15 for a Re_D between 2.1×10^3 and 10^5.

$$f = \frac{0.0791}{Re_D{}^{0.25}} \tag{4.15}$$

with Reynolds number (Re_D) is defined as:

$$Re_D = \frac{\dot{m}_{total} \cdot ID}{\mu} \tag{4.16}$$

using the respective dynamic viscosities of the liquid and vapor.

The overall heat transfer coefficient, $U_{E,i}$, depends on the geometry of the evaporator, on the temperature of the condensing stream, the saturation temperature of each effect, and the fouling factor of the evaporating side. The $U_{E,i}$ is defined as:

$$\frac{1}{U_{E,i} \cdot A_{tot,E,i}} = \frac{1}{\bar{H}_{c,t} \cdot \pi \cdot ID \cdot L_{tube}} + \frac{ln\left(\frac{OD}{ID}\right)}{2 \cdot \pi \cdot k_m \cdot L_{tube}} + \frac{1}{\bar{H}_{b,t} \cdot \pi \cdot OD \cdot L_{tube}} + \frac{R_f''}{\pi \cdot OD \cdot L_{tube}} \tag{4.17}$$

where ID is the inner diameter of the tube, L_{tube} is the total length of the tube, k_m is the conductivity of the tube, and OD is the outer diameter of the tube. The first term expresses the thermal resistance between the water vapor condensing and the inside surface of the tube. The second term shows the thermal resistance of the tube itself the third term represents the thermal resistance between the brine evaporating and the outer tube wall and the fourth term represents the thermal resistance due to fouling using a factor, R_f''.

The average heat transfer coefficient convection between the water vapor condensing and the inside surface of the tube ($\bar{H}_{c,t}$) is determined using a flow condensation correlation suggested by Dobson and Chato (Dobson & Chato, 1998). This correlation defines the local heat transfer coefficient for flow regime wavy or annular depending on the mass flux and the modified Froude number. The local heat transfer coefficient for annular flow is defined as:

$$H = \frac{k_{l,sat}}{ID} \cdot 0.023 \cdot {Re_{D,l}}^{0.8} \cdot {Pr_{l,sat}}^{0.4} \cdot \left(1 + \frac{2.22}{{X_{tt}}^{0.89}}\right)$$

(4.18)

The local heat transfer coefficient for wavy flow is expressed as:

$$H = \frac{k_{l,sat}}{ID} \cdot \left(\left(\frac{0.23}{1 + 1.11 \cdot {X_{tt}}^{0.58}} \right) \left(\frac{G \cdot ID}{\mu_{v,sat}} \right)^{0.12} \left(\frac{\Delta h_{vap}}{c_{l,sat} \cdot (T_{sat} - T_s)} \right)^{0.25} Ga^{0.25} \cdot {Pr_{l,sat}}^{0.25} + AA \cdot Nu_{fc} \right)$$

(4.19)

The annular flow is assumed when the mass flux (G) is greater than 500 [kg/m^2-s], or G is lower than 500 [kg/m^2-s] but the modified Froude number is greater than 20. The mass flux is:

$$G = \frac{4 \cdot \dot{m}}{\pi \cdot ID^2}$$

(4.20)

and the modified Froude number is defined according to:

$$Re_{D,l} \leq 1250 \qquad Fr_{mod} = 0.025 \cdot \frac{{Re_{D,l}}^{1.59}}{Ga^{0.5}} \left(\frac{1 + 1.09 \cdot {X_{tt}}^{0.039}}{X_{tt}} \right)^{1.5}$$

(4.21)

$$Re_{D,l} > 1250 \qquad Fr_{mod} = 1.26 \cdot \frac{{Re_{D,l}}^{1.04}}{Ga^{0.5}} \left(\frac{1 + 1.09 \cdot {X_{tt}}^{0.039}}{X_{tt}} \right)^{1.5}$$

(4.22)

where X_{tt} is the Lockhart Martinelli parameter and $Re_{D,l}$ is the superficial liquid Reynolds number. The Lockhart Martinelli parameter is computed according to:

$$X_{tt} = \sqrt{\frac{\rho_{v,sat}}{\rho_{l,sat}}} \cdot \left(\frac{\mu_{l,sat}}{\mu_{v,sat}} \right)^{0.1} \cdot \left(\frac{(1-x)}{x} \right)^{0.9}$$

(4.23)

where x is the local quality. The superficial liquid Reynolds number is the Reynolds number that is consistent with the liquid flowing alone in the tube.

$$Re_{D,l} = \frac{G \cdot ID \cdot (1-x)}{\mu_{l,sat}}$$

(4.24)

Ga is the Galileo number, defined as:

$$Ga = \frac{g \cdot \rho_{l,sat} \cdot \left(\rho_{l,sat} - \rho_{v,sat} \right) \cdot ID^3}{{\mu_{l,sat}}^2}$$

(4.25)

The parameter AA in equation 4.26 is related to the angle from the top of the tube to the liquid level:

$$AA = \frac{arccos(2 \cdot vf - 1)}{\pi}$$

(4.26)

where vf is the void fraction, the fraction of the volume occupied by vapor, evaluated using the correlation provided by Zivi (Zivi, 1964):

$$vf = \left(1 + \frac{(1-x)}{x}\left(\frac{\rho_{v,sat}}{\rho_{l,sat}}\right)^{2/3}\right)^{-1}$$

(4.27)

The parameter $\mathrm{Nu_{fc}}$ in equation 4.19 is a Nusselt number related to forced convection in the bottom pool, evaluated according to:

$$Nu_{fc} = 0.0195 \cdot {Re_{D,l}}^{0.8} \cdot {Pr_{l,sat}}^{0.4} \sqrt{1.376 + \frac{C_1}{{X_{tt}}^{C_2}}}$$

(4.28)

Parameters C_1 and C_2 in equation 4.28 are evaluated based on the Froude number:

$$Fr = \frac{G^2}{{\rho_{l,sat}}^2 \cdot g \cdot ID}$$

(4.29)

If the Froude number is greater than 0.7 then $C_1 = 7.242$ and $C_2 = 1.655$. Otherwise if Froude number is equal or lower than 0.7 then

$$C_1 = 4.172 + 5.48 \cdot Fr - 1.564 \cdot Fr^2$$

(4.30)

$$C_2 = 1.773 - 0.169 \cdot Fr$$

(4.31)

The average heat transfer coefficient convection between the brine evaporating and the outer tube wall ($\bar{H}_{b,t}$) is determined using the falling thin film correlation suggested by Parken (Parken, Fletcher, Han, & Sernas, 1990). This correlation calculates the boiling heat transfer coefficient for thin water falling film over the outside of horizontal smooth tubes.

$$\bar{H}_{b,t} \left(\frac{\nu^2}{g\, k^3} \right)^{1/3} = 0.00082\, Re^{0.10}\, Pr^{0.65}\, q^{"\,0.40}$$

(4.32)

In this correlation (4.32), Re and Pr are Reynolds and Prandt numbers, respectively, $q^{"}$ is the heat flux, ν is the kinematic viscosity, and k is the thermal conductivity of the seawater. The correlation is valid for 2.54 cm diameter tubes over the following ranges $770 \leq Re \leq 7000$, $1.3 \leq Pr \leq 3.6$, 30 kW/m^2 $\leq q^{"} \leq$ 80 kW/m^2, and 49°C $\leq T \leq$ 127°C. The average convection coefficient, $\bar{h}_{out}$, is influenced by the seawater flow over the tube.

4.1.3.2.Pre-heater

The pre-heater is a shell and tube heat exchanger where a portion of the feed seawater ($\dot{m}_{feed,Ph}[i]$), which has not yet been fed to the downstream effects, is heated by water vapor $\dot{m}_{vapor-heat,E}[i+1]$; consequently, $\dot{m}_{feed,Ph}[i]$ reaches a temperature slightly below the saturation temperature in the evaporator of the same effect. The seawater heated in the pre-heater is divided into two streams: $\dot{m}_{feed,E}[i]$ feeds the evaporator of the same effect, and $\dot{m}_{feed,Ph}[i-1]$ feeds the downstream pre-heater. In the first effect ($i=1$) of a MED plant, $\dot{m}_{vapor-heat,E}[i+1]$ comes only from the evaporator, so that $\dot{m}_{vapor,FB}[i]=0$. From the second effect onward ($i=2,n$) of a MED plant and in each effect ($i=1,n$) of a MED-TC plant, $\dot{m}_{vapor-heat,E}[i+1]$ is formed by mixing the superheated water vapor generated in the evaporator (($\dot{m}_{vapor,FB}[i]$)) and saturated water vapor produced in the flash box ($\dot{m}_{vapor,FB}[i]$) of the same effect.

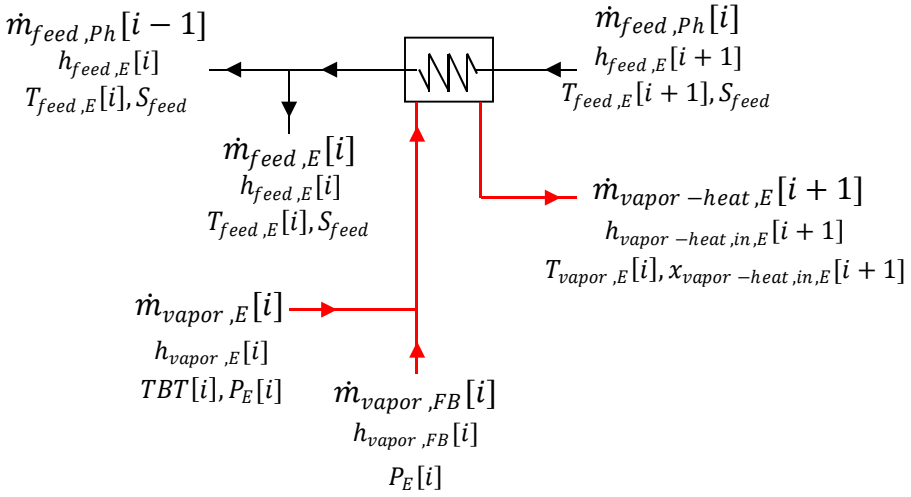

Figure 4 - 7 : Schematic pre-heater

The mass balance in the feed seawater side (cold stream) inside of the pipes in the pre-heater heat exchanger (cold system) is:

$$\dot{m}_{feed,Ph}[i] - \dot{m}_{feed,Ph}[i-1] - \dot{m}_{feed,E}[i] = 0 \tag{4.33}$$

Equation 4.34 shows the mass balance in the water vapor side (hot stream) otsude of the surface of the pre-heater heat exchanger (hot system) is:

$$\dot{m}_{vapor,E}[i] + \dot{m}_{vapor,FB}[i] - \dot{m}_{vapor-heat,E}[i+1] = 0 \tag{4.34}$$

The energy balance in the cold system is:

$$\dot{Q}_{Ph}[i] + \dot{m}_{feed,Ph}[i] \cdot h_{feed,Ph}[i] - \dot{m}_{feed,Ph}[i-1] \cdot h_{feed,Ph}[i-1] - \dot{m}_{feed,E}[i] \cdot h_{feed,E}[i] = 0 \tag{4.35}$$

The energy balance in the hot system is shown in equation 4.36, where $\dot{Q}_{Ph}[i]$ is the heat transfer rate from the hot system to the cold system.

$$\dot{Q}_{Ph}[i] + \dot{m}_{vapor-heat,E}[i+1] \cdot h_{vapor-heat,in,E}[i+1] - \dot{m}_{vapor,E}[i] \cdot h_{vapor,E}[i] - \dot{m}_{vapor,FB}[i] \cdot h_{vapor,FB}[i] = 0 \tag{4.36}$$

In the first effect of the MED plant ($i = 1$), $\dot{Q}_{Ph}[1]$ is only provided by the water vapor generated in the evaporator. From the second effect onward ($i = 2, \dots, n$) of the MED plant and in each effect ($i = 1, 2, \dots, n$) of the MED-TC plant, $\dot{Q}_{Ph}[i]$ is provided by the water vapor produced in both the evaporator and in the flash box. The energy balance is based on enthalpies using the conditions of the pre-heater (temperature, pressure, and quality).

The hot stream (water vapor) in the first section of the heat exchanger enters as superheated steam, and it becomes saturated while advancing through the pre-heater experiencing two-phase conditions in a section of the pre-heater. Consequently, the pre-heater is divided in two sections (Figure 4.8): a superheat section, and a condensing section; therefore, the heat transfer rate in the pre-heater ($\dot{Q}_{Ph}[i]$) is defined as:

$$\dot{Q}_{Ph}[i] = \dot{Q}_{sh,Ph}[i] + \dot{Q}_{sat,Ph}[i] \tag{4.37}$$

Each of the pre-heater sections is modeled as if it were a shell and tube heat exchanger.

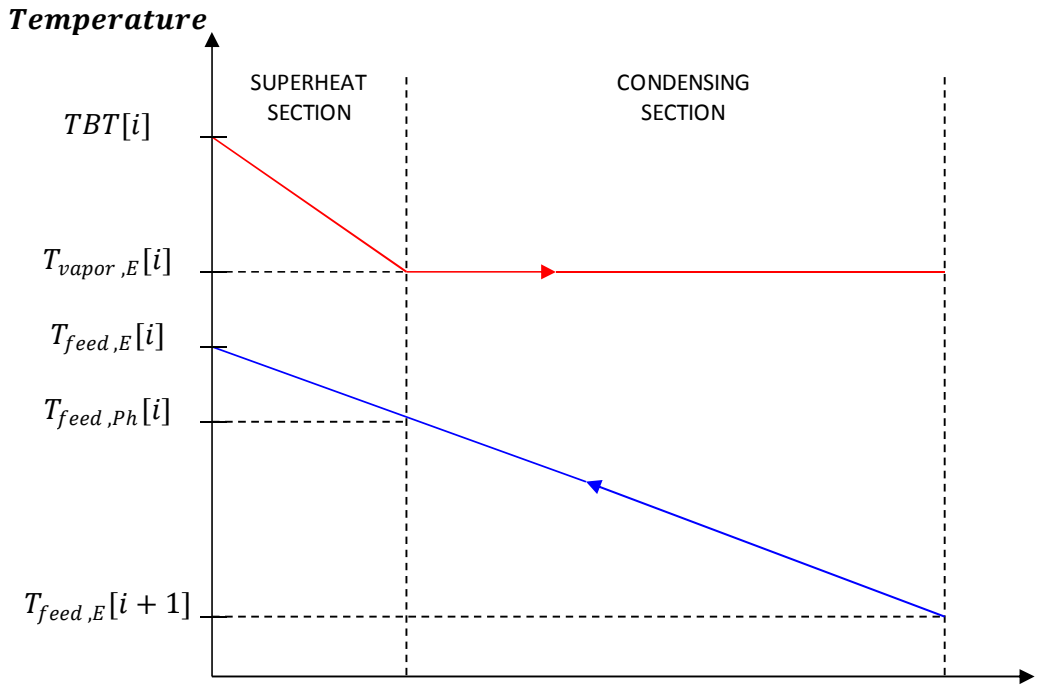

Figure 4 - 8 : Temperature distribution in the pre-heater

Each sub-heat exchanger is solved using the effectiveness-NTU method (Nellis & Klein, 2009), and the calculation process is similar for both sections. The superheat section is developed in detail. The energy balance on the water vapor (hot stream) gives the rate of heat transfer required in the superheat section.

$$\dot{Q}_{sh,Ph}[i] = \dot{m}_{vapor,E}[i] \cdot h_{vapor,E}[i] + \dot{m}_{vapor,FB}[i] \cdot h_{vapor,FB}[i]$$

$$-\dot{m}_{vapor-heat,E}[i+1] \cdot h_{vapor,Ph}[i] \qquad (4.38)$$

The energy balance on the feed seawater (cold stream) is:

$$\dot{Q}_{sh,Ph}[i] = \dot{m}_{feed,Ph}[i] \cdot \left(h_{feed,E}[i] - h_{feed,Ph}[i]\right)$$

(4.39)

The specific heat capacity of water vapor ($\dot{C}_{vapor-heat,sh,Ph}[i]$) is obtained at the average temperature in the superheat section and used to evaluate the capacitance rate of the superheated steam.

$$\dot{C}_{vapor-heat,sh,Ph}[i] = \dot{m}_{vapor-heat,Ph}[i+1] \cdot Cp_{\,vapor-heat,sh,Ph,avg}[i]$$

(4.40)

The specific heat of feed seawater ($Cp_{feed,sh,Ph,avg}[i]$) is obtained at the average temperature in this section, and it is used to calculate the capacitance rate of the feed seawater.

$$\dot{C}_{feed,sh,Ph}[i] = \dot{m}_{feed,Ph}[i] \cdot Cp_{feed,sh,Ph,avg}[i]$$

(4.41)

comparing $\dot{C}_{vapor-heat,sh,Ph}[i]$ and $\dot{C}_{feed,sh,Ph}[i]$ the minimum capacitance rate in the superheat section $\dot{C}_{min,sh,Ph}[i]$ and $\dot{C}_{max,sh,Ph}[i]$ are obtained. The maximum possible heat transfer rate ($\dot{Q}_{sh,Ph,max}[i]$) is defined as:

$$\dot{Q}_{sh,Ph,max}[i] = \dot{C}_{min,sh,Ph}[i] \cdot \left(TBT[i] - T_{feed,Ph}[i]\right)$$

(4.42)

The effectiveness of the superheat section is obtained from:

$$\dot{Q}_{sh,Ph}[i] = \dot{Q}_{sh,Ph,max}[i] \cdot \varepsilon_{sh,Ph}[i]$$

(4.43)

The number of transfer units required in the superheat section, $NTU_{sh,Ph}[i]$, is obtained using the effectiveness-NTU relation for shell and tube heat exchangers (Nellis & Klein, 2009).

$$\varepsilon_{sh,Ph}[i] =$$

$$2\left(1 + C_{R_{sh,Ph}} + \sqrt{1 + {C_{R_{sh,Ph}}}^2} \cdot \frac{1 + exp\left(-NTU_{sh,Ph}[i] \cdot \sqrt{1 + {C_{R_{sh,Ph}}}^2}\right)}{1 - exp\left(-NTU_{sh,Ph}[i] \cdot \sqrt{1 + {C_{R_{sh,Ph}}}^2}\right)}\right)^{-1}$$

(4.44)

where

$$C_{R_{sh,Ph}} = \frac{\dot{C}_{min_{sh,Ph}}}{\dot{C}_{max_{sh,Ph}}}$$

(4.45)

The conductance ($U_{sh,Ph}[i] \cdot A_{tot,sh,Ph}[i]$) required by the superheat section can be computed using $NTU_{sh,Ph}[i]$

$$U_{sh,Ph}[i] \cdot A_{tot,sh,Ph}[i] = \dot{C}_{min,sh,Ph}[i] \cdot NTU_{sh,Ph}[i]$$

(4.46)

The calculated conductance in the superheat section must match the conductance that is required to accomplish the de-superheating process. $A_{tot,E,i}$ is the total outside surface of

the heat exchanger, and $U_{sh,Ph}[i]$ is the overall heat transfer coefficient. $U_{sh,Ph}[i]$ is defined as:

$$\frac{1}{U_{sh,Ph}[i] \cdot A_{tot,sh,Ph}[i]} = \frac{1}{\overline{H}_{in,sh,ph}[i] \cdot \pi \cdot ID \cdot L_{tube}} + \frac{ln\left(\frac{OD}{ID}\right)}{2 \cdot \pi \cdot k_m \cdot L_{tube}}$$

$$+ \frac{1}{\overline{H}_{out,sh,ph}[i] \cdot \pi \cdot OD \cdot L_{tube}} + \frac{R_f''}{\pi \cdot OD \cdot L_{tube}}$$

(4.47)

The first term expresses the thermal resistance between the feed seawater and the inside surface of the tube. The second and fourth terms of equation 4.47 are similar to those explained in the evaporator section. The third term shows the thermal resistance between the water vapor and the outer tube wall.

The average heat transfer coefficient convection between the feed seawater and the inside surface of the tube ($\overline{H}_{in,sh,ph,t}[i]$) is determined using a correlation for turbulent flow in smooth tubes suggested by Gnielinski (Gnielinski, 1976), which provides the local Nusselt number for fully developed turbulent flow (Equation 4.48).

$$Nu_{D,fd} = \frac{\left(\frac{f_{fd}}{8}\right) \cdot (Re_D - 1000) \cdot Pr}{1 + 12.7 \cdot (Pr^{2/3} - 1) \cdot \sqrt{\frac{f_{fd}}{8}}}$$

(4.48)

This equation is valid for Prandtl numbers between 0.5 and 2000, and Reynolds numbers between 2300 and 5 x 10^6. The average Nusselt number is expressed as:

$$\overline{Nu}_D = Nu_{D,fd}\left(1 + \left(\frac{ID}{L}\right)^{0.7}\right)$$

(4.49)

where f_{fd} is the fully developed friction factor. The friction factor for a smooth tube is determined using the Li, Seem, and Li correlation (Li, Seem, & Li, 2011).

$$f_{fd} = 4 \cdot \left(-\frac{0.001570232}{ln\,(Re_D)} + \frac{0.394203137}{ln\,(Re_D)^2} + \frac{2.534153311}{ln\,(Re_D)^3}\right)$$

(4.50)

Finally, the average heat transfer coefficient ($\overline{H}_{in,sh,ph,t}[i]$) convection is determined using equation 4.51.

$$\overline{H}_{in,sh,ph,t}[i] = \frac{\overline{Nu}_D \cdot k}{ID}$$

(4.51)

The average heat transfer coefficient convection between the water vapor and the outer tube wall ($\overline{H}_{out,sh,ph,t}[i]$) is determined using the average Nusselt number for a cylinder in cross flow suggested by Churchill (Churchill & Bernstein, 1977) correlation and Nusselt definition presented in equation 4.51.

$$\overline{Nu}_D = 0.3 + \frac{0.62 \cdot {Re_D}^{0.5} \cdot Pr^{1/3}}{\left(1 + \left(\frac{0.4}{Pr}\right)^{2/3}\right)^{0.25}} \cdot \left(1 + \left(\frac{Re_D}{2.82x10^5}\right)^{0.625}\right)^{0.8}$$

(4.52)

This correlation applies for values of Reynolds numbers between 30 and 1 x 10^8 and Prandtl numbers between 0.7 and 500.

The condensing section is developed in a similar way as the superheat section; however, in the two-phase section, $\dot{C}_{min,sat,Ph}[i]$ is equal to $\dot{C}_{feed,sat,Ph}[i]$ because the capacitance in the water vapor side is infinite while it is condensing. As a consequence of the infinite capacitance of water-vapor in the two-phase section, the capacitance ratio approaches zero, and the equation that provides the number of transfer units is reduced to:

$$\varepsilon_{sat,Ph}[i] = 1 - exp\,(-NTU_{sat,Ph}[i]) \tag{4.53}$$

The average heat transfer coefficient convection between the water vapor and the outer tube wall ($\overline{H}_{out,sat,ph,t}[i]$) in the condensing zone is determined by the means of the correlation for condensation on a single horizontal cylinder proposed by Rohsenow (Rohsenow, Hartnett, & Ganic, 1985).

$$\frac{\overline{h}_{1-tube} \cdot L}{k_{l,sat}} = 0.728 \cdot \left(\frac{\rho_{l,sat} \cdot \left(\rho_{L,sat} - \rho_{v,sat}\right) \cdot g \cdot \left(h_{v,sat} - h_{l,sat}\right) \cdot OD^3}{\mu_{l,sat} \cdot (T_{sat} - T_s) \cdot k_{l,sat}} \right)^{1/4} \tag{4.54}$$

The heat transfer coefficient of film condensation in bundles of tubes takes into account the reduction because the tubes inside the bundle has lower heat transfer coefficient than the coefficient calculated for a single tube (Kakaç & Liu, 1998); therefore, the average heat transfer coefficient for a single tube should be modified based on the number of vertical rows according to:

$$\bar{H}_{out,sat,ph,t}[i] = \bar{h}_{1-tube} \cdot N_{tube,vert}{}^{-1/6} \tag{4.55}$$

4.1.3.3.Flash Box

In a MED plant, there are n-1 flash boxes from the second effect onwards and each is receives condensed fresh water from the outlet (tube-side) of the evaporator. The flash box is assumed to have the same pressure as the corresponding upstream effect (evaporating side). The condensed vapor ($\dot{m}_{vapor-heat,E}[i]$) is directed to the flash box after giving up its heat of condensation in the evaporator. When $\dot{m}_{vapor-heat,E}[i]$ enters in the flash box, a portion of the liquid flashes due to the pressure difference between the condensing side of the evaporator and the flash box. In addition, the flash box receives incoming fresh water coming from the upstream flash box ($\dot{m}_{fw}[i-1]$) that is flashed due to the difference pressure between both flash boxes. A portion of the incoming streams is vaporized due to the change of pressure, and this water vapor ($\dot{m}_{vapor,FB}[i]$) is conducted to the pre-heater. The portion that is not vaporized is directed to the downstream flash box. In each effect of the MED plant, $\dot{m}_{cond,FB}[i] = 0$. In a MED-TC

plant, there are n flash boxes, and in the flash box of the first effect, a portion of the condensed fresh water is directed to the de-superheated and is returned to the boiler that provides the external thermal energy. Figure 4.9 shows the schematic flash box.

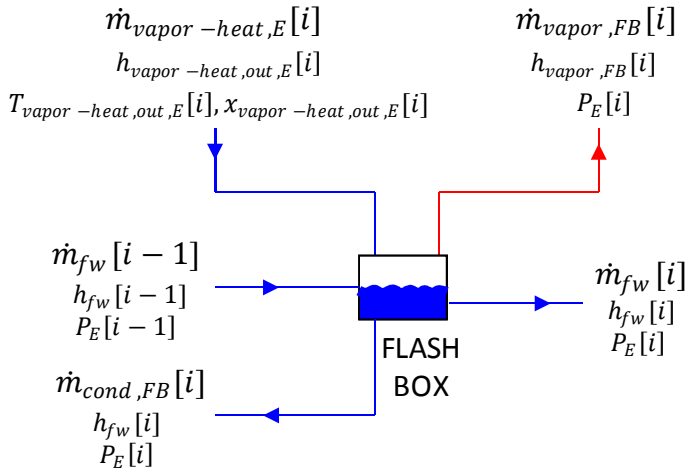

Figure 4 - 9 : Schematic flash box

The mass and energy balances for the flash box (system) are presented in equations 4-56 and 4-57, respectively.

$$\dot{m}_{vapor-heat,E}[i] + \dot{m}_{fw}[i-1] + \dot{m}_{cond,FB}[i] - \dot{m}_{fw}[i] - \dot{m}_{vapor,FB}[i] = 0 \quad (4.56)$$

$$\dot{m}_{vapor-heat,E}[i] \cdot h_{vapor-heat,out,E}[i] + \dot{m}_{fw}[i-1] \cdot h_{fw}[i-1] + \dot{m}_{cond,FB}[i] \cdot h_{fw}[i] - \dot{m}_{fw}[i] \cdot h_{fw}[i] - \dot{m}_{vapor,FB}[i] \cdot h_{vapor,FB}[i] = 0 \quad (4.57)$$

The energy balance in the flash box is based on enthalpies using temperature, pressure, and quality.

4.1.3.4.Condenser

The shell-and-tube condenser has three functions. One is to condense the vapor produced in the evaporator ($\dot{m}_{vapor,E}[n]$) and in the flash box ($\dot{m}_{vapor,FB}[n]$) of the last effect. Another is to preheat the incoming seawater ($\dot{m}_{feed}$), which is directed to the last effect and to the downstream pre-heater. Finally, at the condenser, the pressure of the system is controlled to establish the temperature of the condensation of the vapor. The temperature is controlled by increasing or decreasing the rate of cooling water delivered to the condenser. Figure 4-10 shows the condenser.

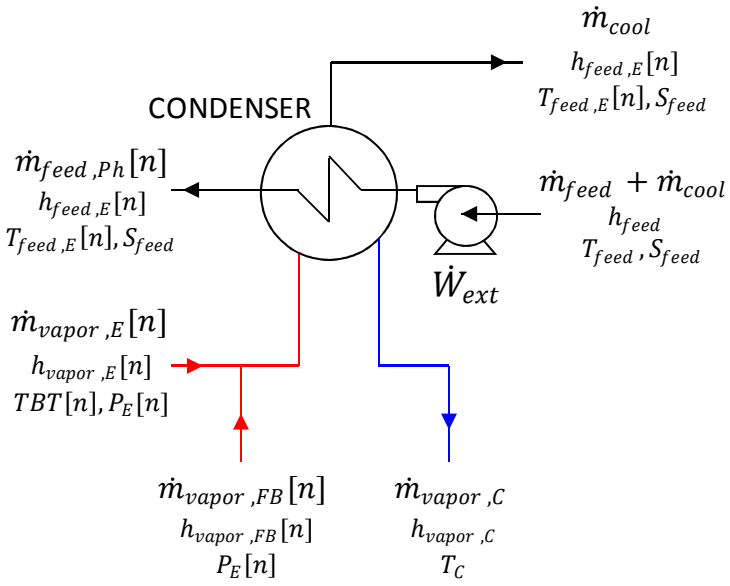

Figure 4 - 10 : Schematic condenser

The mass balance in the feed seawater side (cold stream) inside of the pipes in the condenser heat exchanger (cold system) is:

$$\dot{m}_{feed} + \dot{m}_{cool} = \dot{m}_{feed,Ph}[n] + \dot{m}_{cool} \tag{4.58}$$

Equation 4.59 shows the mass balance in the water vapor side (hot stream) outside of the surface of the condenser heat exchanger (hot system) is:

$$\dot{m}_{vapor,E}[n] + \dot{m}_{vapor,FB}[n] - \dot{m}_{vapor,C} = 0 \tag{4.59}$$

The energy balance in the cold system is:

$$\dot{Q}_C + \dot{m}_{feed} \cdot h_{feed} + \dot{m}_{cool} \cdot h_{feed} - \dot{m}_{feed,Ph}[n] \cdot h_{feed,E}[n] - \dot{m}_{cool} \cdot h_{feed,E}[n] = 0 \tag{4.60}$$

Equation 4.61 shows the energy balance in the hot system, where $\dot{Q}_C$ is the heat transfer rate from the hot system to the cold system.

$$\dot{Q}_C + \dot{m}_{vapor,C} \cdot h_{vapor,C} - \dot{m}_{vapor,E}[n] \cdot h_{vapor,E}[n] - \dot{m}_{vapor,FB}[n] \cdot h_{vapor,FB}[n] = 0 \tag{4.61}$$

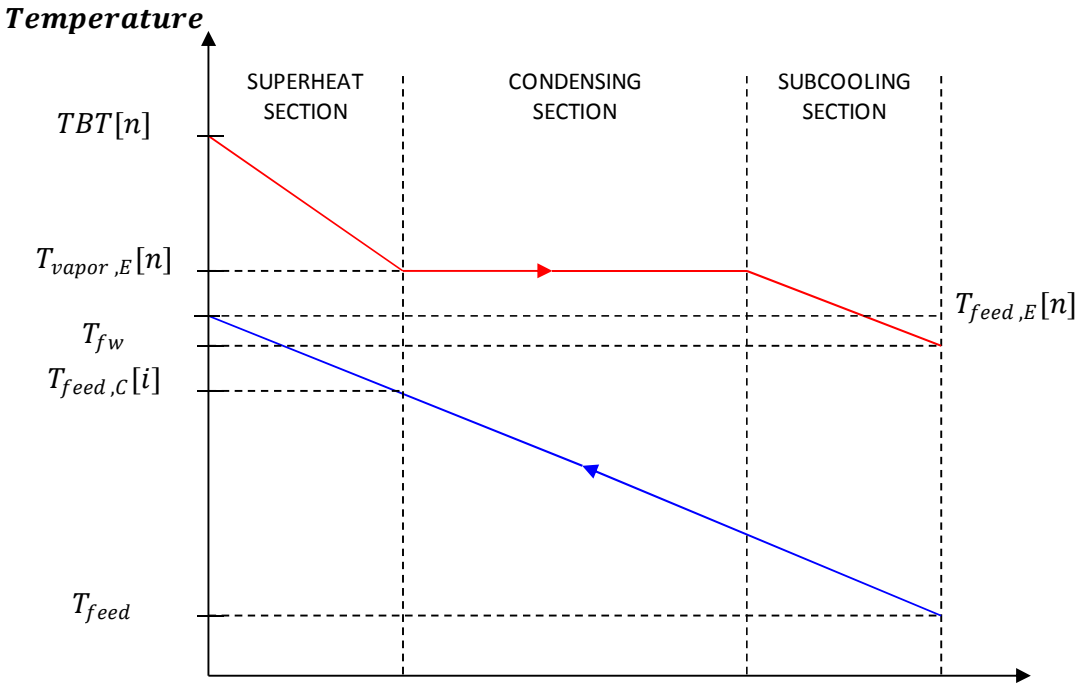

Figure 4 - 11 : Temperature distribution in the condenser

The hot stream (water vapor) in the first section of the heat exchanger enters as superheated steam; it subsequently achieves saturation conditions and condenses while advancing through the condenser, and eventually subcooled water leaves the condenser; consequently, the condenser is divided in three sections (Figure 4.11): a superheat section (sh), a condensing section (sat), and a subcooling section (sc). Therefore, the heat transfer rate in the pre-heater ($\dot{Q}_C$) is defined as:

$$\dot{Q}_C = \dot{Q}_{sh,C} + \dot{Q}_{sat,C} + \dot{Q}_{sc,C} \tag{4.62}$$

Each of the condenser sections is modeled as if it were a shell and tube heat exchanger.

The effectiveness-NTU method is applied to solve each sub-heat exchanger. The calculation process is similar for three sections. The superheat, condensing, and subcooling sections are developed in a similar way to superheat section of the pre-heater (section 4.1.3.2).

4.2. MED-TC model

4.2.1. General description of MED-TC model

In this model, the multi effect desalination model presented in the previous section is combined with a thermo compressor (ejector), and a new model that simulates a multi effect desalination plant with thermal vapor compressor (MED-TC) is created. This model uses the same assumptions as the MED model described in section 4.1. The simplest MED-TC plant considered is comprised of three effects as shown in Figure 4-12.

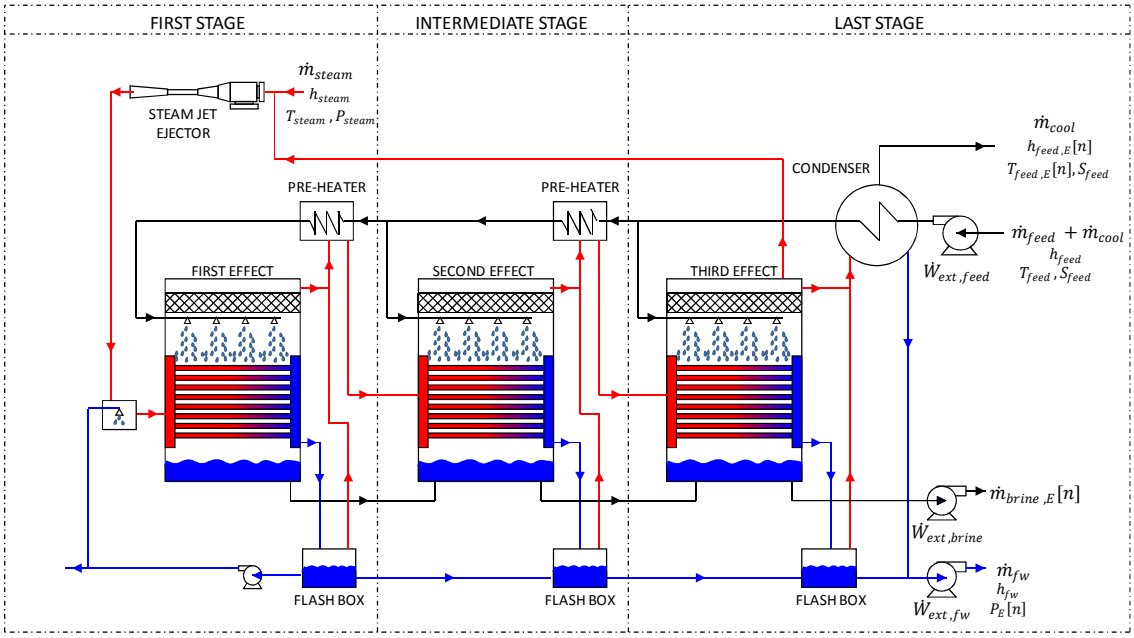

Figure 4 - 12 : Schematic Multi-effect Desalination Plant

The main difference between MED and MED-TC is apparent in the first effect. The first effect received pre-heated seawater, and steam that provides the thermal energy to the process to drive the water purification process. The external source of thermal energy in this plant is supplied by the ejector. The ejector suction is low-pressure water vapor i from one of the effects, which is compressed forming the steam mixture provided in the first effect. The rest of the plant is similar than MED. One to (n-2) intermediate stage follow the first stage, and the last effect is modeled in a separate section where fresh water is delivered from the plant.

The information required by this model includes mass flow rate, temperature and pressure of steam, seawater incoming conditions (temperature and salinity), effect where

the ejector is inducing flow, mass flow rate of feed seawater in each effect, number of effects, dimensions and features of evaporators, pre-heaters and condenser, and temperature of fresh water leaving the plant.

The parameters that the MED-TC model delivers as outputs are the same as provides the MED model. The specific energy consumption (SEC) definition showed in equation 4.2 is similar in MED-TC model

$$SEC\ [kWh/m^3] = \frac{\dot{Q}_{ext} + \dot{W}_{ext,feed} + \dot{W}_{ext,brine} + \dot{W}_{ext,fw}}{\dot{m}_{fw}/\rho} \tag{4.63}$$

where the external heat ($\dot{Q}_{ext}$) provided by the primary steam takes into account the enthalpy difference between the inlet of the ejector ($h_{steam,in}$) and the outlet of the flash box in the first stage ($h_{steam,out}$).

$$\dot{Q}_{ext} = \dot{m}_{steam} \cdot \left(h_{steam,in} - h_{steam,out}\right) \tag{4.64}$$

4.2.2. Stages of MED-TC model

4.2.2.1.First effect of MED-TC model

Figure 4-14 shows the first effect of MED-TC plant. In a MED-TC, the thermal energy is provided using an ejector. Motive steam ($\dot{m}_{steam}$), high pressure superheated steam enters to the ejector and sucks low pressure water vapor ($\dot{m}_{vapor,TC}$) from one of the effect, generally from the last effect; consequently, a superheated steam mixture with

intermediate pressure is formed. This mixture is desuperheated by t adding some fresh water produced in the flash box of the first effect, and saturated steam is obtained that is used as heat source in the first effect. Similar to the MED, the incoming seawater, $\dot{m}_{feed,Ph}[1]$, is preheated by the condenser, by the n-2 preheaters from intermediate stages, and by the preheater in the first effect achieving nearly saturation temperature of the evaporator. The saturated steam flows inside of the tubes of the evaporator, to distill fresh water from incoming seawater, $\dot{m}_{feed,E}[1]$, while it falls down on the outside surface of the tubes. A portion of the incoming seawater is vaporized as a consequence of this heat addition, and water vapor is generated. The saturated steam condenses inside of the tubes and is flashed into the flash box; therefore, a portion of water vapor is produced due to the pressure difference between condensing zone and flash box.

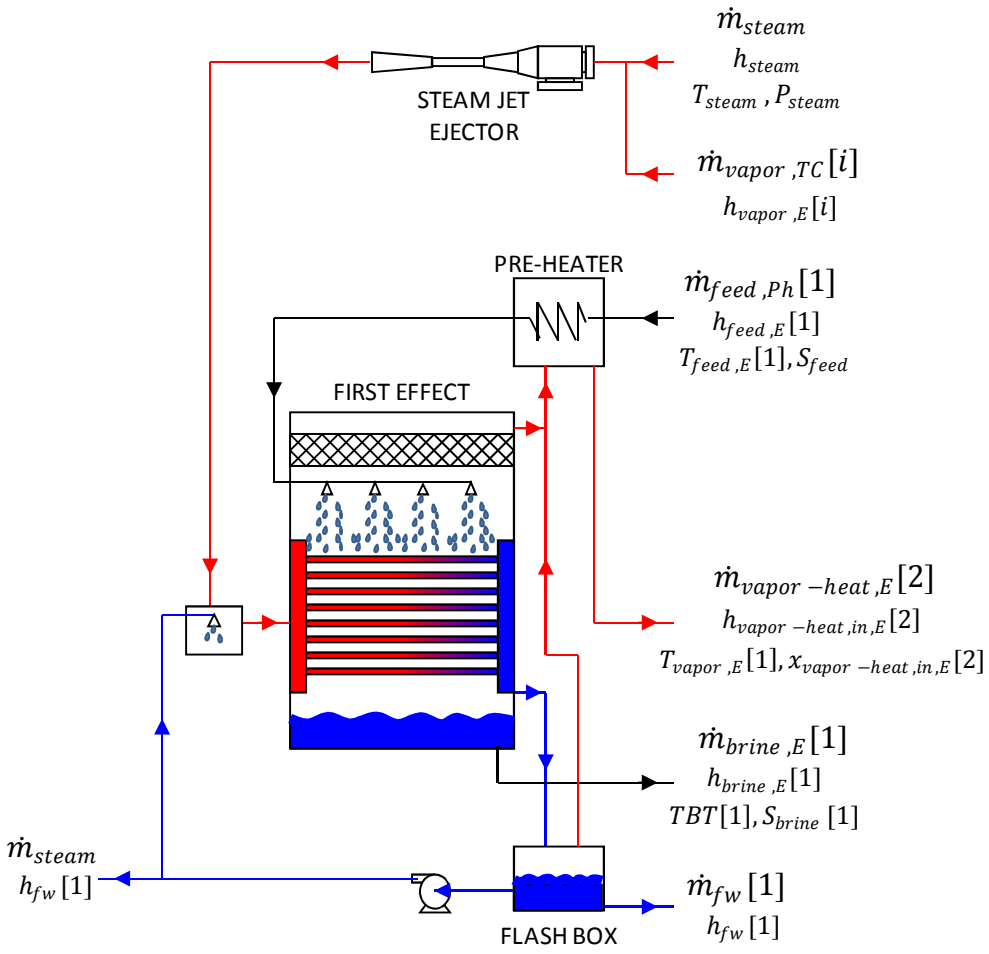

Figure 4 - 13 : Schematic First effect

The water vapor generated in the evaporator is mixed with the water vapor generated in the flash box, and they together, $\dot{m}_{vapor-heat,E}[2]$, flow first through the heat exchanger pre-heater as hot stream and then to the following effect as heat source. The concentrated brine portion of the first effect ($\dot{m}_{brine,E}[1]$) is directed to the chamber of the second effect.

4.2.3. Components of the MED-TC model

4.2.3.1.Ejector

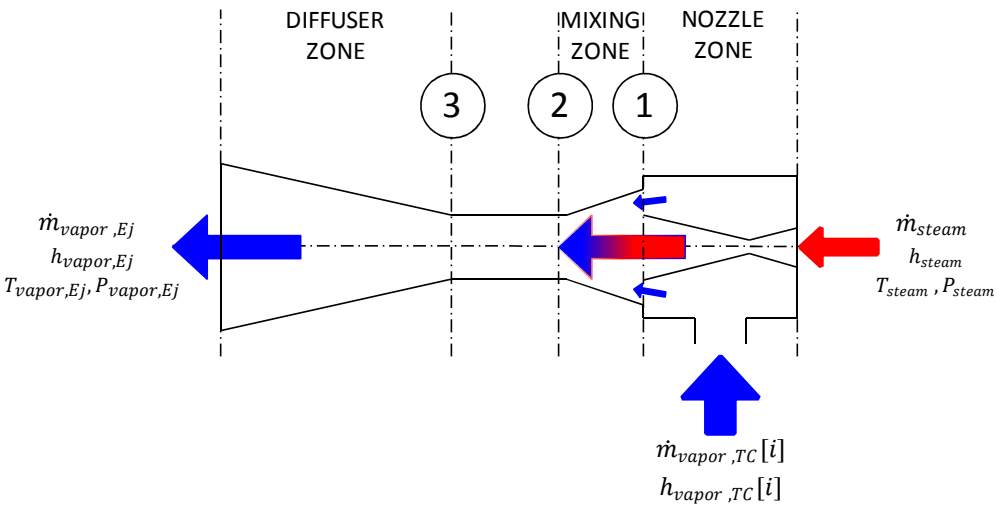

Figure 4 - 14 : Schematic ejector

The high pressure superheated steam or primary steam ($\dot{m}_{steam}$) enters to the primary nozzle expanding and accelerating to supersonic speed through the nozzle; consequently, it creates a low-pressure region at the nozzle exit in the mixing zone due to supersonic speed. The pressure difference between the mixing zone and the secondary steam ($\dot{m}_{vapor,TC}[i]$) inlet drives the secondary steam inside of the ejector. At the beginning of the mixing zone, the primary steam and the secondary steam flow without mixing (section 1 in Figure 4-14). The primary steam expands, diminishing the cross-section area where the secondary steam flows, increasing its speed to sonic value and chokes. After the secondary steam chokes, the two streams, primary and secondary

steam, mix while the primary steam slows down and the secondary steam accelerates (section 2 in Figure 4-14). The pressure of the two streams is uniform at the mixing zone and remains constant until they reach the constant-area tube section ($P_2 = P_1$). In the diffuser zone, the mixture steam reduces the velocity to zero and increases the pressure high enough to cause discharge.

The ejector is simulated using the thermodynamic model proposed by Aly (Aly, Karameldin, & Shamloul, 1999). Aly developed the model applying steady-state equations of energy, momentum and continuity at the nozzle, diffuser and mixing zone to determine the pressure and velocity at each zone. The mass balance is presented in the rate equation 4-65.

$$\dot{m}_{steam} + \dot{m}_{vapor,TC}[i] = \dot{m}_{vapor,Ej} \tag{4.65}$$

In the nozzle section, the energy balance where the primary steam expands through the nozzle with an isentropic efficiency ($\eta_{nozzle} = 0.9$) is shown in equations 4.66 and 4.67.

$$\frac{{V_{steam,1}}^2}{2} = \eta_{nozzle} \cdot \left(h_{steam} - h_{1,is}\right) \tag{4.66}$$

$$h_{steam} - h_1 = \eta_{nozzle} \cdot \left(h_{steam} - h_{1,is}\right) \tag{4.67}$$

The mixing process occurs at constant pressure ($P_2 = P_1$). The pressure in the mixing zone is equal to the vapor pressure, $x_2 = 1$. The momentum conservation in the mixing zone leads to:

$$\dot{m}_{vapor,Ej} \cdot V_2 = \eta_{mixing}\, \dot{m}_{steam}\, V_{steam,1} \tag{4.68}$$

where η_{mixing} is the mixing efficiency, and it is equal to 0.95. The energy balance for this section is presented in equation 4.69.

$$\dot{m}_{vapor,Ej} \cdot \left(h_2 + \frac{{V_2}^2}{2}\right) = \dot{m}_{vapor,TC}[i] \cdot h_{vapor,TC}[i] + \dot{m}_{steam}\left(h_1 + \frac{{V_{steam,1}}^2}{2}\right) \tag{4.69}$$

When the velocity entering in the constant area section is supersonic a normal shock wave occurs. The velocity after shock wave can be expressed

$$V_3 = C_3 \sqrt{\frac{\frac{2}{\gamma - 1} + \frac{{V_2}^2}{{C_2}^2}}{\frac{2\,\gamma \cdot {V_2}^2}{(\gamma - 1) \cdot {C_2}^2} + 1}} \tag{4.70}$$

where the specific heat ratio (γ) is defined as:

$$\gamma = \frac{C_p(T,P)}{C_v(T,P)}$$

(4.71)

The continuity equation before and after shock can be expressed as:

$$\rho_3 = \rho_2 \cdot \frac{V_2}{V_3}$$

(4.72)

and the energy balance may be written as

$$\frac{{V_3}^2}{2} = \eta_{diffuser} \cdot \left(h_{vapor,Ej,is} - h_3\right)$$

(4.73)

In the diffuser zone, the steam mixture passes through the diffuser converting the kinetic energy into pressure energy. The energy balance that represents this phenomenon might be expressed as:

$$h_{vapor,Ej} - h_3 = \eta_{diffuser} \cdot \left(h_{vapor,Ej,is} - h_3\right)$$

(4.74)

where $\eta_{diffuser}$ is the mixing efficiency, and it is equal to 0.9.

4.2.3.2.De-superheated

The de-superheated receives the superheated steam ($\dot{m}_{vapor,Ej}$) generated in the ejector, and mixes with fresh water ($\dot{m}_{dsh}$) coming from the flash box of the first effect. Saturated steam ($\dot{m}_{vapor-heat,E}[1]$) is produced as a result of the mixing of the two incoming streams, and it is supplied as thermal energy source in the first effect.

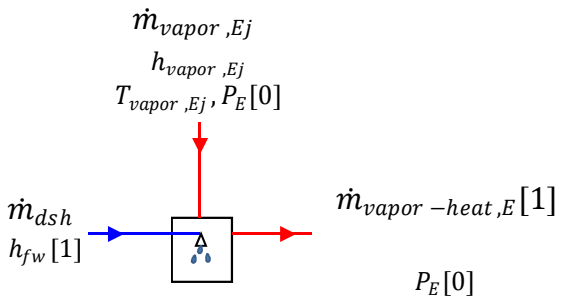

Figure 4 - 15 : Schematic de-superheated

The mass and energy balances in the de-superheated (system) are presented in equations 4-75 and 4-76, respectively.

$$\dot{m}_{dsh} + \dot{m}_{vapor,Ej} - \dot{m}_{vapor-heat,E}[1] = 0 \tag{4.75}$$

$$\dot{m}_{dsh} \cdot h_{fw}[1] + \dot{m}_{vapor,Ej} \cdot h_{vapor,Ej} - \dot{m}_{vapor-heat,E}[1] \cdot h_{vapor-heat,in,E}[1] = 0 \tag{4.76}$$

Chapter 5 : Model validation

5.1. Introduction

The validity of the model is examined in this chapter. The steady state model of the MED-TC desalination plant presented in Chapter 4 is compared against available data from a commercial MED-TC desalination plant located in Bahrain and owned by the Aluminum Bahrain Company (ALBA).

5.2. ALBA MED desalination plant

In 1999, Aluminum Bahrain (ALBA) installed a new MED-TC desalination plant in a petroleum coke calcination facility (de Vries, Froment, & Munro, 2002). Waste heat produced in the calcination process is reused to generate steam in two heat recovery boilers. The steam produced drives the desalination plant that consists of four (4) units and each one produces a nominal output of 124.4 kg/s (10,750 m^3/day) of fresh water with TDS lower than 25 mg/l (de Vries et al., 2002). Each unit has four (4) effects. Effects one (1) and two (2) are composed of two sections (A and B) in parallel, and operate in thermo-compressor mode (Figure 5-1). Each section has two evaporators (1-A and 2-A or 1-B and 2-B) and its own ejector. Effects three (3) and four (4) operate as a conventional MED unit (de Vries et al., 2002).

The feed seawater system consists of three (3) pumps, each with 2,778 kg/s (10,000 m^3/h) capacity, supplying a total flow rate of 5,555 kg/s (20,000 m^3/h) with an additional pump as a backup (de Vries et al., 2002). The total mass flow rate of seawater

demanded by the desalination plant is 3,886.4 kg/s (966.6 kg/s each unit) with the remainder of the total seawater mass flow used for other cooling processes in the calcination plant (de Vries et al., 2002). The feed seawater to the first evaporator in the desalination plant is preheated by 3 successive pre-heaters and the condenser. The first effect pre-heater receives a mixture of steam and non-condensable gases (NCG) from the system for heating the feed seawater and pumping out NCG. Pre-heater two (2) and three (3) receives thermal input by condensing water vapor coming from effect two (2) and three (3), respectively. After being preheated in the condenser, the incoming seawater is divided into two streams: a portion is fed in the last evaporator, and the remaining portion is directed to the next pre-heater. This process is repeated.

The thermal energy required by the desalination process is supplied through two main ejectors with a third ejector used to remove NCG. A total of 16.7 kg/s of high pressure superheated steam at 21 bar and 224°C originates from the two heat recovery boilers and is supplied to all three ejectors (de Vries et al., 2002). Main ejectors installed in this MED plant are reported to have 15% greater efficiency than conventional ejectors (de Vries et al., 2002). Main ejectors induce or draw water vapor from the second effect and mix it with the incoming high-pressure steam. The steam mixture is de-superheated using a portion of fresh water produced in the first effect. Subsequently it enters the evaporator of the first effect where it supplies heat to distillate seawater as it condenses while producing fresh water. A portion of the fresh water produced in the evaporator of the first effect is extracted and recycled to the heat recovery boilers as steam condensate. The water vapor produced in the first effect is used to preheat the feed seawater; afterward, it is directed to the second effect as energy source to drive the distillation

process to produce 24.7 kg/s of water vapor in each section, which feeds into second the effect (de Vries et al., 2002). A portion of the water vapor generated in evaporators 2-A and 2-B goes to the pre-heater and subsequently to the third (3^{rd}) evaporator to produce 13.3 kg/s of water vapor (de Vries et al., 2002). Finally, the water vapor produced in the fourth (4^{th}) effect is condensed in the end condenser.

The system that removes NCG from the plant is formed by an ejector, which receives a portion of high-pressure primary steam to provide a motive force to draw water vapor and NCG from the last section of the condenser. The compressed mixture then condenses in the first pre-heater where NCG are expelled from the system by a small ejector.

The first effect operates at a temperature of 63°C, while the saturation temperature for the vapor at the same pressure is indicated to be 62°C. This means that the BPE at the conditions of the first effect is 1°C. In addition, it is reported the vapor temperatures, at the same pressure of the effect, of effect two (2) and three (3) that are 57°C and 52°C respectively. Moreover, the temperature of the last effect is stated to be 48°C.

Each evaporator of effects one (1) and two (2), sections A and B, has a heat transfer surface of 5,400 m^2 formed by a multiplicity of tubes 22 mm diameter and 7 m length. Evaporators A-1 and A-2 (or B-1 and B-2) are contained in cylindrical shell 5 m diameter by 19.7 m in length (de Vries et al., 2002). Evaporators three (3) and four (4) each have a heat transfer surface area of 2,300 m^2 comprised of a multiplicity of tubes 22

mm diameter and 5 m in length. The tubes are contained in a 4.2 m shell diameter with a total length of 15.4 m (de Vries et al., 2002).

The thermal performance of the ALBA desalination plant is a gain output ratio (GOR) of 7.5. Recall, the GOR is defined as the ratio between the mass flow rate of fresh water and the mass flow rate of high-pressure superheated steam. The specific energy consumption of this plant is 95.4 kWh/kg of fresh water.

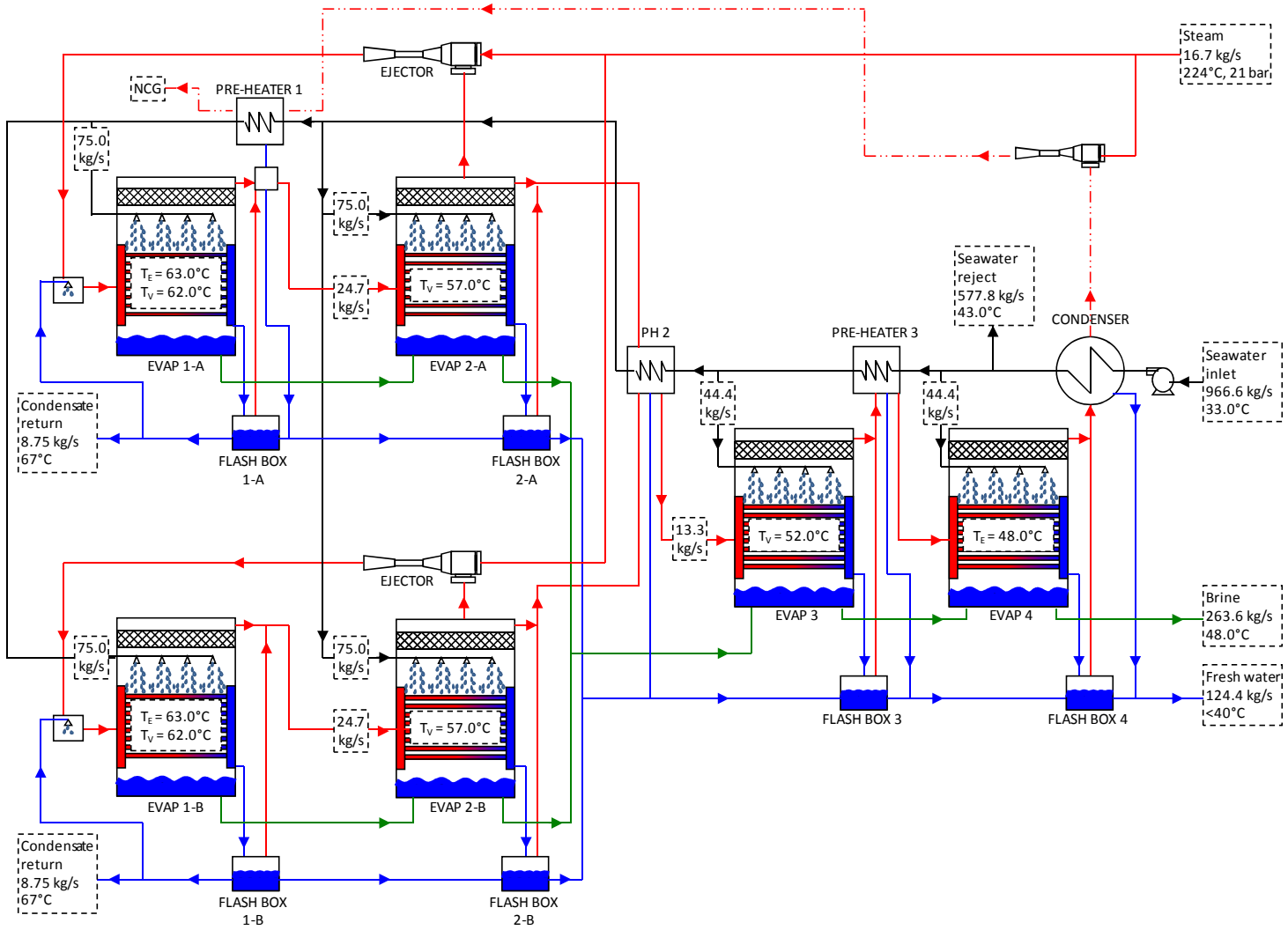

Figure 5 - 1 : ALBA MED-TC plant (de Vries et al., 2002)

5.3. Model results

The MED-TC model presented in Chapter 4 is compared with the available data of the commercial MED-TC plant ALBA, shown in point 5.2, with the intent of validating the MED-TC model. The components of the model are arranged in the same configuration of the ALBA MED-TC as shown in Figure 5-1.

The input data for the model are taken from ALBA MED-TC and shown in Table 5-1. The input data takes into account the following parameters: inlet conditions of seawater (temperature and salinity), mass flow rate of feed seawater to each effect, mass flow rate of cooling seawater, mass flow rate and inlet conditions of steam (pressure and temperature), temperature condensate return, and design features of evaporators (heat transfer surfaces, diameter and length of tubes).

Table 5 - 1 : Input data to the MED-TC

Feed seawater	
temperature (withput preheating)	33 °C
salinity	35 g/kg
mass flow rate effect 1 (section A + B)	150.0 kg/s
mass flow rate effect 2 (section A + B)	150.0 kg/s
mass flow rate effect 3 (section A + B)	44.4 kg/s
mass flow rate effect 4 (section A + B)	44.4 kg/s
Cooling water	
flow rate	602.5 kg/s
Motive steam	
flow rate (section A + B)	16.7 kg/s
pressure	21 bar
temperature	224 °C
Condensate return	
temperature	67 °C
Design features of evaporators	
heat transfer surface evaporators 1 and 2, sections A and B	5400 m^2
heat transfer surface evaporators 3 and 4	2300 m^2
length of tubes evaporators 1 and 2, sections A and B	7 m
length of tubes evaporators 3 and 4	5 m
diameter tubes evaporators 1, 2, 3, and 4	22 mm

The ALBA MED-TC description provided by De Vries et al. (2002) and shown in point 5.2 does not reveal enough information to predict the performance of pre-heaters and the condenser. Consequently, the conductance (UA) in each pre-heater is assumed to be 2,400 kW/°C because this conductance minimizes the difference between the model and the reported data by De Vries et al.. In addition, the mass flow rate of cooling seawater is taken as an input to the model from the data provided to predict the performance of the condenser. DeVries et al., does not explicitly report the seawater salinity; consequently, it is assumed to be 35 g/kg. Although the ejectors installed in ALBA MED-TC are reported to have a 15% greater efficiency compared with

conventional ejectors, the previously developed MED-TC model uses mathematical correlations developed for conventional ejectors. Therefore, the steam mass flow rate drawn from the second effect by the ejector is normalized according to the following expression:

$$\dot{m}_{vapor,TC,Norm}[2] = 1.15 \cdot \dot{m}_{vapor,TC,Model}[2] \tag{5.1}$$

where $\dot{m}_{vapor,TC,Model}[2]$ is the mass flow rate of water vapor drawn by the ejector provided by the model, and $\dot{m}_{vapor,TC,Norm}[2]$ is the mass flow rate of induced water vapor normalized, which includes the effect of 15% greater efficiency. Moreover, the condensate returned is assumed to be equal to the mass flow rate of superheated steam supplied to the MED-TC plant (16.7 kg/s); in contrast, the data reported indicates a greater mass flow rate (17.5 kg/s). Finally, fouling factors are assumed negligible because it is believed that the performance parameters reported comes from a new plant.

The input data that affects the operation of the condenser are: the temperature and salinity of seawater that enters to the condenser are 33°C and 35 g/kg respectively, and the incoming seawater that is composed of feed (388.8 kg/s) and cooling seawater (577.8 kg/s). The mass flow rate of water vapor liquefied in the condenser is 16.9 kg/s. This water comes from the evaporator and the flash box of the fourth effect discounting the water vapor extracted by the NCG ejector; as a result, seawater is heated up to 43.6°C and the cooling stream is released of the plant. The conductance (UA) of the condenser under these conditions is 11,839 kW/°C. After leaving the condenser, feed seawater passes through two pre-heaters raising its temperature as a consequence by a portion of

the water vapor condensing. Water vapor produced in the effect is de-superheated in its pre-heater and subsequent directly to downstream evaporator as heat source; therefore, feed seawater temperature in effect two (2) and three (3) are 48.5°C and 54.7°C, respectively. The first pre-heater heats the feed seawater for the evaporator of the first effect up to 62.3°C while steam coming from the NCG ejector condenses. Each pre-heater has a conductance (UA) of 1,400 kW/°C. The results for pre-heaters and the condenser are shown in Table 5-2.

Table 5 - 2 : Results of MED-TC model for pre-heaters and the condenser

Cooling water	
temperature	43.6 °C
Conductance (UA)	
Pre-heaters (assumption)	2,400 kW/C
Condenser	11,839 kW/C
Temperature feed seawater	
Effect 1	62.3 °C
Effect 2	54.7 °C
Effect 3	48.5 °C
Effect 4	43.6 °C

The most part of total steam (15.7 kg/s) is supplied to main ejectors (7.8 kg/h in each ejector) and draws water vapor from the second effect (28.3 kg/s, normalized value). This steam mixture provides the thermal energy to the evaporator of the first effect. The water vapor drawn into the ejector is compressed increasing its pressure in 1.57 times (CR). The ratio between the steam pressure and the water vapor pressure is 116 (ER), and the ratio between the steam and water vapor mass flow rate is 0.56 (ω), normalized value. The NCG ejector receives 0.94 kg/s of steam inducing almost the same amount of

water vapor from the condenser (ω=1). The CR and ER of this ejector are 2.42 and 222, respectively. The results for ejectors are shown in Table 5-3.

Table 5 - 3 : Results of MED-TC model of ejectors

Main ejector	
Compression ratio (CR)	1.57
Expansion ratio (ER)	116
ω (conventional)	0.64
ω (normalized)	0.56
NCG ejector	
Compression ratio (CR)	2.42
Expansion ratio (ER)	222
ω	1.00

The distillation process is driven by two phenomena. A portion of fresh water vapor is produced by flashing brine as it throttles from the higher pressure upstream evaporator to the successive evaporator that operates at lower pressure. The second mechanism responsible for the production of fresh water vapor is by evaporation of the feed seawater that flows over the outside surface of the evaporator heat exchanger while higher temperature fresh water vapor condenses inside of the pipes of the evaporator's heat exchanger. The overall heat transfer coefficients (U) that control the evaporation process in each evaporator are calculated using the model and shown in Table 5.4 along with other key operating variables. The water vapor produced in each evaporator is slightly superheated because the vapor temperature (at the pressure of the evaporator) is lower than the saturation temperature of the seawater. This temperature difference is

referred to as the *boiling point elevation* (BPE). The BPE is approximately 0.6 °C at these conditions (Table 5-4).

Table 5 - 4 : Results of MED-TC model for evaporators

	Effect 1	*Effect 2*	*Effect 3*	*Effect 4*
Overall heat transfer coefficient (U) - kW/m^2-°C	2.6	2.6	2.8	2.8
Pressure evaporator - kPa	22.9	18.1	13.4	9.5
Temperature evaporator - °C	63.6	58.6	52.2	45.3
Temperature of vapor - °C	63.0	58.0	51.6	44.7
BPE - °C	0.61	0.59	0.57	0.55
Heating water vapor - kg/s	45.2	45.0	14.0	14.0

The metrics that define the performance of MED-TC plant are the thermal efficiency expressed as GOR (7.4) and SEC (96.6 kWh/kg of fresh water), and the rate of fresh water production (122.8 kg/h). Also, the brine rejected by the plant is shown. Table 5-5 show the performance of the MED-TC plant simulated. Key results of the model are presented below in Figure 5-2, the information in black is input data and blue values are outputs.

Table 5 - 5 : System performance

Brine	
flow rate	267.0 kg/s
temperature	45.3 °C
Fresh water production	
flow rate	122.8 kg/s
temperature	38.0 °C
GOR	7.4
SEC	96.6 kWh/m^3

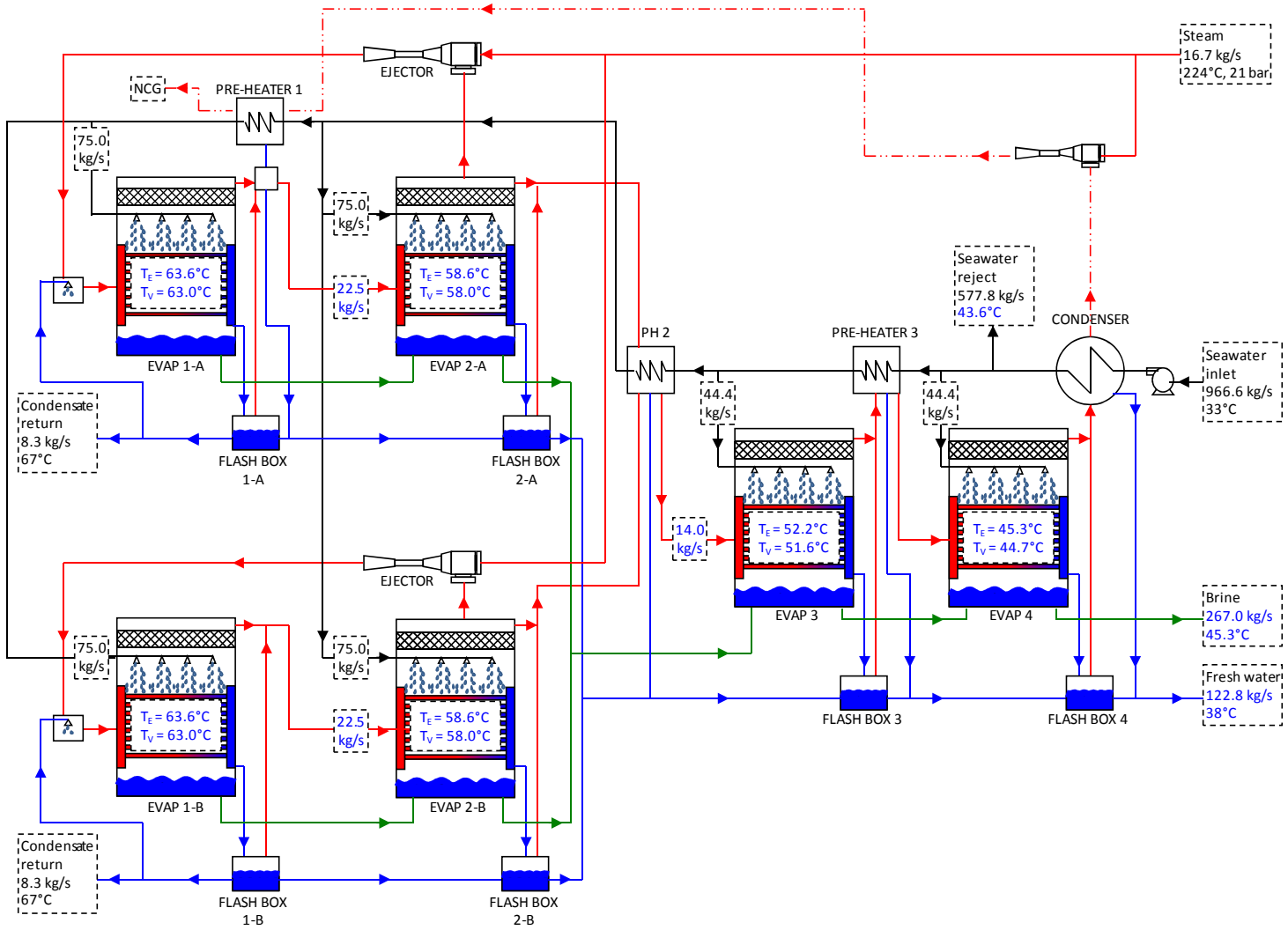

Figure 5 - 2 : MED-TC model

5.4. Validation of the model

The model described in Chapter 4 is used to evaluate the ME-TVC model performance, and its results are compared with the available data of performance of the ALBA MED-TC plant. The model simulates the performance of ALBA MED-TC arranging the same configuration of ALBA showed in Figure 5-1, using as inputs values from the available data from ALBA showed in Table 5-1, and including the assumptions indicated in point 5.2. Table 5-6 presents the comparison between the predicted outputs by the model and the measured outputs from ALBA.

Table 5 - 6 : Comparison of MED-TC model results and data from ALBA MED-TC

	Actual [Vries]	Model	difference
Operating parameters			
water vapor heating			
Effect 1	N.D. kg/s	45.2 kg/s	
Effect 2	49.4 kg/s	45.0 kg/s	-9%
Effect 3	13.3 kg/s	14.0 kg/s	5%
Effect 4	N.D. kg/s	14.0 kg/s	
Temperature evaporator			
Effect 1	63.0 °C	63.6 °C	1%
Effect 2	N.D. °C	58.6 °C	
Effect 3	N.D. °C	52.2 °C	
Effect 4	48.0 °C	45.3 °C	-6%
Vapor tempeerature			
Effect 1	62.0 °C	63.0 °C	2%
Effect 2	57.0 °C	58.0 °C	2%
Effect 3	52.0 °C	51.6 °C	-1%
Effect 4	N.D. °C	44.7 °C	
Cooling water			
temperature	43.0 °C	43.6 °C	1%
Brine			
flow rate	263.6 kg/s	267.0 kg/s	1%
temperature	48 °C	45.3 °C	-6%

N.D.: No Data

In general, the results of the MED-TC model show good agreements with the available measured outputs of ALBA MED-TC. The difference between the values predicted by the model and the values measured are lower than 9%.

The biggest disagreement between the data and simulated results are observed in the mass flow rate of water vapor that provides the thermal energy to drive the distillation process in evaporator of effect two (2). The calculated value is lower in about 9% than

the reported value. This difference may be explained because the mathematical model that predicts the performance of main ejectors underestimates the efficiency of ejectors. This situation can be noted if the mass ratio ω, ω is the mass ratio between steam that enters to the ejector and the water vapor drawn, predicted by the model is compared with the mass ratio ω obtained from Power's graphical data (Power, 1994), which is based in experimental data (see point 3.4, Figure 3-7). The mass ratio (ω) calculated by the model is 0.64 at an expansion ratio (ER) of 116 and a compression ratio (CR) of 1.57. When the Power's graphical data is examined (Figure 3-7) for the same values of CR and ER, mass ratio (ω) is about 0.56 (15% more efficient). In addition, the underestimation in the performance of main ejectors affects other outputs such as water vapor directed to effect three (3), fresh water production, and brine rejection in effect fourth (4^{th}). When main ejector recycles lower amount of water vapor from effect two (2), a greater mass flow rate of water vapor is directed to heat the third effect; consequently, this situation may explained why the mass flow rate calculated is greater in about 5% than the measured value. Also, fresh water production and brine rejected are affected, but with low impact. Comparisons between predicted and reported values of fresh water production and brine rejection show difference of about 1%.

Table 5-6 shows operation temperature of evaporators, vapor temperature corresponding to operation pressure of evaporators, and temperature of cooling water or temperature of feed seawater in effect four (4). Both temperatures in evaporator one (1) have differences lower than 2%. The difference (1°C) between vapor temperature and operation temperature is called BPE, and it seems to be greater than the calculated value and shown in Table 5.4 that is 0.6°C. This difference may be produced because the

salinity of seawater can be greater than 35 g/kg; however, the accuracy of the data does not allow supporting this statement. Also, in vapor temperatures of evaporators two (2) and three (3) difference lower than 2% are noted. However, the last effect presents a greater difference of about 5% between operation temperature predicted and measured. This difference is caused by a greater drop pressure in the last evaporator that produces a greater temperature difference of 2°C (in other effects the temperature difference is lower than 1°C) between the inlet and the outlet. Consequently, the average temperature in the hot side of the evaporator is reduced driving the operation temperature of the evaporator (cold side) to a lower value. The reason, which might explain a greater pressure drop in this effect, could be a greater mass flow rate of water vapor due to the reduction of recycled water vapor in effect 2. Finally, reported and calculated temperatures of cooling water leaving the plant show a difference of about 1%. Small temperature differences observed in Table 5-6 might be explained for several reasons such as underestimation or overestimation of heat transfer coefficients, overestimation of drop pressures, and not enough accurate in the instruments used to measure the reported data.

Table 5-7 shows the comparison between the performance parameters of the plant calculated and measured. The results of the MED-TC model show good agreements with the available measured outputs of ALBA MED-TC noting differences of about 1% between model and real plant. Even though some intermediate results shown in table 5-6 have notable differences between the predicted and the real situation, the performance parameter shows a good agreement because the lower production of water vapor in some section of the plant is compensated for a greater production of water vapor in other section with lower impact in the efficiency of the plant.

Table 5 - 7 : Comparison of MED-TC model results and data from ALBA MED-TC

	Actual [Vries]	Model	difference
System performance			
Fresh water production	124.4 kg/s	122.8 kg/s	-1%
GOR	7.5	7.4	-1%
SEC	95.4 kWh/m^3	96.6 kWh/m^3	1%

Chapter 6 : Solar steam generation plant

6.1. Plant description

The MED-TC desalination plant described in Chapter 5 uses high pressure steam to drive the distillation process. The steam used by the desalination plant can be provided by several sources such as directly from a boiler, from the steam turbine of a power plant, or directly from a solar field. Because one of the objectives of this project is to drive the distillation plant using thermal from a solar energy source, a solar steam generation plant is modeled using TRaNsient SYstems Simulation (TRNSYS) and the integrated performance of both the solar system and the distillation plant working together is analyzed. Figure 6-1 shows the schematic diagram of the solar steam generation plant coupled with the MED-TC plant.

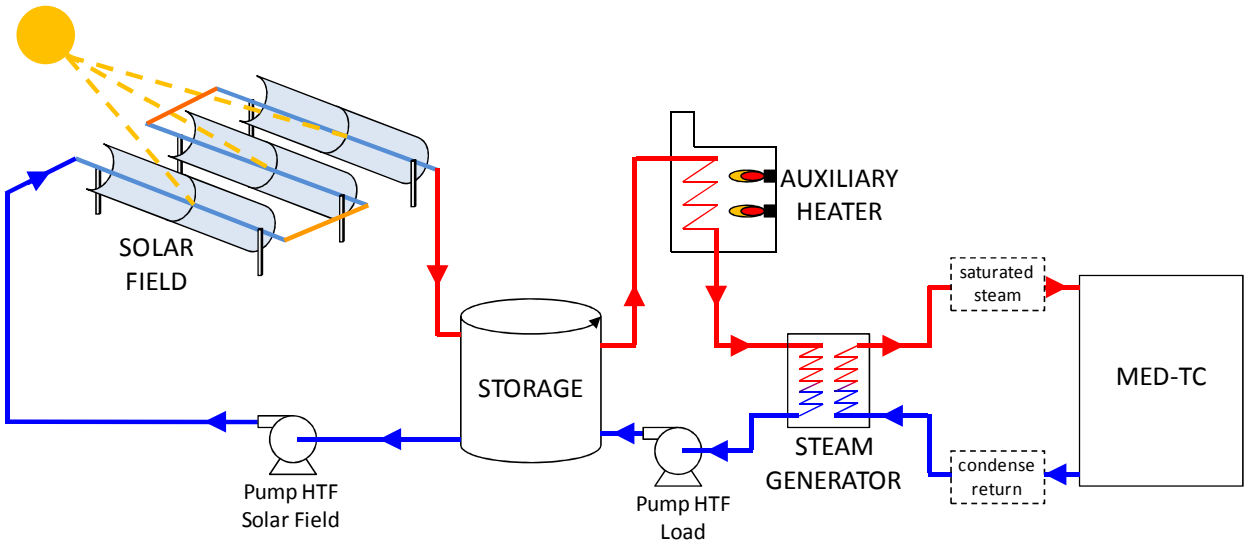

Figure 6 - 1 : Schematic diagram of the solar steam generation plant coupled with the MED-TC plant

The solar steam generation plant is formed by a solar field, a storage tank, an auxiliary heater, and a steam generator. Two independent loops join these components. One is called the source loop that connects the storage tank, the solar field, and return back to the storage tank. The other loop is named load loop, and it connects the storage tank, the auxiliary heater, the steam generator, and return back to the storage tank. The heat transfer fluid (HTF) selected that moves through these loops is Therminol VP-1; and properties of this fluid are provided in Appendix C. In the source loop, the HTF is pumped from the bottom zone of the storage tank to the solar field. The solar field consists of a large number of single axis tracking parabolic trough solar collectors, which are arranged in series and in parallel. In the solar field, cold HTF is distributed through solar collectors and heated by the solar radiation absorbed by solar collectors. The HTF absorbs concentrated solar radiation when it passes through heat collection elements, located in the focal line of each parabolic trough. Hot HTF goes back to the top of the storage tanks where thermal energy is accumulated. The HTF, which flows through the source loop, is temperature controlled by the use of a variable speed pump. The pump works only when enough energy is received in solar collectors to supply hotter water to the top of the storage tank. Once the pump turns on, the flow rate is regulated to maintain a minimum temperature (T_{SP}) at the inlet of the storage tank; consequently the stratification in the storage tank is maintained. T_{SP} is the temperature set point, which is defined as the sum of the saturation temperature of the steam (T_{sat}), the pinch point (PP), and the temperature difference in the load loop (ΔT), see section 6.9.2. In the load

loop, hot HTF is pumped from the top of the storage tank to the auxiliary heater. The auxiliary heater turns on when the HTF coming from the storage tank has a lower temperature than T_{SP}, minimum temperature required by the HTF at the inlet of the steam generator, providing the sufficient energy to the HTF using natural gas as fuel. The steam generator is formed by a pre-heater and a boiler where the HTF is cooled first in the boiler and subsequently in the pre-heater supplying the thermal energy to produce the total steam necessary in the desalination plant. The condensate that returns from the desalination plant enters the pre-heater at a temperature between 63°C and 73°C and leaves the boiler as a saturated steam; both condensate return temperature and steam saturation temperature depends of the steam pressure provided to the desalination plant. The cold HTF is pumped back to the bottom section of the storage tank. The variable speed pump in the load loop controls the flow rate HTF according to the temperature supply at the inlet of the steam generator. When the temperature supply to the steam generator is equal to the T_{SP}, the mass flow rate of the HTF is maximum and leaves the steam generator with a known temperature ($T_{out,SG}$). If the temperature supplies to the steam generator is greater than the T_{SP}, the mass flow rate of HTF is reduced to maintain constant the output temperature ($T_{out,SG}$) of the steam generator. A TRNSYS system schematic for the solar steam generation plant is shown in Figure 6-2.

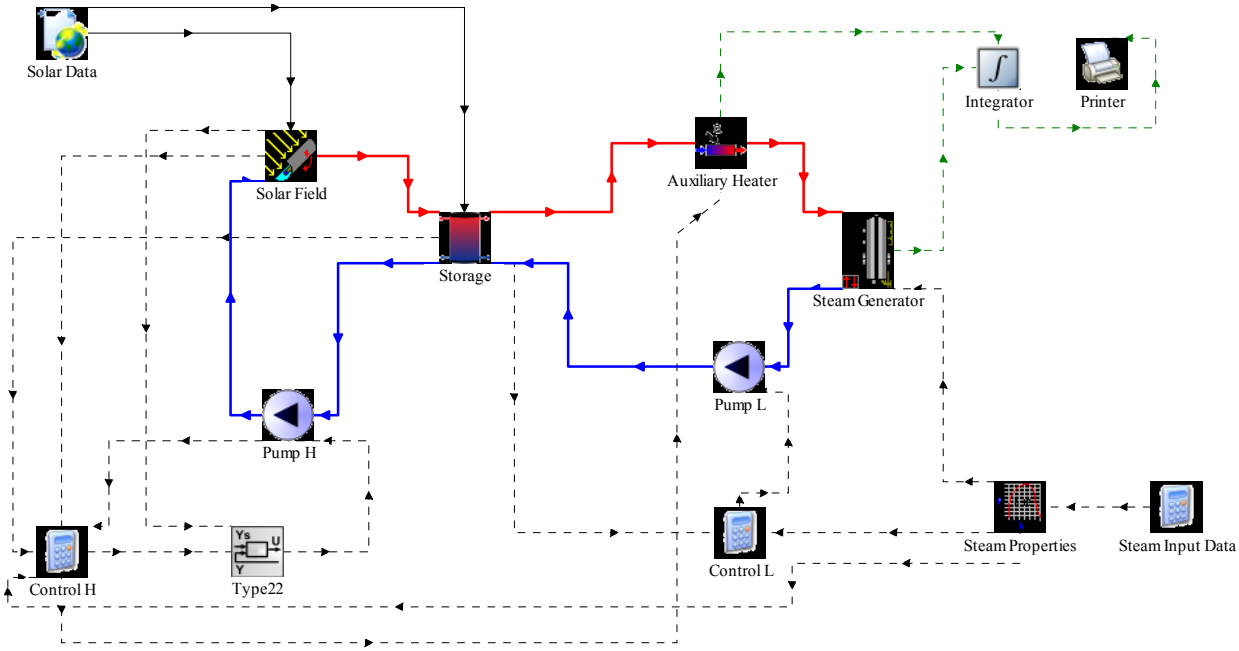

Figure 6 - 2 : Solar steam generation plant

Components of the solar steam generation plant are described in further detail in the following sections. As well calculations of absorbed solar radiation and solar field outlet temperature are explained.

The main results of the solar steam generation plant are the efficiency of the solar field and the fraction of energy provided from solar energy to the desalination plant as a function of collector surface area, collector arrangement, ratio of storage tank versus collector surface, pressure of steam supplied to the desalination plant, and axis of tracking.

6.2. Load

The MED-TC desalination plant described in Chapter 5 is coupled with the steam generation plant described above (section 6.1). The desalination plant operates 24 hours per day and 365 days per year, and it requires a constant supply of saturated steam at a mass flow rate that is a function of the pressure of the steam supplied, as indicated in table 6-1. The steam pressure affects the desalination plant performance, and these effects are analyzed. The desalination plant production is designed to produce 10,800 metric tons of fresh water per day (10,800,000 kg/day or 125 kg/s) to be consistent with the fresh water production of the reference plant. The performance of the distillation plant is tested by supplying saturated steam as thermal energy at a pressure of 1,600 kPa, at 2,100 kPa, and 2,600 kPa. Pressure testing conditions above and below the plant's design point are chosen to analyze the effects on the desalination plant performance. The plant was designed to operate with superheated steam supplied at a pressure 2,100 kPa. When the steam pressure is varied, the pressure of the steam mixture after the ejector changes; thereby, modifying the temperature at which thermal energy is provided to the evaporator comprising the first effect. As a consequence, the first effect temperature changes as well as the temperature that the steam condensate returns to the steam generation plant. If the temperature of the thermal source in the first effect is altered, the temperature of each effect changes varying the point of operation and the performance of each effect; therefore, the steam required to produce the fresh water required also changes. Table 6-1 shows the performance of the desalination plant as a function of the

pressure of the saturated steam necessary to produce 10,800 metric tons of fresh water per day.

Table 6 - 1 : Performance of desalination plant as a function of steam pressure to produce 10,800 ton per day of fresh water

Fresh water production	Steam		Condensate return	GOR	SEC
	Pressure	mass flow rate	Temperature		
ton/day	kPa	kg/h	°C		kWh/m^3
10800	1600	55425	62	8.12	87.4
10800	2100	54300	67	8.29	85.1
10800	2600	52700	72	8.54	82.1

1 ton = 1000 kg

When the desalination plant receives the saturated steam at 1,600 kPa, the temperature in the first effect is reduced diminishing the performance of the plant by 2.7% compared to the design supply pressure of 2,100 kPa. When the saturated steam supply pressure is increased to 2,600 kPa, the temperature in the first effect rises and the plant performance increases by 3.5% compared to the design point pressure of 2,100 kPa.

6.3. Location

Both desalination and solar steam generation plants are assumed to be located in the city of Antofagasta (II Region), Chile. Chile sits along the southwest Pacific Ocean coast of South America. The climate in Chile varies from subtropical in the north to polar in the south (Cáceres, Gruttner, & Contreras, 1992). Antofagasta is a port located in the II Region on the north of the Pacific coast of Chile (1,361 km north from Santiago, Capital of Chile) and surrounded by one of the most arid desert in the world. The climate in this Region (II) varies from moderate subtropical in the coast to alpine in the Andes (Cáceres et al., 1992). The geographical coordinates of the city are -23.65° latitude (ϕ), -70.4° longitude. The average elevation of the Antofagasta city is 276 meters.

The II Region has a surface of 125,305 km^2. The known sources of fresh water in the Region have a total flow of about 12,400 liters per second, 60% is found in a few rivers and 40% is underground (Cáceres et al., 1992). Only a small amount of the available fresh water can be used for human activities because much of the water contains high concentration of salt and/or arsenic (Cáceres et al., 1992). In general, rivers do not reach the coast, and coast cities such as Antofagasta are supplied of water by the means of pipelines coming from the Andes Mountains.

Mining constitutes the main economic activity of the country. Copper is the mining activity most important, and it is followed for other non-metallic mining activities. Copper and non-metallic mines are located mainly in the II Region, same region than Antofagasta. The development of mining projects is continuously growing affecting the water availability because the rapid growth of population in a few close

cities to the industrial projects and new mining projects increases the demand of fresh water. Therefore, the city of Antofagasta that has a population of 360,000 inhabitants (National Institute of Statistics (INE), 2009) will face a shortage of fresh water.

The II Region is characterized by clear skies most of the time and high solar radiation level. Figure 6-3 shows the monthly average solar radiation in horizontal surface in Antofagasta, Chile.

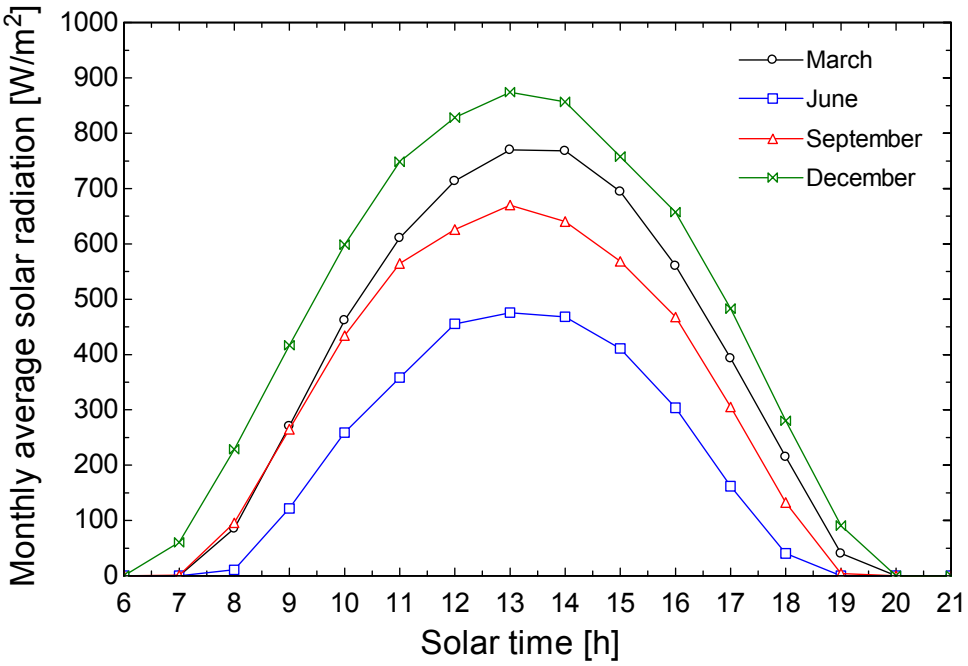

Figure 6 - 3 : Monthly average solar radiation in horizontal surface in Antofagasta, Chile

Levels of solar radiation in the Region of Atacama Desert are very high, making this an ideal application of solar thermal technology.

In conclusion, the city of Antofagasta and the mining projects that surround it face scarcity of water due to the desert climate, with minimal rainfall. Cities and mining industry relies on water, and achieving a solution for the water scarcity in the Region is a challenge. Consequently, the installation of a desalination plant driven by solar thermal energy seems to be a suitable alternative to solve the water shortage and use the high quality solar resource available in this Region.

6.4. Collector arrangement

The solar field is formed by a large number of parabolic trough solar collectors arranged in series and in parallel. The number of collectors in series is identified as N_s, and the number of collectors in parallel is N_p. The solar collectors in series form a row of twenty (20) collectors together ($N_s = 20$). The HTF enters at the first collector of the row and comes out in the 20th collector of the row while its temperature increases gradually in each collector. The number of row or N_p depends of the number of collectors used in the solar field.

The maximum flow rate that flows through a row is calculated assuming a velocity of 2 [m/s] inside of the absorber pipe (OD = 25 mm) to get a reasonable pressure drop. The calculated flow rate is 42 liters per minute per row. The pressure drop through the collectors is 2.8 [bar] for this configuration, which seems to be a reasonable value. As a consequence, the maximum pumping power in the source loop is shown in Table 6-2 assuming a pump efficiency of 60%.

Table 6 - 2 : Maximum pump power, mass flow rate and pressure drop as a function of number of collectors.

Total number of collectors	Number of in series collectors	Number of in parallel collectors	Mass flow rate HTF (source loop) kg/s	Pressure drop kPa	Maximum Pump Power kW
25000	20	1250	17500	276	396
50000	20	2500	35000	276	792
75000	20	3750	52500	276	1188
100000	20	5000	70000	276	1584

6.5. Parabolic trough solar collector

The solar collector used in the solar field is a linear parabolic trough, which is generally used in high temperature applications. The linear parabolic trough solar collector is formed by a parabola made of highly reflective material and a long evacuated tube located in the focal line of the parabola (Figures 6-4 and 6-5). The solar energy received in the parabola is concentrated and directed to the evacuated tube carrying heat transfer fluid, which is heated by absorbed the concentrated solar energy received on the outside surface of the tube. The useful energy output in the parabolic trough collector is dictated by the incident beam radiation on the aperture area of the collector, diffuse radiation is taken into account only when the collector has low concentration ratio (C), C is the ratio of the area of aperture to the area of the receiver (Duffie & Beckman, 2006).

Consequently, the reflector is often tracked so that beam radiation is maximized. The collector can be oriented along both east-west axis and north-south axis. When the collector is oriented along east west axis, it is placed horizontal to the plane of the ground. Figure 6-4 shows a parabolic trough oriented along east-west axis.

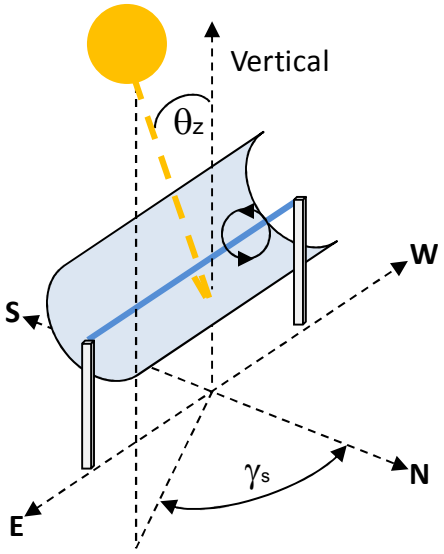

Figure 6 - 4 : A parabolic trough oriented along east-west axis

If the trough collector it is tracked about a north-south axis, it may have a plane tilted with respect to the ground. Figure 6-5 shows a parabolic trough oriented along north-south axis.

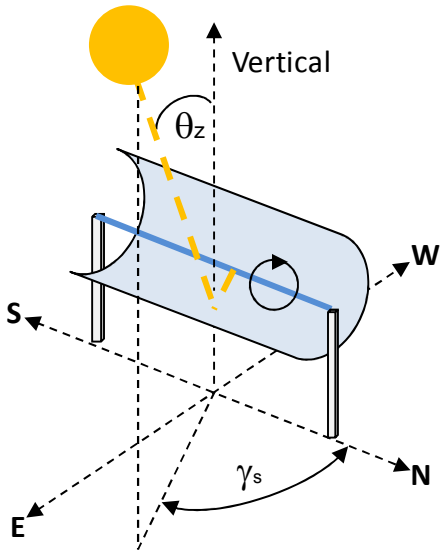

Figure 6 - 5 : A parabolic trough oriented along north-south axis

The effects of both east-west and north-south axis orientations in steam generation are analyzed. Thermal losses from parabolic trough collectors occur only from the absorbing surface which has comparatively small area and high temperature than other collectors (Duffie & Beckman, 2006).

The concentrating solar collector performance is simulated using TRNSYS Type 536. The collector performance depends of collector parameters, configuration of collectors, correction factors due to flow rate (R_1) and number of collector in series (R_2), ambient (T_a) and inlet (T_i) temperatures, and incident beam radiation ($I_{b,T}$). The collector performance equation is defined as (Duffie & Beckman, 2006):

$$\dot{Q}_u = R_1\, R_2\, A_a\, N_p\, N_s \left[F_R(\tau\alpha)_n\, IAM\, I_{b,T} - \frac{F_R U_L}{C}\,(T_i - T_a)\right] \tag{6.1}$$

The relevant collector parameters are: Concentration ratio (C), the intercept efficiency ($F_R(\tau\alpha)_n$), the efficiency slope ($F_R U_L$), incidence angle modifier (*IAM*), and aperture area (A_a). The configuration of collectors in the solar field is defined by the number of collector in series (N_s) and in parallel (N_p).

The temperature of the heat transfer fluid increases as it absorbs solar energy (Q_u) while flowing through the solar field. The outlet temperature (T_{out}) of HTF at the collector is given by equation 6.2 (Duffie & Beckman, 2006).

$$T_{out} = T_{in} + \frac{Q_u}{\dot{m}_H \, Cp_{HTF}} \tag{6.2}$$

where $\dot{m}_{HTF}$ is the mass flow rate of HTF, Cp_{HTF} is the specific heat of HTF.

6.5.1. Parabolic trough solar collector parameters

$F_R(\tau\alpha)_n$, characterizes the energy absorbed in the collector. It represents the fraction of the incident energy received by the collector to the energy actually absorbed. In most concentrating collectors the intercept efficiency ranges from 0.9 to 1.0. $F_R U_L$ is the slope of the collector efficiency curve, and it is used to correlate heat losses from the collector. Additional losses occur when the angle of incidence increases as consequence of additional reflection and absorption in the glass cover. The incidence angle modifier (*IAM*) takes into account the effects of the variation of the angle of incidence and corrects for these additional reflection and absorption losses. In parabolic trough solar collectors, only a dimensional *IAM* is necessary because these kinds of collectors has an axis of

symmetry and are often installed such that they track beam radiation throughout the day (Duffie & Beckman, 2006). These three parameters are given as an empirical fit to experimental data for a given collector type.

For this project, parabolic trough solar collector model SopoNova 4.1 made by Sopogy, Inc. are chosen. The more important collector parameters are presented in Table 6-1. The variation of the incidence angle modifier (*IAM*) is shown versus the incidence angle. The solar collector certification for these collectors is shown in Appendix D.

Table 6 - 3 : Collector parameters (Solar Rating and Certification Corporation, 2011)

Collector parameters		
Collector specifications		
Gross area	6.712	m^2
Aperture area - A_a	5.384	m^2
Concentration ratio - C	61	
Gross length	4.105	m
Test conditions		
Test flow rate - $\dot{m}_t$	0.173	kg/s
Collector technical information		
Collector efficiency factor - $F_R(\tau\alpha)_n$	0.5897	
Collector heat loss coefficient - $F_R U_L$	0.9317	W/m^2-K
Transverse incident angle modifier - IAM		
10°	0.997	°
20°	0.985	°
30°	0.932	°
40°	0.782	°
50°	0.661	°
60°	0.496	°
70°	0.378	°

6.5.2. Correction factors

Collector parameters are obtained at test conditions and when the collector is to be used at a flow rate other than that of the test conditions, correction factors should be applied to $F_R(\tau\alpha)_n$ and $F_R U_L$. R_1 is the flow rate correction factor, and it is defined as (Duffie & Beckman, 2006):

$$R_1 = \frac{N_s \frac{\dot{m}_{HTF}}{N_p} Cp_{HTF}}{A_a} \left[\frac{1 - e^{\left(-F' U_L A_a / \left(N_s \frac{\dot{m}_{HTF}}{N_p} Cp_f C\right)\right)}}{R_{test}} \right] \tag{6.3}$$

where R_{test} is (Duffie & Beckman, 2006)

$$R_{test} = \frac{\dot{m}_t Cp_f}{A_a} \left(1 - e^{\left(-F' U_L A_a / (\dot{m}_t Cp_f C)\right)}\right) \tag{6.4}$$

$F'U_L$ is estimated for the test conditions according to (Duffie & Beckman, 2006):

$$if \;\; F_R U_L \geq \frac{\frac{\dot{m}_f}{N_p} Cp_f C}{A_a}$$

$$F' U_L = F_R U_L \tag{6.5}$$

$$or\ if\ \ F_R U_L < \frac{\frac{\dot{m}_f}{N_p}\ Cp_f\ C}{A_a}$$

$$F' U_L = -\frac{\dot{m}_t\ Cp_f\ C}{A_a}\ ln\left(1 - \frac{F_R U_L\ A_a}{\dot{m}_t\ Cp_f\ C}\right)$$

(6.6)

R_2 is the correction factor that takes into account the number of collector in series (Duffie & Beckman, 2006), and it is defined as:

$$R_2 = \frac{1 - \left(1 - \frac{R_1\ A_a\ F_R U_L}{N_s\ \frac{\dot{m}_{HTF}}{N_p}\ Cp_{HTF}\ C}\right)^{N_s}}{N_s\left(\frac{R_1\ A_a\ F_R U_L}{N_s\ \frac{\dot{m}_{HTF}}{N_p}\ Cp_{HTF}\ C}\right)}$$

(6.7)

6.5.3. Incident beam radiation

The radiation data for Antofagasta, Chile is provided by Meteonorm data base (TMY2). The radiation data are recorded at one hour intervals and on horizontal surface. These data are read and processed by TRNSYS component type 15. The TRNSYS type 15 takes the radiation data provided for horizontal surface and processes these data to convert to incident beam radiation data for a tilted surface ($I_{b,T}$), which is calculated as follows (Duffie & Beckman, 2006):

$$I_{b,T} = \frac{I_b \cos\theta}{\cos\theta_Z} \tag{6.8}$$

where I_b, θ_Z and θ are the beam radiation on horizontal surface, the solar zenith angle and the incident angle. These angles are defined in the following sections 6.5.3.1, 6.5.3.2 and 6.5.3.3

6.5.3.1.Declination

The position of the sun varies throughout the year. The declination angle is the angular position of the sun at solar noon, with respect to the plane of the equator. If the earth rotated upright on its axis, there would be no change in declination angle as the earth revolved around the sun. However, the earth is tilted on its axis at an angle of 23.45°. As the earth rotates around the sun through the course of a year, the declination angle will change, within a range of -23.45° $\leq \delta \leq$ 23.45°. The declination angle can be calculated from the following expression, which was developed by Cooper in 1969 (Duffie & Beckman, 2006):

$$\delta = 23.45 \sin\left(360 \frac{284 + n}{365}\right) \tag{6.9}$$

n is the day number of the year, from 1 (corresponding to January 1) to 365 (corresponding to December 31).

6.5.3.2.Position of sun in sky

The position of the sun in the sky can be specified by giving the hour angle (ω), the solar zenith angle (θ_Z) and the solar azimuth angle (γ_s). The hour angle takes into account the angular displacement of the sun east or west of the local meridian due to earth rotation. ω is negative, in the morning, when the sun is east of the local meridian. ω is positive, in the afternoon, when the sun is west of the local meridian. ω is zero at noon when the sun is in line with the local meridian. The earth rotates at a rate of 15° per hour (Duffie & Beckman, 2006):

$$\omega = 15° \, (St - 12) \tag{6.10}$$

where St is the solar time in hour. The angle between the vertical and the line of sight to the sun is known as the zenith angle (θ_Z), and it is defined as (Duffie & Beckman, 2006):

$$cos\,\theta_Z = sin\,\delta\,sin\,\phi + cos\,\delta\,cos\,\phi\,cos\,\omega \tag{6.11}$$

where δ is the declination angle (see Equation 6.9), ω is the hour angle (see Equation 6.10), and ϕ is the latitude location of the plant. The solar azimuth angle is the angle between the local meridian and the projection of the line of sight of the sun onto the horizontal plane. $\gamma_s = 0$ when the surface is facing the equator. $\gamma_s > 0$ if facing to the west. $\gamma_s < 0$ if facing to the east .

$$\sin \gamma_s = sign(\omega) \left| cos^{-1} \left(\frac{cos\, \theta_Z \, sin\, \phi - sin\, \delta}{sin\, \theta_Z \, cos\, \phi} \right) \right|$$

(6.12)

6.5.3.3.Angle of incidence

The insolation that is directly normal to the collector surface can be focused and thus be available to warm the absorber tubes. The angle of incidence (θ) represents the angle between the beam radiation on a surface and the plane normal to that surface. The angle of incidence will vary over the course of the day (as well as throughout the year) and will heavily influence the performance of the collectors. Figure 6-6 shows the angle of incidence on a parabolic trough solar collector.

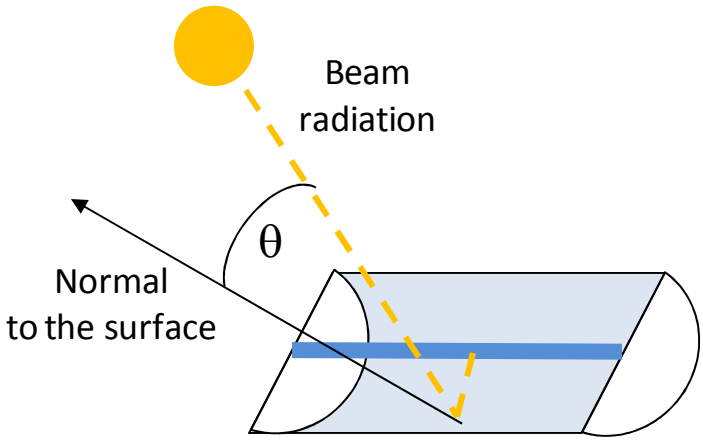

Figure 6 - 6 : Angle of incidence on a parabolic trough solar collector

The parabolic trough solar collectors used in this model are tracked about a single axis and it continually minimizes the angle of incidence. In this project, the model is

tested in two cases: when collectors rotate about a horizontal east-west axis and a horizontal north south axis, and when the collector rotates about a horizontal east-west axis, the angle of incidence (θ) is defined as (Duffie & Beckman, 2006):

$$cos\,\theta = (1 - cos^2\delta\, sin^2\omega)^{0.5} \tag{6.13}$$

where δ is the declination angle, and ω is the hour angle. In this case, the surface slope (β) is continually modified as a function of time and it is given by (Duffie & Beckman, 2006):

$$tan\,\beta = tan\,\theta_z\ |cos\,\gamma_s| \tag{6.14}$$

where θ_z is the zenith angle, and γ_s is the solar azimuth angle. In this case of rotation about a horizontal east-west axis, the surface azimuth (γ) is 180°. The second possible case is when the collector is rotates about a horizontal north-south axis with continuous adjustment to minimize the angle of incidence, the angle of incidence (θ) is defined as (Duffie & Beckman, 2006)

$$cos\,\theta = (cos^2\theta_Z - cos^2\delta\, sin^2\omega)^{0.5} \tag{6.15}$$

The surface slope (β) is continually modified when it rotates about a horizontal north-south axis as a function of time (Duffie & Beckman, 2006), and it is given by:

$$tan\,\beta = tan\,\theta_z\ |cos(\gamma - \gamma_s)| \tag{6.16}$$

In this case, the surface azimuth (γ) is 90°.

The angle of incidence on the collectors can be calculated once the declination angle (δ), the hour angle (ω), the zenith angle (θ_z), and the solar azimuth angle (γ_s) are known.

6.6. Storage

The storage tank is located between the solar field and the steam generator. The storage tank has been implemented into the TRNSYS model, and it is modeled with standard component type 4a. The type 4a model simulates a thermal stratified tank by means of dividing the tank in N fully mixed sections. When N is greater, more stratification is obtained. If only one node is selected (N=1), the tank is modeled as a fully mixed tank, without stratification.

Each node of the storage tank is modeled from its governing differential equation from the energy balance in each node, which is as follows (Duffie & Beckman, 2006):

$$m_i \frac{dT_i}{dt} = \alpha_i \dot{m}_H (T_H - T_i) + \zeta_i \dot{m}_L (T_L - T_i)$$

$$+ \frac{UA}{Cp_{HTF}} (T_a - T_i) \quad + \dot{m}_{m,i}(T_{i-1} - T_i)\big(if\ \dot{m}_{m,i} > 0\big)$$

$$+ \dot{m}_{m,i+1}(T_i - T_{i+1})\big(if\ \dot{m}_{m,i+1} < 0\big)$$

(6.17)

where m_i is the mass of the heat transfer fluid in the node "i" of the tank, Cp_{HTF} is the specific heat capacity of the heat transfer fluid in the tank, UA is the loss coefficient from the tank, $\dot{m}_H$ is the mass flow rate of the HTF entering from the solar field, $\dot{m}_L$ is the mass flow rate of the HTF entering from the load (steam generator), T_i is the temperature of the HTF in the node "i", T_H is the temperature of the HTF entering from the solar field, T_L is the temperature of the HTF entering from the load (steam generator), T_a is the ambient temperature surrounding the tank, $\frac{dT_i}{dt}$ is the change in average temperature of the node "i" as a function of time.

$\dot{m}_{m,i}$ is the mixed-flow rate that is the net mass flow rate between nodes, which can move either down or up. The direction of this flow depends in the magnitudes of the solar field and load (steam generator) mass flow rates. The following equations express the net mass flow rate between nodes (Duffie & Beckman, 2006).

$$\dot{m}_{m,1} = 0$$

(6.18)

$$\dot{m}_{m,i} = \dot{m}_H \sum_{j=1}^{i-1} \alpha_j - \dot{m}_L \sum_{j=i+1}^{N} \zeta_j \tag{6.19}$$

$$\dot{m}_{m,N+1} = 0 \tag{6.20}$$

α and ζ are collector control functions. α can be defined to determine which node received HTF from the solar field, and ζ control which node receive HTF from the load. $\alpha_i = 1$ when $i = 1$ and $T_H > T_i$ or when $T_{i-1} \geq T_H > T_i$, otherwise $\alpha_i = 0$. $\zeta_i = 1$ when $i = N$ and $T_L < T_N$ or when $T_{i-1} \geq T_L > T_i$, otherwise $\zeta_i = 0$.

In this project, the storage tank is model as a single tank maintaining a ratio equal to one (1) between the diameter and the height of the storage tank, and stratified with two (2) nodes (N=2). The hot stream coming from the solar field enters in the first node (i = 1). The cold stream from the load (steam generator) enters to the last node (i = 2). The simulation will be run for different ratios of volume of storage versus area of collectors between 25 and 200 liters/m^2. The specific heat capacity (Cp_{HTF}) of the fluid in the tank is supplied to type 4a as a parameter, and it is assumed to be constant. The specific heat capacity of the HTF is evaluated at the temperature of 200 °C as the reference state. The loss coefficient (UA) for the tank itself is neglected (0 [kW/K]). Figure 6-7 shows the flow diagram for the storage tank used in the solar steam generation plant.

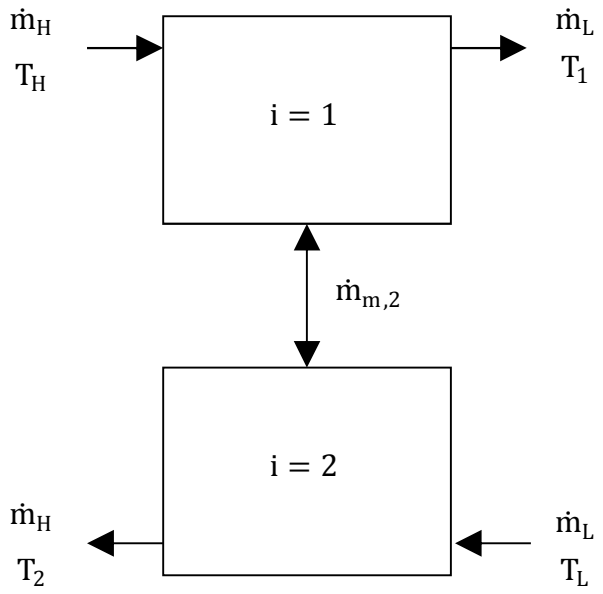

Figure 6 - 7 : Flow diagram for the storage tank used in the solar steam generation plant.

Equation 6.17 can be written as a system of first-order linear differential equations, like equation 6.21, and may be solved analytically each time step (Δt) for every node of the tank.

$$\frac{dT}{dt} = aT + b \tag{6.21}$$

TRNSYS provides a subroutine to solve these differential equations.

6.7. Auxiliary heater

The auxiliary heater turns on when the HTF coming from the storage tank has a temperature lower than T_{SP} (set point), which is set as minimum condition in the inlet of the steam generator. The auxiliary heater provides the required energy by the HTF to increase its temperature from the temperature at the top of the storage tank (T_1) to T_{SP} at the inlet of the steam generator. The auxiliary heater turns off if T_1 is greater than T_{SP}. The auxiliary heater uses as fuel natural gas and has a thermal efficiency (η_{AH}) of 80% (with a lower heating value). The auxiliary heater is simulated using the TRNSYS component type 6. The thermal power ($\dot{Q}_{AH}$) provided by the auxiliary heater is given as:

$$\dot{Q}_{AH} = \frac{\dot{m}_{HTF}\, Cp_{HTF}\, (T_{SP} - T_1)}{\eta_{AH}} \tag{6.22}$$

6.8. Steam generator

The steam generator is modeled using the TRNSYS component type 637. This component models is a heat recovery steam generator, a device which uses a high-temperature fluid as thermal energy source to produce steam. The steam produced can be either saturated or superheated. The steam generator is compounded for a super-heater, a boiler and a pre-heater section. The heat exchangers can be parallel or counter-flow.

In this plant, the steam generator is formed by a pre-heater and a boiler section (Figure 6-8). The heat exchanger is configured for counter-flow. The high temperature fluid is the HTF, which comes from the auxiliary heater.

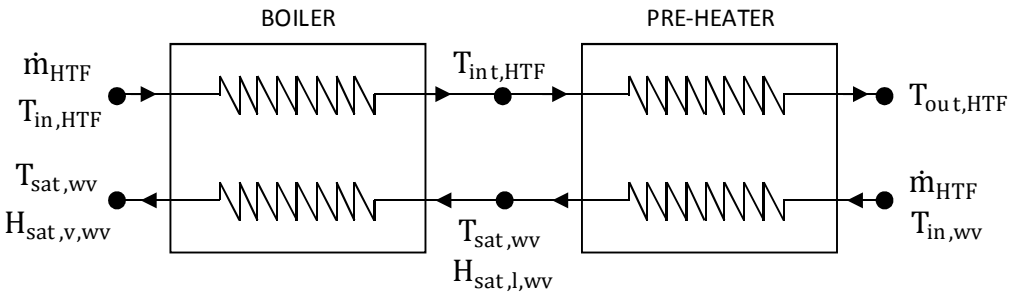

Figure 6 - 8 : Schematic of the steam generator

In the boiler, the HTF enters with a temperature ($T_{int,HTF}$), and it leaves with a temperature ($T_{int,HTF}$). $T_{int,HTF}$ is similar to the temperature in the top of the storage tank (T_1) when T_1 is greater than T_{SP}, or $T_{int,HTF}$ is equal to T_{SP} if T_1 is lower than T_{SP},. While the HTF is cooled in the boiler, the condensate is converted from liquid saturated to vapor saturated. The energy balance of the boiler heat exchanger is expressed as:

$$\dot{m}_{wv}\left(h_{sat,v,wv} - h_{sat,l,wv}\right) = \dot{m}_{HTF}\, Cp_{HTF}\left(T_{in,HTF} - T_{int,HTF}\right) \tag{6.23}$$

Once the HTF leaves the boiler, it is directed to the pre-heater. The HTF is cooled from $T_{int,HTF}$ to $T_{out,HTF}$ supplying the energy to pre-heat the condensate from the temperature that returns from the desalination plant (67°C) to the saturation temperature. The energy balance in the pre-heater heat exchanger is defined as:

$$\dot{m}_{wv}\left(h_{sat,l,wv} - h_{in,wv}\right) = \dot{m}_{HTF}\, Cp_{HTF}\left(T_{int,HTF} - T_{out,HTF}\right)$$

(6.24)

The steam outlet condition and the pinch point of the heat exchanger are the parameters of this component. Because the steam supplied to the desalination plant is saturated, the steam outlet condition depends only of the pressure, which is varied as indicated in section 6.1. The pinch point is set to be equal to 5°C.

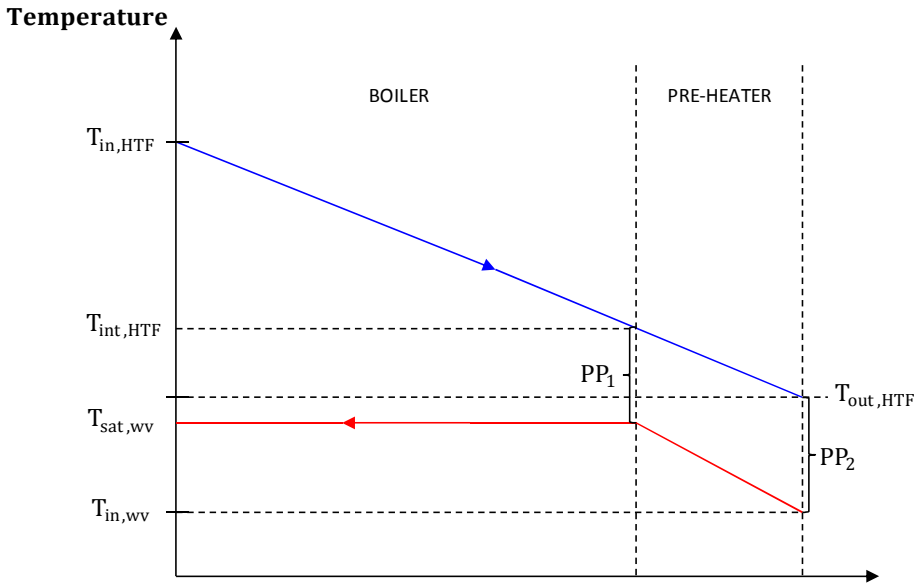

Figure 6 - 9 : Temperature distribution in the steam generator

The heat recovery steam generator calculates the temperature of the HTF leaving the steam generator. The steam generator turns off if the pinch-point temperature difference is achieved. The pinch-point temperature difference is defined to be the minimum temperature difference between the hot-source fluid and the steam that allows for heat

transfer between the fluids. The pinch-point is checked at the steam saturated liquid point.

$$PP_1 = T_{int,HTF} - T_{sat,wv} \tag{6.25}$$

and at the outlet of the hot source flow.

$$PP_2 = T_{out,HTF} - T_{in,wv} \tag{6.26}$$

Figure 6-9 shows the temperature distribution in the steam generator and the two possible pinch points.

6.9. Control systems

6.9.1. Pump solar field

The loop that connects the storage tank to the solar field and return back to the storage tank, is temperature controlled by the use of a variable speed pump that maintain a minimum temperature supply (T_{SP}, set point) to the storage tank. The temperature set point (T_{SP}) is defined at section 6.9.2. The variable speed pump is controlled using a feedback iterative control, which is modeled with TRNSYS component type 22. This control reads the temperature at the outlet of the solar field and compares with the set point. When the outlet temperature of the solar field is lower than the set point, the control modifies the velocity of the pump and consequently the mass flow rate of HTF

maintaining constant the outlet temperature of the solar field. If the outlet collector temperature is greater than the set point temperature, the pump operates with maximum mass flow rate. The pump turns off when the temperature provided by the solar field is lower than the temperature at the top of the storage tank.

6.9.2. Pump steam generator

The loop that connects the storage tank, the auxiliary heater, the steam generator and returns back to the storage tank is controlled by the use of a variable speed pump that maintains a constant temperature at the outlet of the steam generator ($T_{out,SG}$). The temperature at the inlet of the steam generator has a minimum value of T_{SP} (set point). T_{SP} is defined as the sum of the saturation temperature of the steam generated (T_{sat}), the pinch point (PP), and a temperature difference (ΔT).

$$T_{SP} = T_{sat} + PP + \Delta T \tag{6.27}$$

The temperature at the outlet of the steam generator is defined as

$$T_{out,SG} = T_{sat} + PP \tag{6.28}$$

The temperature difference (ΔT) is a design parameter and it sets the maximum mass flow rate of the HTF in the loop as shown in equation 6.29. When the temperature supply to the steam generator is equal to the T_{SP}, the mass flow rate of the HTF is at a maximum and it leaves the steam generator with a known temperature ($T_{out,SG}$).

$$\dot{m}_{HTF,max} = \frac{\dot{Q}_{req}}{Cp_{HTF}\,\Delta T}$$

(6.29)

The temperature difference (ΔT) is defined in section 6.10.1. When the inlet temperature to the steam generator is greater than the set point temperature (T_{SP}), the mass flow rate of HTF is reduced to maintain a constant outlet temperature ($T_{out,SG}$). At this condition, the mass flow rate in the loop is calculated as

$$\dot{m}_{HTF}(t) = \frac{\Delta T}{T_1(t) - T_{out,SG}}\ \dot{m}_{HTF,max}$$

(6.30)

6.10. Results and discussion

6.10.1. Temperature difference in the steam generator

In the load loop when the temperature at the inlet of the steam generator is equal to T_{SP} (set point), the HTF mass flow rate is maximum and the temperature difference between the inlet and outlet of the steam generator is ΔT. The temperature difference (ΔT) should be defined to obtain the maximum flow rate that flows through the load loop as is defined in equation 6.31.

$$\dot{m}_{HTF,max} = \frac{\dot{Q}_{req}}{Cp_{HTF}\,\Delta T}$$

(6.31)

The design mass flow rate of heat transfer fluid circulating through the load loop, $\dot{m}_{HTF,max}$, affects the parasitic electrical energy consumption by the circulating pump. When ΔT is low, the solar energy absorbed is reduced, but the energy pump is maximum. If the design ΔT increases, the solar energy absorbed is decreased, but the parasitic energy associated with pumping is reduced. Consequently, an optimization O function (O) that maximizes the fraction of solar energy by the system taking into account the effects of parasitic energy consumption is defined as

$$O = \frac{\int \dot{Q}_u \, dt}{\int \dot{Q}_u \, dt + \int \dot{Q}_{AH} \, dt + \int \dot{W}_{p,L} \, dt/\eta_c}$$

(6.32)

The optimization function is defined as the ratio between the energy solar absorbed in the solar field ($\int \dot{Q}_u \, dt$) and the total primary energy supplied to the desalination plant. The total energy supplied takes into account the energy solar absorbed in the solar field ($\int \dot{Q}_u \, dt$), the energy supplied in the auxiliary heater ($\int \dot{Q}_{AH} \, dt$), and the primary pumping energy (parasitic) in the load loop ($\int \dot{W}_{p,L} \, dt/\eta_c$). η_c is the efficiency of conversion from fossil fuel to electricity, which is assumed to be 35%. The electrical pumping power $\dot{W}_{p,L}$ is defined as:

$$\dot{W}_{p,L} = \dot{m}_{HTF}(t) \, \frac{\Delta P}{\eta_p \, \rho_{HTF}}$$

(6.33)

Where η_p is the overall pump efficiency, ΔP is the drop pressure in the steam generator and in the auxiliary heater, and ρ_{HTF} is the HTF density. η_p is assumed to be 60%, The

The optimization function is calculated over a range of temperature differences from 1.5°C to 40°C. The results of the optimization function as a function of temperature difference are shown in Figure 6-10.

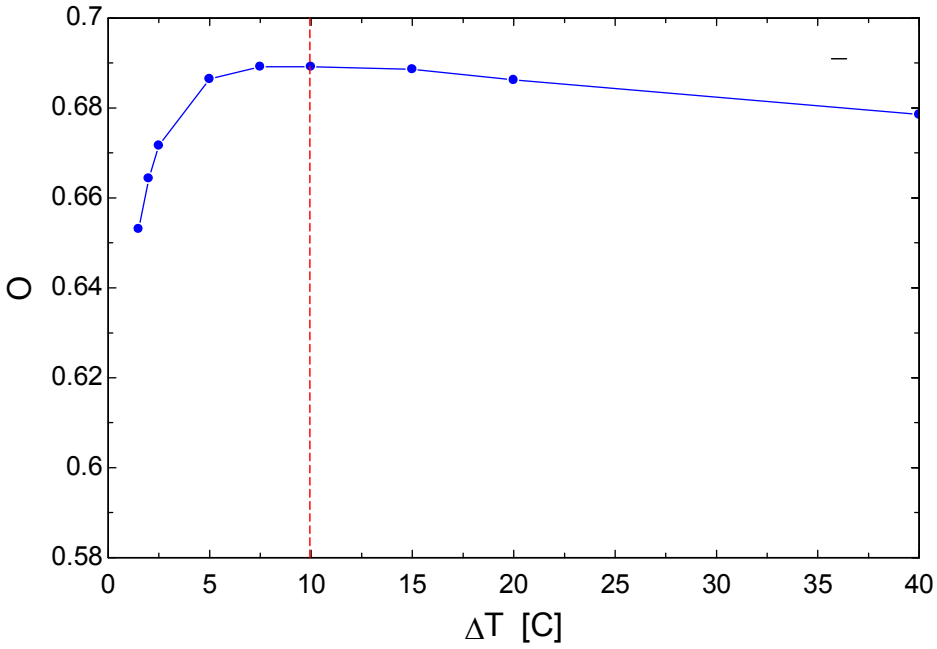

Figure 6 - 10 : Optimization function as a function of temperature difference, 100,000 number of collectors, north-south axis oriented, 75 liters of storage per square meter of solar collectors, and the steam pressure is 2,100 kPa

The optimization function exhibits a maximum when the temperature difference is equal to 10°C.

6.10.2. Collector orientation

The solar fraction is defined as:

$$Solar\ fraction = \frac{\int \dot{Q}_u\, dt}{\int \dot{Q}_u\, dt + \int \dot{Q}_{AH}\, dt} \tag{6.34}$$

The solar fraction is the ratio between the energy solar absorbed in the solar field ($\int \dot{Q}_u\, dt$) and the total primary thermal energy supplied to the desalination plant. The total energy supplied takes into account the energy solar absorbed in the solar field ($\int \dot{Q}_u\, dt$) and the energy supplied in the auxiliary heater ($\int \dot{Q}_{AH}\, dt$).

The solar field is oriented along to a north-south axis, and the solar fraction is calculated as a function of the number of collectors. Also, in a separate calculation, the solar fraction is determined when collectors are oriented along to east-west axis. Figure 6-11 shows the solar fraction obtained when collectors are oriented along north-south axis and east-west axis.

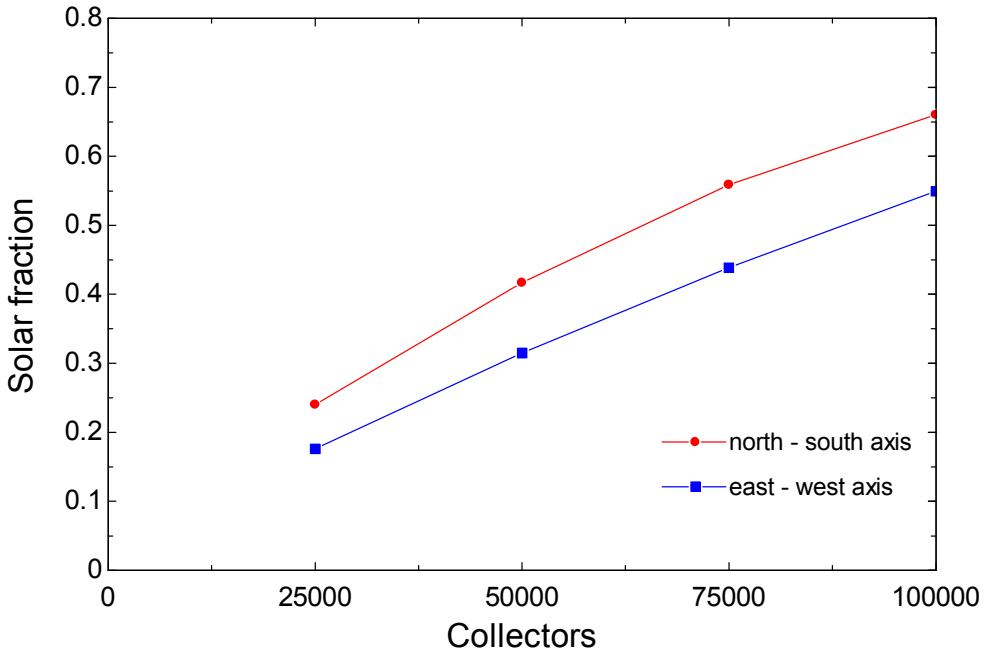

Figure 6 - 11 : Solar fraction as a function of number of collectors for two different orientations: north-south axis and east west axis

It is observed a greater solar fraction occurs when collectors are oriented north-south axis compared to an east-west axis orientation. The solar fraction advantage of a north-south axis orientation over an east-west orientation is almost constant with a 10% advantage for the north-south case.

Figure 6-12 presents the monthly solar fraction for the two orientations.

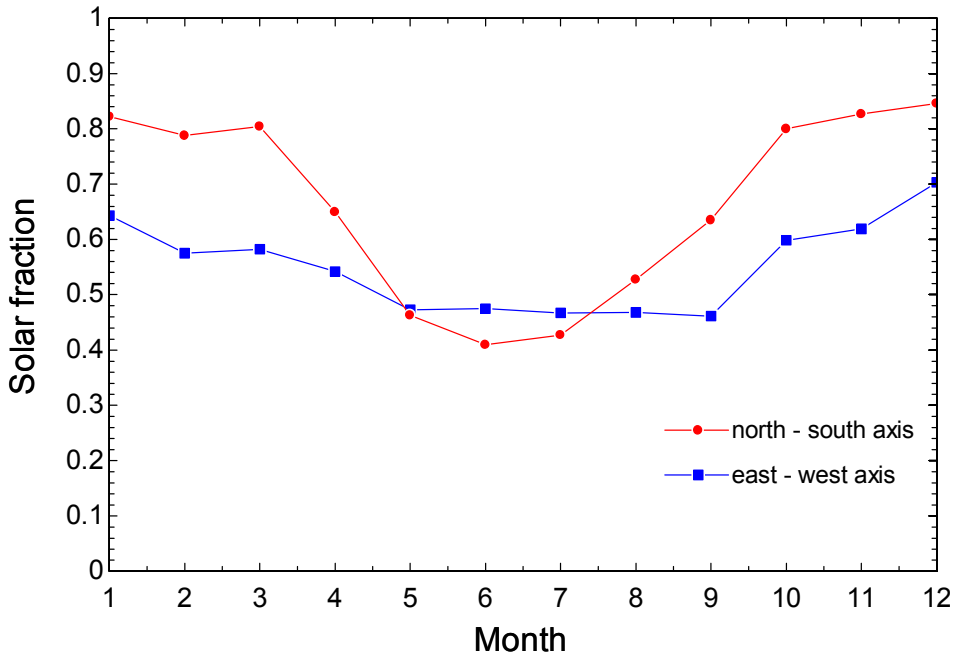

Figure 6 - 12 : Solar fraction as a function of month for two different orientations: north-south axis and east west axis

Because of Antofagasta is located in the south hemisphere, the summer is between December 21 to March 21 and the winter is between June 21 and September 21. The north-south axis orientation case shows a wider variation in the monthly average solar fraction between summer and winter; about 90% in summer and lower than 60% in winter. Only three months (May, June and July) have a solar fraction lower than east-west axis orientation. The north-south axis has a lower range (between 60% and 80%) but generally trend lower than north-south axis.

In conclusion, using the same collector area, a higher annual solar fraction is obtained with north-south axis. It means, if the capital cost is the most important the north-south orientation is the best. However, the monthly average for collectors oriented

east-west is more flat than north-south that presents a wide variation. If more collectors oriented east-west are installed, they are able to supply a greater solar fraction without refusing energy.

6.10.3. Storage size, number of collectors and steam pressure supply

The solar field efficiency is defined as the ratio between the solar energy absorbed by the HTF and the incident beam radiation in the solar field. The solar efficiency is expressed as:

$$\eta_{field} = \frac{\int \dot{Q}_u \, dt}{A_a \, N_p \, N_s \, \int I_{b,T} \, dt} \tag{6.35}$$

The solar field efficiency is calculated when the solar plant produces saturated steam at the three different pressures and as a function of the number of collectors that form the solar field. The solar field efficiency is insensitive to changes in the steam pressures. Figure 6-13 shows the solar field efficiency as a function of the number of collectors.

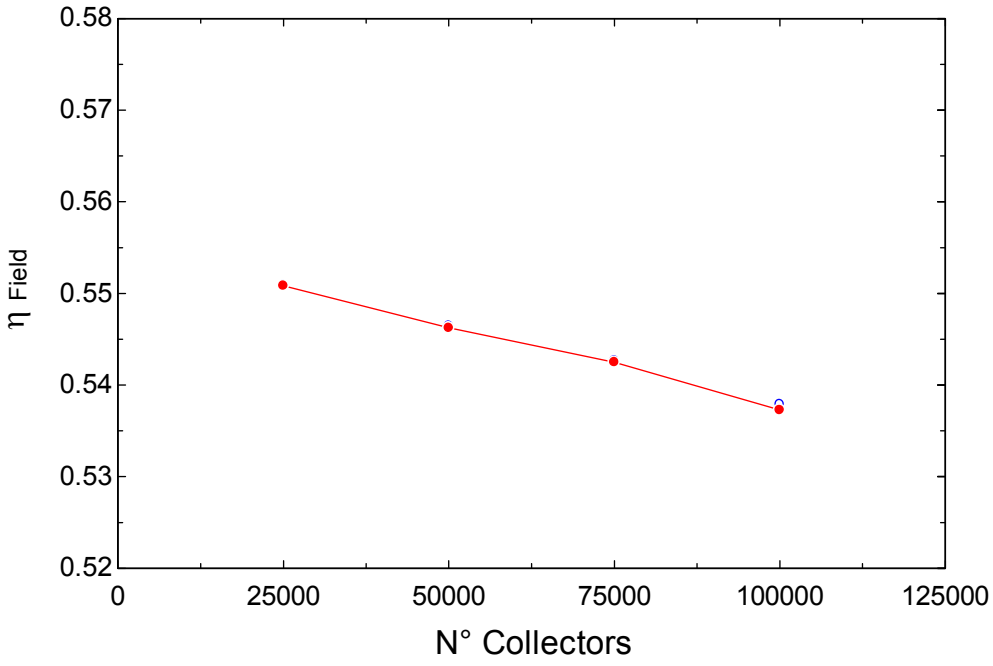

Figure 6 - 13 : The solar field efficiency as a function of number of collectors

The solar field efficiency decreases as the number of collector increases. The decrease in solar field efficiency is a consequence of the higher average HTF temperature achieved in the solar field when the number of collectors increases. When the HTF average temperature increases, the thermal losses in collectors increase.

Figure 6-14 shows the fraction of energy covered using solar energy to produce the steam required by the desalination plant at continuous operation, called solar fraction. The effect of increasing the storage capacity of the solar field in the solar fraction is analyzed. The normalized storage volume (storage volume per m^2 of collector area) is varied between 25 and 200 liters/m^2. The system's solar fraction increases asymptotically as the normalized storage capacity increases.. In addition, the effect of more collectors on the solar fraction is shown. Finally, the effect of supply saturated

steam at three pressures 1,600, 2,100, and 2,600 kPa is investigated. As noted previously, the effect of supply steam pressure has relatively little effect on the solar fraction.

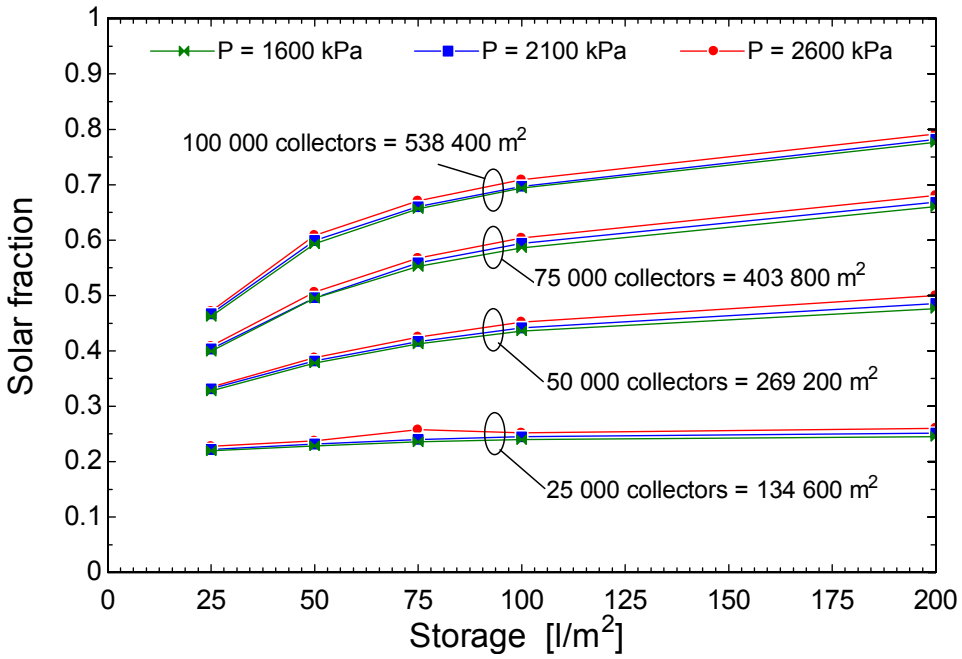

Figure 6 - 14 : Solar fraction as a a function of storage tank size for different number of collectors and steam pressure supply, $\Delta T = 10$

The solar fraction covered installing 25,000 collectors, which results in an area of collection (only area of parabolic collectors) of 134,600 m^2, is about 30%. The variation of the storage volume does not affect the performance of the solar field because most of the energy absorbed by the solar system is lower than the energy required to produce saturated steam and is used immediately. When 50,000 collectors, corresponding to an area of collection of 269,200 m^2, are installed the solar fraction is between 45% and 55%, depending on the storage volume. The optimum normalized storage volume is

approximately 75 l/m^2 of collector area for this condition. In addition, the best performance is observed when the steam pressure supply is 2,100 kPa. Solar fractions between 55% and 75% can be achieved when the solar field has 75,000 collectors. A solar field comprised of 100,000 collectors can achieve solar fractions in the range of 60% to 85%. The effect of the storage capacity on the performance of the solar field is notable when the number of collectors is greater than 50,000. The solar fraction increases when the storage capacity also increases. It is noted that the solar system works well when the storage capacity is between 75 and 100 l/m^2 because addition of more storage capacity increases the solar fraction but the rate of efficiency increase diminishes. When 100,000 collectors are used in the solar field, the optimum storages is closer to 100 l/m^2. Even though the performance of the solar steam generation plant is greater at the higher pressure (2,100 kPa), it is not observed as a significant effect in the performance of the solar field if the steam is supplied with different pressure.

In conclusion, the performance of the solar field is not significantly better when the pressure of steam provided to the desalination plant decreases. The solar field performance increases with an increasing number of collectors. The optimum storage size is found to be between 75 and 100 liters per square meter of solar collector area. When the number of collectors is doubled, the solar fraction is not doubled. A solar fraction of about 70% is achieved when 100,000 collectors are installed in the solar field.

Chapter 7 : Conclusions and recommendations

7.1. Conclusions

In costal places where fresh water is scarce and solar levels are high, the utilization of solar thermal energy to drive a desalination plant driven may be a sustainable option for producing fresh water. A literature review of some desalination technologies has been conducted. The two desalination technologies found appropriate to be combined with solar thermal energy include multi-effect desalination (MED) and multi-effect desalination combined with a thermo-compressor (MED-TC). Both MED and MED-TC technologies can be effective when driven with the lower temperatures available using parabolic trough collector technologies. This form of solar energy conversion effectively provides the lower grade thermal energy needed by the desalination approaches considered. The most important advantages of MED-TC plants over MED plants is that MED-TC is able to produce the same amount of fresh water using the half of energy than MED with the same number of effects. This fact is important if the capital cost is the relevant parameter. However, MED-TC plant has a great limitation because the number of effects is dictated by the pressure of the high pressure of steam used as a source of thermal energy; therefore, the maximum GOR is limited to be about eight (8). With future work, MED plants may have a greater potential of development if coupled with solar energy compared with MED-TC because it is possible to add more and more effects to improve efficiency if the temperature in the first

effect can be increased. Normally, a MED plant can achieve a GOR of 16, but the maximum depends of the number of effects.

Both MED and MED-TC plants have been modeled in EES. The MED-TC model results have been compared against operational data from the ALBA MED-TC plant installed in Bahrain. The model is capable of predicting intermediate results such as the temperature and pressure of each effect as well as the water vapor and brine mass flow rates produced in each effect. In addition, the total fresh water production and overall plant performance parameters are calculated. The intermediate temperature/pressure results for each effect are predicted with a difference lower than 10%. However, the fresh water production and the plant performance show difference lower than 2% with the real data. The MED-TC model has served as a tool for understanding how affects in the plant performance the variation of some parameters. Increasing the temperature of the first effect in the desalination plant can improve the efficiency of the plant. An increment of 5°C in the source of thermal energy for the first effect increases the efficiency of the desalination plant in 3.5%. If this temperature is reduced in 5°C the efficiency of the plant decreases in about 2%. The MED plant model is not validated because detail data has not been found.

A solar steam generation plant also has been modeled using parabolic trough solar collectors in TRNSYS. The solar plant produces the steam to drive the desalination plant, and the performance of both working together is tested. Both plant solar steam generator and desalination plants are located in the city of Antofagasta, Chile. This city faces a shortage of fresh water because is located in a dry zone with poor supply of water.

Its population is growing, and a great number of industrial projects are been installed in zones that surround this city. Also, it is located in the coast and receives high levels of solar radiation. The testing conditions are: the desalination plant should produce 10,800 metric tons of fresh water per day and the solar steam generation plant must continuously supply saturated steam at three alternative plant design steam pressures (1,600, 2,100, and 2,600 kPa). The best performance of the solar steam generation plant coupled with the desalination plant is obtained when the collectors are oriented along a north-south axis absorbing 10% more solar radiation than the east-west axis orientation. The optimum temperature difference in the load loop at maximum flow rate in the steam generator is 10°C. Also, a storage size between 75 and 100 liters per square meter of solar collector offers good performance. In addition, the annual solar field efficiency varies between 55 and 53%. The solar field efficiency is reduced while the average temperature of the HTF in the loops rises increasing the thermal losses in the collectors; however, the efficiency seems to be insensitive to variation in the steam pressure required. Finally, if 100,000 parabolic trough collectors are installed with an area of collection equivalent to 538,400 m^2, the fraction of the energy required for the desalination plant covered with solar energy (i.e. the solar fraction) is about 70% without considering parasitic power requirements. The solar fraction does not change significantly as the pressure of the saturated steam generated varies.

7.2. Recommendations for future work

The MED-TC model predicts the performance of the data used in the validation within a difference below to 1%; however, it is believed that the MED-TC plant uses, as a base to the model is not the optimum design from an energetic point of view. An optimization of the solar MED-TC plant should be studied. In addition, the MED-TC model can be coded in Fortran to create TRNSYS component; consequently, the performance of both plants working together can be optimized. Also, an estimation of the capital cost of both technologies could be included in this analysis. This situation will permit optimizing MED designs taking into account the life cycle of the system. Additionally, the desalination component could be included in the System Advisor Model (SAM) to analyze the technical and financial performance facilitating the decision making for people interested in considering the installation of a desalination plant driven with solar thermal energy in different locations.

Some cases in the literature combine MED or MED-TC plants with solar thermal tower power plant (Rankine cycle) that drives the desalination by the means to bleed steam from the steam turbine, but desalination is treated as black box. They use the standard design of MED and MED-TC used in conventional facilities. It is believed that the optimum design of these plants working separately is not necessarily the same as when they work together. When they work together, capital cost of both plants are relevant and may be possible to justify the construction of a MED plant with a large number of effects to increase the efficiency of the desalination plant and reduce the size of the solar field. In further analysis, these trade-offs should be studied.

The parasitic power elements in the steam generation plant, mainly the HTF pumps, have not been as rigorously modeled. Parasitic power consumption calculations in the source loop are based on pressure drop through the heat exchangers assuming the length of the heat exchange (steam generator) as 40 ft. and a reasonable velocity inside of pipes. Further studies might include the design of the heat exchanger in the solar plant to obtain more accurate parasitic power predictions.

The integration of the desalination model with other solar steam sources may be interesting. Future work should explore how this kind of plant performance with solar power plant driven by solar energy and bleeding a fraction of steam from the steam turbine to drive the desalination plant. Also, a MED plant should be tested if the thermal source provided is hot water or the HTF directly.

References

Al-Ahmad, M., & Aleem, F. A. (1993). Scale formation and fouling problems effect on the performance of MSF and RO desalination plants in saudi arabia. *Desalination, 93*(1-3), 287-310.

Al-Karaghouli, A., Renne, D., & Kazmerski, L. L. (2009). Solar and wind opportunities for water desalination in the arab regions. *Renewable and Sustainable Energy Reviews, 13*(9), 2397-2407.

Aly, N. H., Karameldin, A., & Shamloul, M. M. (1999). Modelling and simulation of steam jet ejectors. *Desalination, 123*(1), 1-8.

Bin Amer, A. O. (2009). Development and optimization of ME-TVC desalination system. *Desalination, 249*(3), 1315-1331.

Bodendieck, F., & Genthner, K. (1999). The effects of different venting and deaeration concepts on the performance and energy consumption of MSF distillers.

Borsani, R., & Rebagliati, S. (2005). Fundamentals and costing of MSF desalination plants and comparison with other technologies. *Desalination, 182*(1-3), 29-37.

Cáceres, V. L., Gruttner, D. E., & Contreras, N. R. (1992). Water recycling in arid regions: Chilean case. *Ambio, 21*(2), pp. 138-144.

Cheng, H., Hu, Y., & Zhao, J. (2009). *Meeting China's Water Shortage Crisis: Current Practices and Challenges*- American Chemical Society.

Churchill, S. W., & Bernstein, M. (1977). A correlating equation for forced convection from gases and liquids to a circular cylinder in crossflow. *J. Heat Transfer, 99*, 300-306.

de Vries, A. J., Froment, T., & Munro, A. (2002). Aluminum bahrain ALBA new desalination facility, one of the biggest MED plant in the world Manama, Bahrain.,

Dobson, M. K., & Chato, J. C. (1998). Condensation in smooth horizontal tubes *J. Heat Transfer, 120*, 193-213.

Duffie, J., & Beckman, W. (2006). *Solar engineering of thermal processes* (3rd ed. ed.)Hoboken, N.J. : Wiley,.

Eames, I. W., Aphornratana, S., & Haider, H. (1995). A theoretical and experimental study of a small-scale steam jet refrigerator. *International Journal of Refrigeration, 18*(6), 378-386.

El-Dessouky, H. T., & Ettouney, H. M. (2002). *Fundamentals of salt water desalination*. Amsterdam: Elsevier.

Fritzmann, C., Löwenberg, J., Wintgens, T., & Melin, T. (2007). State-of-the-art of reverse osmosis desalination. *Desalination, 216*(1-3), 1-76.

Glade, H., & Al-Rawajfeh, A. E. (2008). Modeling of CO2 release and the carbonate system in multiple-effect distillers. *Desalination, 222*(1-3), 605-625.

Gnielinski, V. (1976). New equations for heat and mass transfer in turbulent pipe and channel flow *Int. Chem. Eng., 16*, 359-368.

He, S., Li, Y., & Wang, R. Z. (2009). Progress of mathematical modeling on ejectors. *Renewable and Sustainable Energy Reviews, 13*, 1760-1780.

Holman, J. P. (1997). *Heat transfer* (8th edition ed.). New York: McGraw-Hill.

Kakaç, S., & Liu, H. (1998). *Heat exchangers: Selection, rating, and thermal design*. Boca Raton, Florida: CRC Press.

Karagiannis, I. C., & Soldatos, P. G. (2008). Water desalination cost literature: Review and assessment. *Desalination, 223*(1-3), 448-456.

Keenan, J. H., Neumann, E. P., & Lustwerk, F. (1950). An investigation of ejector design by analysis and experiment. *Journal of Applied Mechanics, 17*, 299-399.

Khan, A. H. (1986). *Desalination processes and multistage flash distillation practice*. Amsterdam: Elsevier.

Khawaji, A. D., Kutubkhanah, I. K., & Wie, J. (2008). Advances in seawater desalination technologies. *Desalination, 221*(1-3), 47-69.

Klein, S. (2010). *Engineering Equation Solver (EES) for Microsoft Windows Operating System Commercial and Professional Versions*F-Chart Software.

Knudsen, J. G. (1990). Fouling in heat exchangers. *, Hemisphere Handbook of Heat Exchangers Design,*

Leblanc, J., Andrews, J., & Akbarzadeh, A. (2010). Low-temperature solar?thermal multi-effect evaporation desalination systems. *International Journal of Energy Research, 34*(5), 393-403.

Li, P., Seem, J. E., & Li, Y. (2011). A new explicit equation for accurate friction factor calculation of smooth pipes. *International Journal of Refrigeration, 34*(6), 1535-1541.

Ludwig, H., & Hetschel, M. (1990). Treatment of distillates and permeates from sea water desalination plants to make potable water, . *Saline Water Processing,*

Meteonorm. (2011). *Global Irradiance World*

Miller, J. E. (2003). Review of water resources and desalination technologies *SAND0800,*

Millero, F. J. (1996). *Chemical oceanography* (2nd edition ed.). Boca Raton: CRC press.

Narayan, G. P., Sharqawy, M. H., Summers, E. K., Lienhard, J. H., Zubair, S. M., & Antar, M. A. (2010). The potential of solar-driven humidification–dehumidification desalination for small-scale decentralized water production. *Renewable and Sustainable Energy Reviews, 14*(4), 1187-1201.

National Institute of Statistics (INE). (2009). *Demographic Annual Reports*. Chile: INE.

Nellis, G., & Klein, S. (2009). *Heat transfer*. New York: Cambridge University Press, New York.

Office of Saline Water (O.S.W). (1973). *Final report horizontal spray film (HTEX) and vertical tube (VTEX) evaporator, office of saline water (O.S.W)*. Paramus N .0,: Burs and Row Construction Corp.

Ould Didi, M. B., Kattan, N., & Thome, J. R. (2002). Prediction of two-phase pressure gradients of refrigerants in horizontal tubes. *International Journal of Refrigeration, 25*(7), 935-947.

Palen, J. W. (1988). Falling film evaporation in vertical tubes . (pp. 189-217). Alhambra, California, U.S.A.: Heat Transfer Research, Inc.

Pankratz, T., & Tonner, J. (2003). *Desalination.com: An environmental primer* . Houston, TX.: Lone Oak Publishing.

Pankratz, T. (2010). *IDA desalination yearbook 2009-2010*. United Kingdom: Oxford.

Parken, W. H., Fletcher, L. S., Han, J. C., & Sernas, V. (1990). Heat transfer through falling film evaporation and boiling on horizontal tubes. *J. Heat Transfer, 112:3*, 744-750.

Power, R. B. (1994). *Steam jet ejectors for the process industries*New York, NY (United States); McGraw-Hill.

Revenga, C., Brunner, J., Henninger, N., Kassem, K., & Payne, N. (2000). *Pilot analysis of global ecosystems*. Washington, DC: World Resources Institute and Worldwatch Institute.

Rohsenow, W. M., Hartnett, J. P., & Ganic, E. N. (1985). *Handbook of heat transfer applications* . New York: McGraw-Hill.

Sampathkumar, K., Arjunan, T. V., Pitchandi, P., & Senthilkumar, P. (2010). Active solar distillation—A detailed review. *Renewable and Sustainable Energy Reviews, 14*(6), 1503-1526.

Semiat, R. (2008). *Energy Issues in Desalination Processes*American Chemical Society.

Semiat, R., & Galperin, Y. (2001). Effect of non-condensable gases on heat transfer in the tower MED seawater desalination plant. *Desalination, 140*(1), 27-46.

Sharqawy, M. H., Lienhard, J. H., & Zubair, S. M. (2010). Thermophysical properties of seawater: A review of existing correlations and data. *Desalination and Water Treatment, 16*, 354-380.

Slesarenko, V. (1977). Hydrodynamics and heat transfer during seawater boiling in thin-film desalination plants. *Desalination, 21*(3), 275-283.

Solar Rating and Certification Corporation. (2011). Summary of SRCC certified concentrating solar collectors, December 2011

Soteris A., K. (2005). Seawater desalination using renewable energy sources. *Progress in Energy and Combustion Science, 31*(3), 242-281.

U.S Census Bureau. (2011). International data base.

U.S. EPA. (2011). Clean water and drinking water.Retrieved December 2011,

Uche, J., Artal, J., & Serra, L. (2003). Comparison of heat transfer coefficient correlations for thermal desalination units. *Desalination, 152*(1-3), 195-200.

United Nations. (2008). *The millennium development goals report*United Nations Department of Economic and Social Affairs.

Utomo, T., Ji, M., Choi, D., Rahman, M. S., Jeong, H., & Chung, H. (2008). CFD investigation on the flow structure inside thermo vapour compressor. Seoul, Korea, 1891-1898.

Vyas, S. K. (2003). A small scale multiple effect distillation (MED) system for rural drinking water supply. (Doctoral dissertation, IIT). *Department of Applied Mechanics,*

Yang, L., & Shen, S. (2008). Experimental study of falling film evaporation heat transfer outside horizontal tubes. *Desalination, 220*(1-3), 654-660.

Zivi, S. M. (1964). Estimation of steady-state steam void-fraction by means of the principle of minimum entropy production. *J. Heat Transfer, 86*, 247-252.

Appendix A : MED Model (General)

```
"*************************************************************************************************************"
"subprogram evaporation convection heat transfer coefficient outside of horizontal tubes"
"*************************************************************************************************************"
subprogram evap(T_w_o,T_sat,GAMMA,S:h_e,q_e)
    T_avg = (T_w_o + T_sat) / 2
    rho = SW_Density(T_avg,S)                          "density feed brine, kg/m^3"
    mu = SW_Viscosity(T_avg,S)
    nu = SW_KViscosity(T_avg,S)                        "kinematic viscosity feed brine, m^2/s"
    k = SW_Conductivity(T_avg,S)                       "conductivity feed brine, W/m-C"
    Pr = SW_Prandtl(T_avg,S)                           "prandt number feed brine"
    Re = 4 * GAMMA / mu                                "reynold number feed brine"
    q_e = h_e * (T_w_o - T_sat)                        "heat flux, W/m^2"
    h_e *  (nu^2 / (g# * k^3))^(1/3) = 0.00082 * Re^0.10 * Pr^0.65 * q_e^0.4
                                                       "conv heat transfer coeff, W/m^2-C"
end

"*************************************************************************************************************"
"INPUT DATA"
"*************************************************************************************************************"

N = 4                                                  "number of effects"
S_feed = 35 [g/kg]                                     "salinity of feed water" "INPUT"

Duplicate i = 1,N
    "feed water"
    OD[i] = 22 [mm] * convert(mm,m)                    "outside diameter tubes evaporator, m"
    th[i] = 1.2 [mm] * convert(mm,m)                   "thickness tube, m"
    N_e[i] = 2                                         "number of evaporators"
    A_e[i] = 5400 [m^2]                                "heat transfer area per evaporator, m^2"
    L[i] = 7 [m]                                       "long of tubes evaporator, m"
    m_dot_feed_E[i] = 540000 [kg/h] * convert(kg/h,kg/s) "feed water mass flow rate evaporator 1"
                                                       "INPUT"
    m_dot_vapor_TC[i] = 0                              "boundary condition"
```

```
end

FF = 0.0000 [m^2-C/W]                                   "Fouling Factor" "INPUT"

GAMMA = 0.5 [m^3/h-m] * rho_b * convert(kg/h-m,kg/s-m)
                                                        **********define**********"
rho_b = SW_Density(T_feed_E[1],S_feed)                  "density brine"
x_vaporheat_in_E[1] = 1                                 "quality steam supply first effect"

"brine produced"
m_dot_brine_E[0] = 0                                    "boundary condition"
h_brine_E[0] = 0                                        "boundary condition"
S_brine_E[0] = 0                                        "boundary condition"

h_vaporheat_in_E[1] = Enthalpy(Steam,x=1,P=P_E[0])      "enthalpy steam supply first effect"
P_E[0] = P_sat(Steam,T=T_vapor_E[0])                    "pressure steam supplied at the first
effect"
T_vaporheat_out_E[1] =  71 [C]                          "INPUT" "temperature primary steam
                                                        condensed"

m_dot_fw = 140                                          "GOAL"

"*************************************************************************************************************"
"EVAPORATOR"
"*************************************************************************************************************"

Duplicate i = 1,N

    ID[i] = OD[i] - 2 * th[i]                           "inside diameter tubes evaporator, m"
    A_tot_E[i] = A_e[i] * N_e[i]                        "total heat transfer area, m^2 "
    A_tot_E[i] = N_t[i] * L[i] * OD[i] * pi#            "number of tubes evaporator"

    h_feed_E[i] = SW_Enthalpy(T_feed_E[i],S_feed) * convert(J/kg,kJ/kg)
                                                         "enthalpy of feed water"
    h_vapor_E[i] = Enthalpy(Steam,T=TBT[i],P=P_E[i])    "enthalpy of water-vapor generated"
    h_brine_E[i] = SW_Enthalpy(TBT[i],S_brine_E[i]) * convert(J/kg,kJ/kg)
```

```
                                                    "enthalpy of brine"

m_dot_feed_E[i] + m_dot_brine_E[i-1] - m_dot_vapor_E[i] - m_dot_brine_E[i] =  0
                                                    "MASS BALANCE"

m_dot_brine_E[i] * S_brine_E[i] = m_dot_feed_E[i] * S_feed + m_dot_brine_E[i-1] *
S_brine_E[i-1]
                                                    "SALT BALANCE"
{S_brine_E[i] = 51 [g/kg]}                          "*****GUESS VALUE*****"

Q_dot_E[i] = -(m_dot_feed_E[i] * h_feed_E[i] + m_dot_brine_E[i-1] * h_brine_E[i-1] -
(m_dot_vapor_E[i]) * h_vapor_E[i] -  m_dot_brine_E[i] * h_brine_E[i])
Q_dot_E[i] = m_dot_vaporheat_E[i] * (h_vaporheat_in_E[i] - h_vaporheat_out_E[i])
                                                    "ENERGY BALANCE"

P_E[i] = P_sat(Steam,T=T_vapor_E[i])                "pressure evaporator 1"
TBT[i] = T_vapor_E[i] + BPE[i]                      "vapor temperature"
BPE[i] = SW_BPE(TBT[i],S_brine_E[i])                "boiling point elevation"

m_dot_v_t[i] = m_dot_vaporheat_E[i] / N_t[i]         "water-vapor mass flow rate per tube
                                                    evap 1"
DELTAP_E[i] = DELTAP_2Phase_horiz('steam', m_dot_v_t[i]/A_c[i], P_E[i-1], ID[i], L[i], 1,
x_vaporheat_out_E[i])                               "pressure drop"

A_c[i] = pi# *  ID[i]^2 / 4                         "cross area pipe"
P_c[i] = P_E[i-1] - DELTAP_E[i]                     "cond pressure outlet condensing side "
T_vaporheat_out_E[i] = T_sat(Steam,P=P_c[i])        "sat T condensing side in the inside"
h_vaporheat_out_E[i] = Enthalpy(Steam,T=T_vaporheat_out_E[i],x=x_vaporheat_out_E[i])
                                                    "boiling point elevation"

k[i] = k_('Copper', (T_w_t_i[i] + T_w_t_o[i])/2)    "thermal conductivity"

T_avg[i] = (T_vaporheat_out_E[i]  + T_vapor_E[i-1])/2"avg T between in and out cond side"
DELTAT[i] = T_avg[i] - TBT[i]                       "temperature difference"
```

```
    Call Cond_HorizontalTube_avg('steam', m_dot_v_t[i], T_avg[i], T_w_t_i[i], ID[i], 1,
    x_vaporheat_out_E[i]: H_c_t[i])                    "avg conv heat transfer coeff cond side"
    H_c_t[i] * convert(W,kW) * ID[i] * pi# * L[i] * (T_avg[i] - T_w_t_i[i]) = m_dot_v_t[i] *
    (h_vaporheat_in_E[i] - h_vaporheat_out_E2[i])
    Q_dot_E[i] = H_c_t[i] * convert(W,kW) * ID[i] * pi# * L[i] * (T_avg[i] - T_w_t_i[i]) * N_t[i]

    h_vaporheat_out_E2[i] = Enthalpy(Steam,T=T_vaporheat_out_E[i],x=x_vaporheat_out_E2[i])

    N_t[i] / (A_tot_E[i] * U_E[i]) = (1/(H_b_t[i] * pi# * OD[i] * L[i]) + 1/(H_c_t[i] * pi# * ID[i] * L[i]) +
    ln(OD[i]/ID[i])/(2 * pi# * k[i] * L[i]) + FF/(pi# * OD[i] * L[i]))  * convert(C/W,C/kW)
                                                       "overall heat transfer coefficient"
    (T_w_t_o[i] - TBT[i]) / (1/(H_b_t[i] * pi# * OD[i] * L[i]) + FF/(pi# * OD[i] * L[i])) = pi# * L[i] * ID[i] *
    H_c_t[i] * (T_avg[i] - T_w_t_i[i])                 "energy balance"
    2 * pi# * L[i] * k[i] / ln(OD[i]/ID[i]) * (T_w_t_i[i] - T_w_t_o[i]) = pi# * L[i] * ID[i] * H_c_t[i] *
    (T_avg[i] - T_w_t_i[i])                            "energy balance"

    CALL evap(T_w_t_o[i],TBT[i],GAMMA,S_feed:H_b_t[i],q_dot_b_t[i])
                                                       "avg conv heat transfer coeff evap side"

    x_vaporheat_out_E[i] = x_vaporheat_out_E2[i]

end

"*****************************************************************************************************"
"CONDENSER"
"*****************************************************************************************************"

m_dot_feed = sum(m_dot_feed_E[i],i=1,N)                "mass flow rate of feed seawater"
T_feed = 33 [C]                                        "INPUT" "temperature of feed seawater"

m_dot_fw = m_dot_fw[n] + m_dot_vapor_E[n] + m_dot_vapor_FB[n]
                                                       "mass flow rate of fresh water"
SEC =  (m_dot_vaporheat_E[1] * (h_vaporheat_in_E[1] - h_vaporheat_out_E[1])) / m_dot_fw *
1000 [kg/m^3]  * convert(kJ,kWh)                       "specific energy consumption"
GOR = m_dot_fw / (m_dot_vaporheat_E[1])                "gain output ratio"
```

```
Cp_feed_sh_C_avg = (Cp_feed_sh_in_C + Cp_feed_sh_out_C)/2
                                                    "avg spec feed seawater SH section"
Cp_feed_sh_in_C = SW_SpcHeat(T_feed_sh_C,S_feed) * convert(J/kg,kJ/kg)
                                                    "spec incoming feed seawater SH sect"
Cp_feed_sh_out_C = SW_SpcHeat(T_feed_E[n],S_feed) * convert(J/kg,kJ/kg)
                                                    "spec outgoing feed seawater SH sect"

T_feed_E[n] = T_feed_sh_C

"saturated section"
 epsilon_sat_C =HX('counterflow{shell&tube_1}', Ntu_sat_C, C_min_sat_C,9999[kW/K], 'epsilon')
                                                    "effectiveness-NTU relation"
epsilon_sat_C = Q_sat_C / Q_sat_C_max               "effectiveness"

Q_sat_C_max = C_min_sat_C * (T_vapor_E[n] - T_feed_sat_C)
                                                    "maximum heat transfer rate"

C_min_sat_C = (m_dot_feed + m_dot_cool) * Cp_feed_sat_C_avg
                                                    "minimum capacitance"
Cp_feed_sat_C_avg = (Cp_feed_sat_in_C + Cp_feed_sat_out_C)/2
                                                     "avg spec heat feed seawater sat sect"
Cp_feed_sat_in_C =  Cp_feed_sc_out_C                "spec heat in feed seawater sat sect"
Cp_feed_sat_out_C = Cp_feed_sh_in_C                 "spec heat out feed seawater sat sect"
Q_sat_C = (m_dot_feed + m_dot_cool) * Cp_feed_sh_C_avg * (T_feed_sh_C - T_feed_sat_C)
                                                    "heat transfer rate condenser sat sect"
Q_sat_C = (m_dot_vapor_E[n] + m_dot_vapor_FB[n]) * (h_vapor_C - h_cond)
                                                    "heat transfer rate condenser sat sect"
h_vapor_C = Enthalpy(Water,P=P_E[n],x=1)            "enthalpy of saturation vapor"
h_cond = Enthalpy(Water,T=T_vapor_E[n],x=0)         "enthalpy of saturation liquid"
NTU_sat_C = UA_sat_C / C_min_sat_C                  "number of transfer units"

"subcooling section"
epsilon_sc_C =HX('counterflow{shell&tube_1}', NTU_sc_C, C_min_sc_C, C_max_sc_C,
'epsilon')                                          "effectiveness-NTU relation"
epsilon_sc_C = Q_sc_C / Q_sc_C_max                  "effectiveness"
```

```
Q_sc_C_max = C_min_sc_C * (T_vapor_E[n] - T_feed_sat_C)
                                                    "maximum heat transfer rate"

C_min_sc_C = min((m_dot_feed + m_dot_cool) * Cp_feed_sc_C_avg,(m_dot_vapor_E[n] +
m_dot_vapor_FB[n]) * Cp_fw_avg)                     "minimum capacitance"
C_max_sc_C = max((m_dot_feed + m_dot_cool) * Cp_feed_sc_C_avg,(m_dot_vapor_E[n] +
m_dot_vapor_FB[n]) * Cp_fw_avg)                     "maximum capacitance"
Cp_fw_avg = (specheat(Steam,T=T_vapor_E[n],x=0) + specheat(steam,T=T_fw,x=0))/2
                                                    "avg spec heat cond fwater scool sect"
Cp_feed_sc_C_avg = (Cp_feed_sc_in_C + Cp_feed_sc_out_C)/2
                                                    "avg spec heat feed seawat scool sect"
Cp_feed_sc_in_C = SW_SpcHeat(T_feed,S_feed) * convert(J/kg,kJ/kg)
                                                    "spec heat feed in seawater scool sect"
Cp_feed_sc_out_C = SW_SpcHeat(T_feed_sat_C,S_feed) * convert(J/kg,kJ/kg)
                                                    "spec heat feed out seawater scool sect"
Q_sc_C = (m_dot_feed + m_dot_cool) * Cp_feed_sc_C_avg * (T_feed_sat_C - T_feed)
                                                    "heat transfer rate condenser scool sect"
Q_sc_C = (m_dot_vapor_E[n] + m_dot_vapor_FB[n]) * (h_cond - h_fw)
                                                    "heat transfer rate condenser scool sect"
h_fw = Enthalpy(Water,T=T_fw,x=0)
NTU_sc_C = UA_sc_C / C_min_sc_C                     "number of transfer units"
T_fw = 38                                           "temperature fresh water"

UA_sat_C + UA_sc_C = 10000

"***************************************************************************************************************"
"PRE-HEATER"
"***************************************************************************************************************"

m_dot_feed_Ph[n] = m_dot_feed                       "mass balance"

Duplicate i=1,N-1

    m_dot_vapor_Ph[i] = m_dot_vapor_E[i] + m_dot_vapor_FB[i]
                                                    "mass balance hot stream"
```

```
m_dot_feed_Ph[i] = m_dot_feed_Ph[i+1] - m_dot_feed_E[i+1]
                                                    "mass balance cold stream"

m_dot_vapor_Ph[i] * (1 - x_vaporheat_in_E[i+1]) = m_dot_d_Ph[i]
m_dot_vapor_Ph[i] * (x_vaporheat_in_E[i+1]) = m_dot_vaporheat_E[i+1]

Cp_feed_sh_Ph_avg[i] = (Cp_feed_sh_in_Ph[i] + Cp_feed_sh_out_Ph[i])/2
                                                    "avg spec heat feed seawater SH sect"
Cp_feed_sh_in_Ph[i] = SW_SpcHeat(T_feed_int_E[i],S_feed) * convert(J/kg,kJ/kg)
                                                    "spec heat in feed seawater SH sect"
Cp_feed_sh_out_Ph[i] = SW_SpcHeat(T_feed_E[i],S_feed) * convert(J/kg,kJ/kg)
                                                    "spec heat out feed seawater SH sect"

"saturation section"
T_feed_int_E[i] = T_feed_E[i]

epsilon_sat_Ph[i] =HX('counterflow{shell&tube_1}', Ntu_sat_Ph[i],
C_min_sat_Ph[i],9999[kW/K], 'epsilon')              "effectiveness-NTU relation"
epsilon_sat_Ph[i] = Q_sat_Ph[i] / Q_sat_Ph_max[i]   "effectiveness"

Q_sat_Ph_max[i] = C_min_sat_Ph[i] * (T_vapor_E[i] - T_feed_E[i+1])
                                                    "maximum heat transfer rate"

C_min_sat_Ph[i] = m_dot_feed_Ph[i] * Cp_feed_sat_Ph_avg[i]
                                                    "minimum capacitance"
Cp_feed_sat_Ph_avg[i] = (Cp_feed_sat_in_Ph[i] + Cp_feed_sat_out_Ph[i])/2
                                                    "avg spec heat feed seawater sat sect"
Cp_feed_sat_in_Ph[i] = SW_SpcHeat(T_feed_E[i+1],S_feed) * convert(J/kg,kJ/kg)
                                                    "spec heat feed in seawater sat sect"
Cp_feed_sat_out_Ph[i] = Cp_feed_sh_in_Ph[i]         "spec heat feed out seawater sat sect"
Q_sat_Ph[i] = m_dot_feed_Ph[i] * Cp_feed_sh_Ph_avg[i] * (T_feed_int_E[i] - T_feed_E[i+1])
                                                    "heat transfer rate PH sat sect"
Q_sat_Ph[i] = m_dot_vapor_Ph[i] * (h_vapor_Ph[i] - h_vapor_out_Ph[i+1])
                                                    "heat transfer rate PH sat sect"

NTU_sat_Ph[i] = UA_sat_Ph[i] / C_min_sat_Ph[i]      "number of transfer units"
```

```
    h_vapor_Ph[i] = Enthalpy(Water,P=P_E[i],x=1)          "enthalpy saturated vapor pre-heater"
    h_vapor_out_Ph[i+1] = Enthalpy(Water,T=T_vapor_E[i],x=x_vaporheat_in_E[i+1])
                                                          "enthalpy water vapor leaving PH"
    h_vaporheat_in_E[i+1] = Enthalpy(Water,T=T_vapor_E[i],x=1)
    UA_sat_Ph[i] = 1400 [kW/C]

end

"*************************************************************************************************************"
"FLASHING BOX"
"*************************************************************************************************************"

m_dot_fw[0] = 0 [kg/s]                                    "boundary condition"
h_fw[0] = 0                                               "boundary condition"
m_dot_vapor_FB[0] = 0
m_dot_d_Ph[0] = 0                                         "boundary condition"

m_dot_cond_FB[1] = 0
m_dot_vapor_FB[1] = 0
m_dot_fw[1] = 0
h_fw[1] = 0

duplicate i = 2,n
    m_dot_cond_FB[i] = 0 [kg/s]                           "boundary condition"
    m_dot_d_Ph[i-1] + m_dot_fw[i-1] + m_dot_vaporheat_E[i] - m_dot_cond_FB[i] =
    m_dot_vapor_FB[i] + m_dot_fw[i]                       "mass balance"
    m_dot_d_Ph[i-1] * h_fw[i-1] + m_dot_fw[i-1] * h_fw[i-1] + m_dot_vaporheat_E[i] *
    h_vaporheat_out_E[i] - m_dot_cond_FB[i] * h_fw[i] = m_dot_vapor_FB[i] * h_vapor_FB[i] +
    m_dot_fw[i] * h_fw[i]                                 "energy balance"
    h_fw[i] = Enthalpy(Water,x=0,P=P_E[i])                "enthalpy condensed fresh water"
    h_vapor_FB[i] = Enthalpy(Water,x=1,P=P_E[i])          "enthalpy vapor produced in flash box"
end
```

Appendix B : MED-TC validated Model

```
"*************************************************************************************************************"
"subprogram evaporation convection heat transfer coefficient outside of horizontal tubes"

subprogram evap(T_w_o,T_sat,GAMMA,S:h_e,q_e)
    T_avg = (T_w_o + T_sat) / 2
    rho = SW_Density(T_avg,S)                          "density feed brine, kg/m^3"
    mu = SW_Viscosity(T_avg,S)
    nu = SW_KViscosity(T_avg,S)                        "kinematic viscosity feed brine, m^2/s"
    k = SW_Conductivity(T_avg,S)                       "conductivity feed brine, W/m-C"
    Pr = SW_Prandtl(T_avg,S)                           "prandt number feed brine"
    Re = 4 * GAMMA / mu                                "reynold number feed brine"
    q_e = h_e * (T_w_o - T_sat)                        "heat flux, W/m^2"
    h_e *  (nu^2 / (g# * k^3))^(1/3) = 0.00082 * Re^0.10 * Pr^0.65 * q_e^0.4
                                                       "conv heat transfer coeff, W/m^2-C"
end


procedure Shockwave(P_2,C_2, V_2, h_2, rho_2,s_2: V_3, h_3,s_3)
gamma_ej = {1.3} 1.135                                 "INPUT" "specific heat ratio"

if (V_2>=C_2) then
    C = C_2
    repeat
    C_3 = C
    V_3 = ((2/(gamma_ej - 1) + V_2^2/C_2^2)/(2 * gamma_ej * V_2^2 / ((gamma_ej - 1)*C_2^2) -
    1))^0.5 * C_3                                      "velocity after shock wave"
    h_3 = (h_2*convert(kJ/kg,J/kg) + V_2^2/2 - V_3^2/2) /  convert(kJ/kg,J/kg)
                                                       "energy balance before and after shock "
    rho_3 = rho_2 * V_2/V_3                            "continuity before and after shock wave"
    s_3 = Entropy(Steam,v=1/rho_3,h=h_3)
    P_3 = Pressure(Steam,h=h_3,v=1/rho_3)
    h_liq = Enthalpy(Steam,x=0,P=P_3)
    h_vap = Enthalpy(Steam,x=1,P=P_3)
    if (h_3 > h_vap) then
    C =SoundSpeed(Steam,h=h_3,P=P_3)
    s_3 = Entropy(Steam,P=P_3,h=h_3)                   "entropy after shock wave"
else
    x_3 = Quality(Steam,v=1/rho_3,h=h_3)
    C =SoundSpeed(Steam,x=1,P=P_3)                     "sound velocity after shock wave"
    s_3 = Entropy(Steam,P=P_3,x=x_3)                   "entropy after shock wave"
endif
until (C=C_3)
else
    V_3 = V_2
    h_3 = h_2
    s_3 = s_2
endif
end
```

```
"****************************************************************************************************"
"INPUT DATA"
"****************************************************************************************************"

N = 4                                              "number of effects"
S_feed = 35 [g/kg]                                 "salinity of feed water" "INPUT"

"evaporator 1"
OD[1] = 22 [mm] * convert(mm,m)                    "outside diameter tubes evaporator, m"
th[1] = 1.2 [mm] * convert(mm,m)                   "thickness tube, m"
N_e[1] = 2                                         "number of evaporators"
A_e[1] = 5400 [m^2]                                "heat transfer area per evaporator, m^2"
L[1] = 7 [m]                                       "long of tubes evaporator, m"

"evaporator 2"
OD[2] = OD[1]                                      "outside diameter tubes evaporator, m"
th[2] = th[1]                                      "thickness tube, m"
N_e[2] = 2                                         "number of evaporators"
A_e[2] = 5400 [m^2]                                "heat transfer area per evaporator, m^2"
L[2] = 7 [m]

"evaporator 3"
OD[3] = OD[1]                                      "outside diameter tubes evaporator, m"
th[3] = th[1]                                      "thickness tube, m"
N_e[3] = 1
A_e[3] = 2300 [m^2]                                "heat transfer area evaporator, m^2"
L[3] = 5 [m]                                       "long of tubes evaporator, m"

"evaporator 4"
OD[4] = OD[1]                                      "outside diameter tubes evaporator, m"
th[4] = th[1]                                      "thickness tube, m"
N_e[4] = 1
A_e[4] = 2300 [m^2]                                "heat transfer area evaporator, m^2"
L[4] = 5 [m]                                       "long of tubes evaporator, m"

FF = 0.0000 [m^2-C/W]                              "Fouling Factor" "INPUT"
GAMMA = 0.5 [m^3/h-m] * rho_b * convert(kg/h-m,kg/s-m)
                                                   "*************define******************"
rho_b = SW_Density(T_feed_E[1],S_feed)             "density brine"

"feed water"
m_dot_feed_E[1] = 540000 [kg/h] * convert(kg/h,kg/s)     "feed water mass flow rate evaporator 1"
"INPUT"
m_dot_feed_E[2] = 540000 [kg/h]  * convert(kg/h,kg/s)    "feed water  mass flow rate evaporator
2" "INPUT"
m_dot_feed_E[3] = 160000 [kg/h]  * convert(kg/h,kg/s)    "feed water  mass flow rate evaporator
2" "INPUT"
m_dot_feed_E[4] = 160000 [kg/h] * convert(kg/h,kg/s)     "feed water mass flow rate evaporator 1"
"INPUT"

"brine produced"
m_dot_brine_E[0] = 0                               "boundary condition"
```

```
h_brine_E[0] = 0                                        "boundary condition"
S_brine_E[0] = 0                                        "boundary condition"

"extraction"
m_dot_vapor_TC[1] = 0                                   "boundary condition"
m_dot_vapor_TC[3] = 0                                   "boundary condition"
m_dot_vapor_TC[4] = 0                                   "boundary condition"


"*************************************************************************************************************"
"EVAPORATOR"
"*************************************************************************************************************"

Duplicate i = 1,N

    ID[i] = OD[i] - 2 * th[i]                           "inside diameter tubes evaporator, m"
    A_tot_E[i] = A_e[i] * N_e[i]                        "total heat transfer area, m^2 "
    A_tot_E[i] = N_t[i] * L[i] * OD[i] * pi#            "number of tubes evaporator"
    h_feed_E[i] = SW_Enthalpy(T_feed_E[i],S_feed) * convert(J/kg,kJ/kg)
                                                        "enthalpy of feed water"
    h_vapor_E[i] = Enthalpy(Steam,T=TBT[i],P=P_E[i])    "enthalpy of water-vapor generated"
    h_brine_E[i] = SW_Enthalpy(TBT[i],S_brine_E[i]) * convert(J/kg,kJ/kg)
                                                        "enthalpy of brine"
    m_dot_feed_E[i] + m_dot_brine_E[i-1] - m_dot_vapor_E[i] - m_dot_brine_E[i] -
    m_dot_vapor_TC[i] * ZZZ=  0                         "MASS BALANCE"
    m_dot_brine_E[i] * S_brine_E[i] = m_dot_feed_E[i] * S_feed + m_dot_brine_E[i-1] *
    S_brine_E[i-1]                                      "SALT BALANCE"
    {S_brine_E[i] = 51 [g/kg]                           "*****GUESS VALUE*****"}

    Q_dot_E[i] = -(m_dot_feed_E[i] * h_feed_E[i] + m_dot_brine_E[i-1] * h_brine_E[i-1] -
    (m_dot_vapor_E[i] + m_dot_vapor_TC[i] * ZZZ) * h_vapor_E[i] -  m_dot_brine_E[i] *
    h_brine_E[i])
    Q_dot_E[i] = m_dot_vaporheat_E[i] * (h_vaporheat_in_E[i] - h_vaporheat_out_E[i])
                                                        "ENERGY BALANCE"

    P_E[i] = P_sat(Steam,T=T_vapor_E[i])                "pressure evaporator 1"
    TBT[i] = T_vapor_E[i] + BPE[i]                      "vapor temperature"
    BPE[i] = SW_BPE(TBT[i],S_brine_E[i])                "boiling point elevation"

    m_dot_v_t[i] = m_dot_vaporheat_E[i] / N_t[i]        "water-vap mass flow rate x tube evap1"
    DELTAP_E[i] = DELTAP_2Phase_horiz('steam', m_dot_v_t[i]/A_c[i], P_E[i-1], ID[i], L[i],
    1{x_vaporheat_in_E[i]}, x_vaporheat_out_E[i])       "pressure drop"

    A_c[i] = pi# *  ID[i]^2 / 4                         "cross area pipe"
    P_c[i] = P_E[i-1] - DELTAP_E[i]                     "cond press out condensing side "
    T_vaporheat_out_E[i] = T_sat(Steam,P=P_c[i])        "sat T condensing side in the inside"
    h_vaporheat_out_E[i] = Enthalpy(Steam,T=T_vaporheat_out_E[i],x=x_vaporheat_out_E[i])
                                                        "boiling point elevation"

    k[i] = k_('Copper', (T_w_t_i[i] + T_w_t_o[i])/2)    "thermal conductivity"

    T_avg[i] = (T_vaporheat_out_E[i]  + T_vapor_E[i-1])/2
                                                        "avg T inlet and outlet condensing side"
    DELTAT[i] = T_avg[i] - TBT[i]                       "temperature difference"
```

```
    Call Cond_HorizontalTube_avg('steam', m_dot_v_t[i], T_avg[i], T_w_t_i[i], ID[i],
    1{x_vaporheat_in_E[i]}, x_vaporheat_out_E[i]: H_c_t[i])
                                                    "avg conv heat transfer coeff cond side"
    H_c_t[i] * convert(W,kW) * ID[i] * pi# * L[i] * (T_avg[i] - T_w_t_i[i]) = m_dot_v_t[i] *
    (h_vaporheat_in_E[i] - h_vaporheat_out_E2[i])
    Q_dot_E[i] = H_c_t[i] * convert(W,kW) * ID[i] * pi# * L[i] * (T_avg[i] - T_w_t_i[i]) * N_t[i]

    h_vaporheat_out_E2[i] = Enthalpy(Steam,T=T_vaporheat_out_E[i],x=x_vaporheat_out_E2[i])

    N_t[i] / (A_tot_E[i] * U_E[i]) = (1/(H_b_t[i] * pi# * OD[i] * L[i]) + 1/(H_c_t[i] * pi# * ID[i] * L[i]) +
    ln(OD[i]/ID[i])/(2 * pi# * k[i] * L[i]) + FF/(pi# * OD[i] * L[i]))  * convert(C/W,C/kW)
                                                    "overall heat transfer coefficient"
    (T_w_t_o[i] - TBT[i]) / (1/(H_b_t[i] * pi# * OD[i] * L[i]) + FF/(pi# * OD[i] * L[i])) = pi# * L[i] * ID[i] *
    H_c_t[i] * (T_avg[i] - T_w_t_i[i])              "energy balance"
    2 * pi# * L[i] * k[i] / ln(OD[i]/ID[i]) * (T_w_t_i[i] - T_w_t_o[i]) = pi# * L[i] * ID[i] * H_c_t[i] *
    (T_avg[i] - T_w_t_i[i])                         "energy balance"

    CALL evap(T_w_t_o[i],TBT[i],GAMMA,S_feed:H_b_t[i],q_dot_b_t[i])
                                                    "avg conv heat transfer coeff evap side"

    x_vaporheat_out_E[i = x_vaporheat_out_E2[i

end

x_vaporheat_in_E[1] = 1                             "quality steam supply first effect"

"*************************************************************************************************************"
"CONDENSER"
"*************************************************************************************************************"

m_dot_feed = sum(m_dot_feed_E[i],i=1,N)             "mass flow rate of feed seawater"
T_feed = 33 [C]                                     "INPUT"  "temperature of feed seawater"

m_dot_fw = m_dot_fw[4] + m_dot_vapor_E[4] + m_dot_vapor_FB[4] - m_dot_vapor_TC_NCG
                                                    "mass flow rate of fresh water"
SEC =  ((m_dot_steam + m_dot_steam_NCG) * (h_steam - h_fw[1])) / m_dot_fw * 1000 [kg/m^3]
* convert(kJ,kWh)                                  "specific energy consumption"
GOR = m_dot_fw / (m_dot_steam + m_dot_steam_NCG)"gain output ratio"

SEC2 =  ((m_dot_steam + m_dot_steam_NCG) * (h_steam - h_fw[1])) / 124.4 * 1000 [kg/m^3]  *
convert(kJ,kWh)                                     "specific energy consumption"
GOR2 = 124.4 / (m_dot_steam + m_dot_steam_NCG)      "gain output ratio"

"superheated section"
epsilon_sh_C =HX('counterflow{shell&tube_1}', NTU_sh_C, C_min_sh_C, C_max_sh_C,
'epsilon')                                          "effectiveness-NTU relation"
epsilon_sh_C = Q_sh_C / Q_sh_C_max                  "effectiveness"

Q_sh_C_max = C_min_sh_C * (TBT[n] - T_feed_sh_C)  "maximum heat transfer rate"

C_min_sh_C = min((m_dot_feed + m_dot_cool) * Cp_feed_sh_C_avg,(m_dot_vapor_E[n] +
m_dot_vapor_FB[n] - m_dot_vapor_TC_NCG) * Cp_vaporheat_avg)
                                                    "minimum capacitance"
```

```
C_max_sh_C = max((m_dot_feed + m_dot_cool) * Cp_feed_sh_C_avg,(m_dot_vapor_E[n] +
m_dot_vapor_FB[n] - m_dot_vapor_TC_NCG) * Cp_vaporheat_avg)
                                                    "maximum capacitance"
Cp_vaporheat_avg = (specheat(Steam,T=TBT[n],P=P_E[n]) +
specheat(steam,T=T_vapor_E[n],x=1))/2               "avg spec heat water vapor SH section"
Cp_feed_sh_C_avg = (Cp_feed_sh_in_C + Cp_feed_sh_out_C)/2
                                                    "avg spec feed seawater SH section"
Cp_feed_sh_in_C = SW_SpcHeat(T_feed_sh_C,S_feed) * convert(J/kg,kJ/kg)
                                                    "spec in feed seawater SH section"
Cp_feed_sh_out_C = SW_SpcHeat(T_feed_E[n],S_feed) * convert(J/kg,kJ/kg)
                                                    "spec out feed seawater SH section"
Q_sh_C = (m_dot_feed + m_dot_cool) * Cp_feed_sh_C_avg * (T_feed_E[n] - T_feed_sh_C)
                                                    "heat transfer rate condenser SH sect"
Q_sh_C = (m_dot_vapor_E[n] - m_dot_vapor_TC_NCG) * h_vapor_E[n] + m_dot_vapor_FB[n] *
h_vapor_FB[n] - (m_dot_vapor_E[n] + m_dot_vapor_FB[n] - m_dot_vapor_TC_NCG) *
h_vapor_C                                           "heat transfer rate condenser SH sect"
NTU_sh_C = UA_sh_C / C_min_sh_C                     "number of transfer units"

"saturated section"
epsilon_sat_C =HX('counterflow{shell&tube_1}', Ntu_sat_C, C_min_sat_C,9999[kW/K], 'epsilon')
                                                    "effectiveness-NTU relation"
epsilon_sat_C = Q_sat_C / Q_sat_C_max               "effectiveness"

Q_sat_C_max = C_min_sat_C * (T_vapor_E[n] - T_feed_sat_C)
                                                    "maximum heat transfer rate"

C_min_sat_C = (m_dot_feed + m_dot_cool) * Cp_feed_sat_C_avg
                                                    "minimum capacitance"
Cp_feed_sat_C_avg = (Cp_feed_sat_in_C + Cp_feed_sat_out_C)/2
                                                    "avg spec heat feed seawater sat sect"
Cp_feed_sat_in_C =  Cp_feed_sc_out_C                "spec heat in feed seawater sat section"
Cp_feed_sat_out_C = Cp_feed_sh_in_C                 "spec heat out feed seawater sat sect"
Q_sat_C = (m_dot_feed + m_dot_cool) * Cp_feed_sh_C_avg * (T_feed_sh_C - T_feed_sat_C)
                                                    "heat transfer rate condenser sat sect"
Q_sat_C = (m_dot_vapor_E[n] + m_dot_vapor_FB[n] - m_dot_vapor_TC_NCG) * (h_vapor_C -
h_cond)                                             "heat transfer rate condenser sat sect"
h_vapor_C = Enthalpy(Water,P=P_E[n],x=1)            "enthalpy of saturation vapor"
h_cond = Enthalpy(Water,T=T_vapor_E[n],x=0)         "enthalpy of saturation liquid"
NTU_sat_C = UA_sat_C / C_min_sat_C                  "number of transfer units"

"subcooling section"
epsilon_sc_C =HX('shell&tube_1', NTU_sc_C, C_min_sc_C, C_max_sc_C, 'epsilon')
                                                    "effectiveness-NTU relation"
epsilon_sc_C = Q_sc_C / Q_sc_C_max                  "effectiveness"

Q_sc_C_max = C_min_sc_C * (T_vapor_E[n] - T_feed_sat_C)
                                                    "maximum heat transfer rate"

C_min_sc_C = min((m_dot_feed + m_dot_cool) * Cp_feed_sc_C_avg,(m_dot_vapor_E[n] +
m_dot_vapor_FB[n] - m_dot_vapor_TC_NCG) * Cp_fw_avg)
                                                    "minimum capacitance"
C_max_sc_C = max((m_dot_feed + m_dot_cool) * Cp_feed_sc_C_avg,(m_dot_vapor_E[n] +
m_dot_vapor_FB[n] - m_dot_vapor_TC_NCG) * Cp_fw_avg)
                                                    "maximum capacitance"
```

```
Cp_fw_avg = (specheat(Steam,T=T_vapor_E[n],x=0) + specheat(steam,T=T_fw,x=0))/2
                                                        "avg spec heat cond fwater scool sect"
Cp_feed_sc_C_avg = (Cp_feed_sc_in_C + Cp_feed_sc_out_C)/2
                                                        "avg spec heat feed seawater scool "
Cp_feed_sc_in_C = SW_SpcHeat(T_feed,S_feed) * convert(J/kg,kJ/kg)
                                                        "spec heat feed in seawater scool "
Cp_feed_sc_out_C = SW_SpcHeat(T_feed_sat_C,S_feed) * convert(J/kg,kJ/kg)
                                                        "spec heat feed out seawater subcool"
Q_sc_C = (m_dot_feed + m_dot_cool) * Cp_feed_sc_C_avg * (T_feed_sat_C - T_feed)
                                                        "heat transfer rate condenser scool "
Q_sc_C = (m_dot_vapor_E[n] + m_dot_vapor_FB[n] - m_dot_vapor_TC_NCG) * (h_cond - h_fw)
                                                        "heat transfer rate condenser subcool"
h_fw = Enthalpy(Water,T=T_fw,x=0)
NTU_sc_C = UA_sc_C / C_min_sc_C                         "number of transfer units"
T_fw{ - T_feed = 3 [C]}= 38                             "temperature fresh water"

m_dot_cool = 2080000 [kg/h] * convert(kg/h,kg/s)

"*****************************************************************************************************"
"PRE-HEATER"
"*****************************************************************************************************"

m_dot_feed_Ph[4] = m_dot_feed                           "mass balance"

Duplicate i=2,3

m_dot_vapor_Ph[i] = m_dot_vapor_E[i] + m_dot_vapor_FB[i]
                                                        "mass balance hot stream"
m_dot_feed_Ph[i] = m_dot_feed_Ph[i+1] - m_dot_feed_E[i+1]
                                                        "mass balance cold stream"

m_dot_vapor_Ph[i] * (1 - x_vaporheat_in_E[i+1]) = m_dot_d_Ph[i]
m_dot_vapor_Ph[i] * (x_vaporheat_in_E[i+1]) = m_dot_vaporheat_E[i+1]

"superheated section"
epsilon_sh_Ph[i] =HX('counterflow{shell&tube_1}', NTU_sh_Ph[i], C_min_sh_Ph[i],
C_max_sh_Ph[i], 'epsilon')                              "effectiveness-NTU relation"
epsilon_sh_Ph[i] = Q_sh_Ph[i] / Q_sh_Ph_max[i]          "effectiveness"

Q_sh_Ph_max[i] = C_min_sh_Ph[i] * (TBT[i] - T_feed_int_E[i])
                                                        "maximum heat transfer rate"

C_min_sh_Ph[i] = min(m_dot_feed_Ph[i] * Cp_feed_sh_Ph_avg[i],m_dot_vapor_Ph[i] *
Cp_vaporheat_avg[i])                                    "minimum capacitance"
C_max_sh_Ph[i] = max(m_dot_feed_Ph[i] * Cp_feed_sh_Ph_avg[i],m_dot_vapor_Ph[i] *
Cp_vaporheat_avg[i])                                    "maximum capacitance"
Cp_vaporheat_avg[i] = (specheat(Steam,T=TBT[i],P=P_E[i]) +
specheat(steam,T=T_vapor_E[i],x=1))/2                   "avg spec heat water vapor SH section"
Cp_feed_sh_Ph_avg[i] = (Cp_feed_sh_in_Ph[i] + Cp_feed_sh_out_Ph[i])/2
                                                        "avg spec heat feed seawater SH sect"
Cp_feed_sh_in_Ph[i] = SW_SpcHeat(T_feed_int_E[i],S_feed) * convert(J/kg,kJ/kg)
                                                        "spec heat in feed seawater SH section"
Cp_feed_sh_out_Ph[i] = SW_SpcHeat(T_feed_E[i],S_feed) * convert(J/kg,kJ/kg)
                                                        "spec heat out feed seawater SH sect"
```

```
Q_sh_Ph[i] = m_dot_feed_Ph[i] * Cp_feed_sh_Ph_avg[i] * (T_feed_E[i] - T_feed_int_E[i])
                                                    "heat transfer rate PH superheat sect"
Q_sh_Ph[i] = m_dot_vapor_Ph[i] * (h_vapor_E[i] - h_vapor_Ph[i])
                                                    "heat transfer rate PH superheat sect"
NTU_sh_Ph[i] = UA_sh_Ph[i] / C_min_sh_Ph[i]         "number of transfer units"

"saturation section"
epsilon_sat_Ph[i] =HX('shell&tube_1', Ntu_sat_Ph[i], C_min_sat_Ph[i],9999[kW/K], 'epsilon')
                                                    "effectiveness-NTU relation"
epsilon_sat_Ph[i] = Q_sat_Ph[i] / Q_sat_Ph_max[i]   "effectiveness"

Q_sat_Ph_max[i] = C_min_sat_Ph[i] * (T_vapor_E[i] - T_feed_E[i+1])
                                                    "maximum heat transfer rate"

C_min_sat_Ph[i] = m_dot_feed_Ph[i] * Cp_feed_sat_Ph_avg[i]
                                                    "minimum capacitance"
Cp_feed_sat_Ph_avg[i] = (Cp_feed_sat_in_Ph[i] + Cp_feed_sat_out_Ph[i])/2
                                                    "avg spec heat feed seawater sat sect"
Cp_feed_sat_in_Ph[i] = SW_SpcHeat(T_feed_E[i+1],S_feed) * convert(J/kg,kJ/kg)
                                                    "spec heat feed in seawater sat section"
Cp_feed_sat_out_Ph[i] = Cp_feed_sh_in_Ph[i]
                                                    "spec heat feed out seawater sat sect"
Q_sat_Ph[i] = m_dot_feed_Ph[i] * Cp_feed_sh_Ph_avg[i] * (T_feed_int_E[i] - T_feed_E[i+1])
                                                    "heat transfer rate PH saturation sect"
Q_sat_Ph[i] = m_dot_vapor_Ph[i] * (h_vapor_Ph[i] - h_vapor_out_Ph[i+1]
{h_vaporheat_in_E[i+1]})                            "heat transfer rate PH saturation sect"
h_vapor_Ph[i] = Enthalpy(Water,P=P_E[i],x=1)        "enthalpy saturated vapor pre-heater"
{h_vaporheat_in_E[i+1]}h_vapor_out_Ph[i+1] =
Enthalpy(Water,T=T_vapor_E[i],x=x_vaporheat_in_E[i+1])
                                                    "enthalpy water vapor leaving PH"
NTU_sat_Ph[i] = UA_sat_Ph[i] / C_min_sat_Ph[i]      "number of transfer units"

h_vaporheat_in_E[i+1] = Enthalpy(Water,T=T_vapor_E[i],x=1)

UA_sat_Ph[i] + UA_sh_Ph[i] = 2400 [kW/C]

end

"*********************************************************************************************************************"

"FLASHING BOX"
"*********************************************************************************************************************"

m_dot_fw[0] = 0 [kg/s]                              "boundary condition"
m_dot_cond_FB[1] = m_dot_steam + m_dot_dsh          "mass balance"
m_dot_cond_FB[2] = 0 [kg/s]                         "boundary condition"
m_dot_cond_FB[3] = 0 [kg/s]                         "boundary condition"
m_dot_cond_FB[4] = 0 [kg/s]                         "boundary condition"
h_fw[0] = 0                                         "boundary condition"
m_dot_vapor_FB[0] = 0
m_dot_d_Ph[0] = 0                                   "boundary condition"

duplicate i = 1,4
```

```
m_dot_d_Ph[i-1] + m_dot_fw[i-1] + m_dot_vaporheat_E[i] - m_dot_cond_FB[i] =
m_dot_vapor_FB[i] + m_dot_fw[i]                          "mass balance"
m_dot_d_Ph[i-1] * h_fw[i-1] + m_dot_fw[i-1] * h_fw[i-1] + m_dot_vaporheat_E[i] *
h_vaporheat_out_E[i] - m_dot_cond_FB[i] * h_fw[i] = m_dot_vapor_FB[i] * h_vapor_FB[i] +
m_dot_fw[i] * h_fw[i]                                    "energy balance"
h_fw[i] = Enthalpy(Water,x=0,P=P_E[i])                   "enthalpy condensed fresh water"
h_vapor_FB[i] = Enthalpy(Water,x=1,P=P_E[i])             "enthalpy vapor produced in flash box"
end

"*****************************************************************************************************************"
"DESUPERHEATER"
"*****************************************************************************************************************"

m_dot_vapor_Ej = m_dot_steam + m_dot_vapor_TC[2]  "mass balance ejector"
m_dot_vapor_Ej2 * h_vapor_Ej2 + m_dot_dsh * h_fw[1] = m_dot_vaporheat_E[1] *
h_vaporheat_in_E[1]                                      "energy balance" "@"
m_dot_vaporheat_E[1] = m_dot_vapor_Ej2 + m_dot_dsh"mass balance" "@"
h_steam = Enthalpy(Steam,T=T_steam,P=P_steam)       "enthalpy steam from external source"
h_vapor_Ej2 = Enthalpy(Steam,T=T_vapor_Ej,P=P_E[0])"enthalpy secondary steam ejector"
h_vaporheat_in_E[1] = Enthalpy(Steam,x=1,P=P_E[0])   "enthalpy steam supply first effect"

"*****************************************************************************************************************"
"EJECTOR"
"*****************************************************************************************************************"

omega = m_dot_steam/m_dot_vapor_TC[2]
gamma_ej = {1.3} 1.135                                   "INPUT""specific heat ratio"

eta_n = 0.9                                              "INPUT""nozzle efficiency"
eta_d = 0.9                                              "INPUT""diffuser efficiency"
eta_m = 0.95                                             "INPUT""mixing efficiency"

T_vaporheat_out_E[1] =  67 [C]                           "INPUT""T primary steam condensed"
P_E[0] = P_sat(Steam,T=T_vapor_E[0])                     "pressure steam supplied at the 1 effect"
P_steam = 21 [bar] * convert(bar,kPa)                    "INPUT""pressure primary steam"
m_dot_steam + m_dot_steam_NCG = 60000 [kg/h] * convert(kg/h,kg/s)
                                                         "INPUT" "mass flow rate primary steam"
T_steam = 224  [C]                                       "INPUT""temperature primary steam"
s_steam = Entropy(Steam,T=T_steam,P=P_steam)             "entropy primary steam at the inlet"

h_steam - h_1 = eta_n * (h_steam - h_1_s)                "isentropic efficiency nozzle"
V_1^2/2 = eta_n * (h_steam - h_1_s) * convert(kJ/kg,J/kg)

h_1_s = Enthalpy(Steam,P=P_1,s=s_1)                      "isentropic enthalpy nozzle"
h_1 = Enthalpy(Steam,x=x_1,P=P_1)                        "enthalpy in the nozzle"
s_1 = s_steam                                            "isentropic compression"


m_dot_vapor_Ej * V_2 = eta_m * m_dot_steam * V_1         "mom cons nozzle and mixing zone"
m_dot_vapor_Ej * (h_2*convert(kJ/kg,J/kg) + V_2^2/2) = m_dot_vapor_TC[2] * h_vapor_E[2]
*convert(kJ/kg,J/kg) + m_dot_steam * (h_1*convert(kJ/kg,J/kg) +V_1^2/2)
                                                         "energy bal nozzle and mixing zone"

P_2 = P_1                                                "pressure before shock wave"
```

```
x_2 = 1                                                    "quality before shock wave"
C_2 = SoundSpeed(Steam,x=x_2,P=P_2)                        "sound velocity before shock wave"
h_2 = Enthalpy(Steam,P=P_2,x=x_2)
s_2 = Entropy(Steam,P=P_2,x=x_2)                           "enthalpy before shock wave"
rho_2 = Density(Steam,x=x_2,P=P_2)                         "density before shock wave"

call Shockwave(P_2,C_2, V_2, h_2, rho_2,s_2: V_3, h_3,s_3)

h_3 - h_vapor_Ej = eta_d * (h_3 - h_m_s)                   "isentropic efficiency diffuser"
V_3^2/2 = eta_d * (h_m_s - h_3) * convert(kJ/kg,J/kg)      "energy bal after shock and diffuser"

h_m_s = Enthalpy(Steam,P=P_E[0],s=s_m)                     "isentropic outlet enthalpy ejector"
h_vapor_Ej = Enthalpy(Steam,T=T_m,P=P_E[0])                "outlet enthalpy ejector"
s_m = s_3                                                  "isentropic expansion"

Dsgn=P_steam/P_E[2]
CR = P_E[0]/P_E[2]                                         "compression ratio"
ER = P_steam/P_E[2]                                        "expansion ratio"
omega_3 = 0.235 * (P_E[0])^1.19 * ER^0.015 / P_E[2]^1.04

m_dot_steam + m_dot_vapor_TC[2] * ZZZ = m_dot_vapor_Ej2
m_dot_steam * h_steam + m_dot_vapor_TC[2] * ZZZ * h_vapor_E[2] = m_dot_vapor_Ej2 *
h_vapor_Ej2

ZZZ = 1.15

omega2 = m_dot_steam/(m_dot_vapor_TC[2]*ZZZ)

"*************************************************************************************************************"
"EJECTOR NCG"
"*************************************************************************************************************"

omega_NCG_2 = m_dot_steam_NCG/m_dot_vapor_TC_NCG

m_dot_vapor_Ej_NCG = m_dot_steam_NCG + m_dot_vapor_TC_NCG
                                                           "mass balance ejector"
m_dot_vapor_Ej_NCG * h_vapor_Ej_NCG = m_dot_steam_NCG * h_steam+
m_dot_vapor_TC_NCG * h_vapor_C                             "mass balance ejector"

h_vapor_Ej_NCG = Enthalpy(Steam,T=T_m_NCG,P=P_E[1])
                                                           "outlet enthalpy ejector"

CR_NCG = P_E[1]/P_E[4]                                     "compression ratio"
ER_NCG = P_steam/P_E[4]                                    "expansion ratio"
omega_NCG_2 = 0.235 * (P_E[1])^1.19 * ER_NCG^0.015 / P_E[4]^1.04

"*************************************************************************************************************"
"PRE-HEATER"
"*************************************************************************************************************"

Duplicate i=1,1

m_dot_vapor_Ph[i] = m_dot_vapor_Ej_NCG                     "mass balance hot stream"
m_dot_feed_Ph[i] = m_dot_feed_Ph[i+1] - m_dot_feed_E[i+1]
```

```
                                                    "mass balance cold stream"

m_dot_d_Ph[i] = m_dot_vapor_Ph[i] - m_zz[i]
m_dot_vaporheat_E[i+1] = m_dot_vapor_E[i] + m_dot_vapor_FB[i] + m_zz[i]
m_dot_vaporheat_E[i+1] * h_vaporheat_in_E[i+1] = m_dot_vapor_E[i] * h_vapor_E[i]+
m_dot_vapor_FB[i] * h_vapor_FB[i] + m_zz[i] * h_vapor_out_Ph[i+1]
h_vaporheat_in_E[i+1] = Enthalpy(Steam,x=1,P=P_E[i])

"superheated section"
epsilon_sh_Ph[i] =HX('counterflow{shell&tube_1}', NTU_sh_Ph[i], C_min_sh_Ph[i],
C_max_sh_Ph[i], 'epsilon')                          "effectiveness-NTU relation"
epsilon_sh_Ph[i] = Q_sh_Ph[i] / Q_sh_Ph_max[i]      "effectiveness"

Q_sh_Ph_max[i] = C_min_sh_Ph[i] * (T_m_NCG - T_feed_int_E[i])
                                                    "maximum heat transfer rate"

C_min_sh_Ph[i] = min(m_dot_feed_Ph[i] * Cp_feed_sh_Ph_avg[i],m_dot_vapor_Ph[i] *
Cp_vaporheat_avg[i])                                 "minimum capacitance"
C_max_sh_Ph[i] = max(m_dot_feed_Ph[i] * Cp_feed_sh_Ph_avg[i],m_dot_vapor_Ph[i] *
Cp_vaporheat_avg[i])                                "maximum capacitance"
Cp_vaporheat_avg[i] = (specheat(Steam,T=T_m_NCG,P=P_E[i]) +
specheat(steam,T=T_vapor_E[i],x=1))/2               "avg spec heat water vapor SH sect"
Cp_feed_sh_Ph_avg[i] = (Cp_feed_sh_in_Ph[i] + Cp_feed_sh_out_Ph[i])/2
                                                    "avg spec heat feed seawater SH sect"
Cp_feed_sh_in_Ph[i] = SW_SpcHeat(T_feed_int_E[i],S_feed) * convert(J/kg,kJ/kg)
                                                    "spec heat in feed seawater SH sect"
Cp_feed_sh_out_Ph[i] = SW_SpcHeat(T_feed_E[i],S_feed) * convert(J/kg,kJ/kg)
                                                    "spec heat out feed seawater SH sect"
Q_sh_Ph[i] = m_dot_feed_Ph[i] * Cp_feed_sh_Ph_avg[i] * (T_feed_E[i] - T_feed_int_E[i])
                                                    "heat transfer rate pre-heater SH sect"
Q_sh_Ph[i] = m_dot_vapor_Ph[i] * (h_vapor_Ej_NCG - h_vapor_Ph[i])
                                                    "heat transfer rate pre-heater SH sect"
NTU_sh_Ph[i] = UA_sh_Ph[i] / C_min_sh_Ph[i]         "number of transfer units"

"saturation section"
epsilon_sat_Ph[i] =HX('shell&tube_1', Ntu_sat_Ph[i], C_min_sat_Ph[i],9999[kW/K], 'epsilon')
                                                    "effectiveness-NTU relation"
epsilon_sat_Ph[i] = Q_sat_Ph[i] / Q_sat_Ph_max[i]   "effectiveness"

Q_sat_Ph_max[i] = C_min_sat_Ph[i] * (T_vapor_E[i] - T_feed_E[i+1])
                                                    "maximum heat transfer rate"

C_min_sat_Ph[i] = m_dot_feed_Ph[i] * Cp_feed_sat_Ph_avg[i]
                                                    "minimum capacitance"
Cp_feed_sat_Ph_avg[i] = (Cp_feed_sat_in_Ph[i] + Cp_feed_sat_out_Ph[i])/2
                                                    "avg spec heat feed seawater sat sect"
Cp_feed_sat_in_Ph[i] = SW_SpcHeat(T_feed_E[i+1],S_feed) * convert(J/kg,kJ/kg)
                                                    "spec heat feed in seawater sat sect"
Cp_feed_sat_out_Ph[i] = Cp_feed_sh_in_Ph[i]         "spec heat feed out seawater sat sect"
Q_sat_Ph[i] = m_dot_feed_Ph[i] * Cp_feed_sh_Ph_avg[i] * (T_feed_int_E[i] - T_feed_E[i+1])
                                                    "heat transfer rate pre-heater sat sect"
Q_sat_Ph[i] = m_dot_vapor_Ph[i] * (h_vapor_Ph[i] - h_vapor_out_Ph[i+1])
                                                    "heat transfer rate pre-heater sat sect"
h_vapor_Ph[i] = Enthalpy(Water,P=P_E[i],x=1)        "enthalpy saturated vapor pre-heater"
```

```
h_vapor_out_Ph[i+1] = Enthalpy(Water,T=T_vapor_E[i],x=0)
                                                    "enthalpy water vapor leaving PH"
NTU_sat_Ph[i] = UA_sat_Ph[i] / C_min_sat_Ph[i]      "number of transfer units"

UA_sat_Ph[i] + UA_sh_Ph[i] = 1400 [kW/C]

end

"*************************************************************************************************************"
```

Appendix C : Therminol VP-1 properties

Appendix D : Certification of parabolic trough solar collector (SopoNova 4.1 made by Sopogy, Inc.) -